Dissertation

submitted to the
Combined Faculties for the Natural Sciences and for Mathematics
of the Ruperto-Carola University of Heidelberg, Germany
for the degree of
Doctor of Natural Sciences

presented by

Diplom-Physiker Jens Fohlmeister
Born in Brandenburg (Havel), Germany

Oral examination: 29th October 2008

Carbon isotopes in stalagmites and drip water
-
Tracers of soil processes

Referees: **Prof. Dr. Augusto Mangini**
Prof. Dr. Werner Aeschbach-Hertig

Abstract

Stalagmites in caves are new climate archives recording meteorological parameters and processes occurring in the soil above caves. Due to advances in mass spectroscopy (TIMS and ICPMS) stalagmites can be dated reliably by the ^{230}Th/U-method. Carbon isotopes, recorded in stalagmites, are of interest because they depend on climate influenced soil processes above caves. In this thesis ^{14}C and ^{13}C in speleothem environments were used as tracers to investigate soil processes for the present day situation and during the Holocene.

The present day situation is studied by using monthly collected drip water samples from two caves (Ernesto cave in Trentino, Italy, and Bunker cave in Sauerland, Germany), which were analysed for their carbon isotope content. To interpret the isotopic composition a drip water model including various modes of limestone dissolution with respect to carbon isotopes was developed for the first time. The modelled carbon isotope composition of the drip water agrees well with the measurements. The annual trend in the carbon isotopes, observed in the drip water samples, can be attributed to changes in the water supply in the soil for Ernesto cave and to changes of the soil air carbon isotopic composition for Bunker cave.

The information about the soil-cave-systems obtained in the investigation of the present day situation was applied to interpret the carbon isotopes of Holocene stalagmites of both caves. An inverse modelling method was developed to determine the soil CO_2 content from measured carbon isotope pairs (^{14}C, δ^{13}C). The results indicate that the soil CO_2 content increased during the late Holocene in the soil above Ernesto cave due to a rising vegetation density. The Bunker cave stalagmite reveals a constant soil pCO_2 in the past.

Zusammenfassung

Stalagmiten sind neue Klimaarchive, die meteorologische Parameter und Bodenprozesse über der Höhle speichern. Fortschritte in der Massenspektroskopie (TIMS, ICPMS) ermöglichen das genaue Datieren von Stalagmiten mit der ^{230}Th/U-Methode. Die Kohlenstoffisotope in Stalagmiten sind von besonderem Interesse, da sie klimaabhängige Bodenprozesse über der Höhle widerspiegeln. Die vorliegende Arbeit benutzt die Kohlenstoffisotope ^{14}C und ^{13}C in Speleothemen als Spurenstoffe, um Bodenprozesse in der Gegenwart und während des Holozän zu untersuchen.

Zum Erforschen der gegenwärtigen Situation der Bodenprozesse von zwei Höhlensystemen (Ernestohöhle in Trentino, Italien und Bunkerhöhle im Sauerland, Deutschland) wurden Kohlenstoffisotopmessungen an monatlich gesammelten Tropfwasserproben durchgeführt. Für die Interpretation der Messungen wurde ein Tropfwassermodel unter Einbeziehung von Kohlenstoffisotopen entwickelt, das zum ersten Mal auch verschiedene Kalksteinlösungsvorgänge im Boden über der Höhle berücksichtigt. Die modellierten Kohlenstoffisotope stimmen mit den gemessenen überein. Der beobachtete Jahreszyklus der Kohlenstoffisotope im Tropfwasser kann Änderungen in der Niederschlags- und Verdunstungsmenge über der Ernestohöhle zugeschrieben werden. Für die Bunkerhöhle kann die Änderung der Tropfwasserkohlenstoffisotopie auf die jahreszeitlich variierende Bodenluftkohlenstoffisotopie zurückgeführt werden.

Die erworbenen Informationen über die Boden-Höhlen-Systeme aus der Tropfwasseruntersuchung tragen dazu bei, die gemessenen Kohlenstoffisotopien zweier holozäner Stalagmiten beider Höhlen besser zu interpretieren. Ein inverser Modellierungsansatz berechnet aus gepaarten ^{14}C und δ^{13}C Werten der Stalagmiten den Boden-CO_2-Gehalt über der Höhle. Während im Boden über der Bunkerhöhle keine CO_2-Schwankungen festgestellt werden können, stieg der Boden-CO_2-Wert über der Ernestohöhle während des betrachteten Zeitraumes im späten Holozän an.

Contents

List of Figures

List of Tables

Chapter 1

^{14}C in speleothems

The beginnings of radiocarbon measurements in speleothems go back to the 1950s shortly after the discovery of the carbon radionuclide by Libby et al. (1949). Franke (1951), Broecker et al. (1960), Hendy and Wilson (1968) and Geyh and Franke (1970) were among the first who used radiocarbon of stalagmite calcite to date speleothems. But very soon it was recognized (e.g. Hendy and Wilson, 1968; Hendy, 1970), that the most serious difficulty with this method of dating is the estimation of initial ^{14}C activity of the carbon in the calcite. In the early days of radiocarbon dating scientists assumed a constant atmospheric ^{14}C level of the atmosphere in the past. That yielded large errors in dating depending on the former atmospheric radiocarbon level. Even under the assumption of a constant atmospheric radiocarbon concentration, the injection of dead carbon[1] from the host rock is assumed to vary in different caves from 0 % to 50 % (Hendy, 1970, 1971; Salomons and Mook, 1986; Schwarcz, 1986, and see Chapter 3 for further explanations) and can thus introduce an uncertainty of more than 5000 years in the age determination. Therefore radiocarbon dating of stalagmites was no longer used in the 70's and 80's of the 20th century.

With the rise of the alpha counting U-series dating technique absolute dates of stalagmites can be determined. The disadvantage was the huge sample amount needed for a good dating statistics. Since the late 1980s up to now the ^{230}Th/U age determination improved significantly by thermal ionisation mass spectrometry (TIMS) and, more recently, multi collector – inductively coupled plasma mass spectrometry (MC–ICPMS). With a higher dating precision and much smaller sample sizes the interest on speleothems as climate archives returned.

The stable isotope and trace element analysis of stalagmites was established soon after reliably ages could be determined and leads up to now to several high resolution records (e.g. Drysdale et al., 2004; Dykoski et al., 2005; Cruz Jr. et al., 2006; Vollweiler et al., 2006) Additionally, the radiocarbon analysis found the way back into the speleothem community (Genty et al., 1998; Genty and Massault, 1999; Wang et al., 2001; Beck et al., 2001). Now ^{14}C measurements were not used for dating purposes anymore. Due to the fact that precise ages were determined by U-series dating, it is possible to use ^{14}C as a geochemical tracer in order to understand the processes occurring in the karst and soil above the cave.

The idea behind the thesis In this thesis radiocarbon in speleothem drip water and speleothem stalagmites is used as a tracer for soil processes occurring above caves. Paired carbon isotope values (^{14}C and δ^{13}C) are used to estimate the partial pressure of carbon dioxide (pCO_2) in the soil above the cave at the time of drip water collection and stalagmite

[1]The term **dead carbon** means that the material is completely depleted in its ^{14}C content.

growth. The basic idea is schematically described in the next paragraphs.

This PhD started on an assumption based on the paper of Hendy (1970), that it could be possible to derive the soil atmosphere pCO_2 above the cave by the content of the carbon isotopes in stalagmites. The soil pCO_2 is produced by decomposition of organic matter and by root respiration. Both processes are temperature and precipitation dependent (Dörr and Münnich, 1980, 1986; Cerling, 1984) and take place primarily in the uppermost half meter of the soil.

The basis is a graphic proposed in Hendy (1970), which is redrawn in Figure 1.1. Here the ^{14}C and $\delta^{13}C$ concentration of a saturated solution derived by an open dissolution system (the blue line connecting points A to B) and by a closed dissolution system (the blue line connecting points D and E) in dependence of pCO_2 is plotted[2]. The open limestone dissolution occurs if the solution is in contact with the soil atmosphere during the calcite is dissolved. In the closed system no contact to soil air is present during the limestone dissolution (see Sec. 3.3).

The isotopic composition of the saturated solution depends strongly on the initial pCO_2 value of the water. The initial pCO_2 value of the water in turn depends on the amount of soil CO_2. Hence especially in the closed dissolution system the large differences of ^{14}C in drip water provide an insight into the soil pCO_2 values.

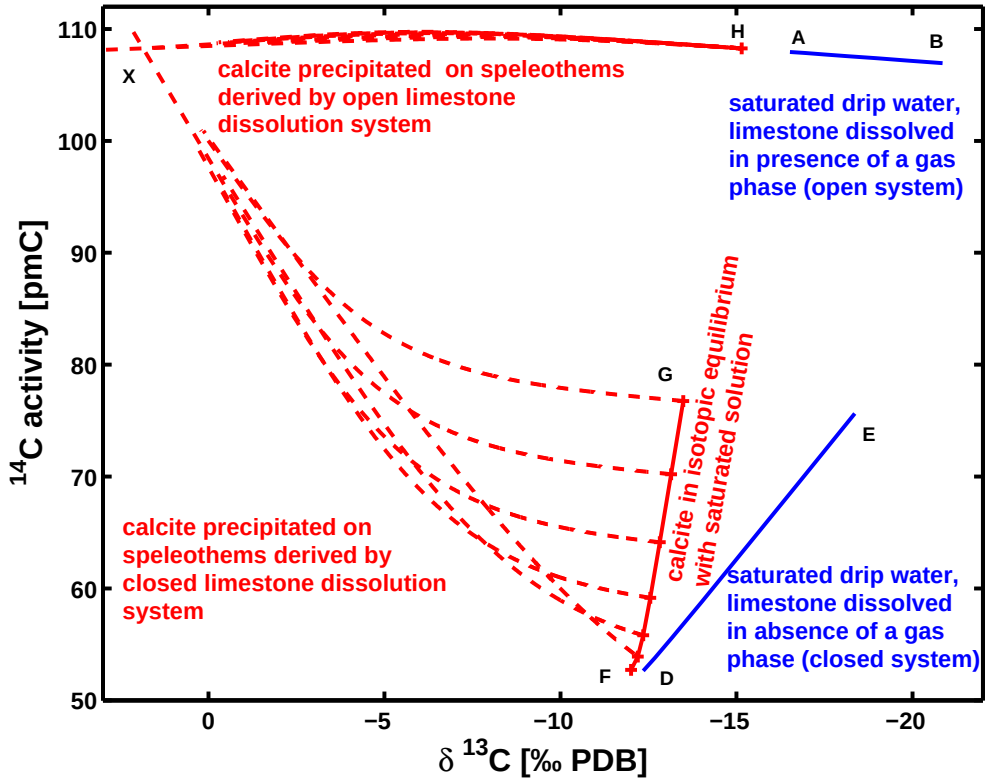

Figure 1.1: Relationship between ^{14}C and $\delta^{13}C$ content in cave environments, redrawn after Hendy (1970). The original plot initiated this thesis about carbon isotopes in speleothems. More details about this figure are given in the text (In Sections 5 and 6 the plot is explained in more detail.)

[2]The lower the $\delta^{13}C$ values, the more pCO_2 is available in the soil.

The carbon isotope dependence of pCO_2 is passed to the calcite derived by the saturated solution. The line connecting points F and G for the closed system and point H for the open system represent the isotopic composition of the first calcite precipitated from the solution. The start points of the single red dashed lines (point H for the open system and the red solid line between points F and G for the closed system) are also in dependence on the soil pCO_2 above the cave. The red dashed lines, drawn to the upper left (point X), show the carbon isotope development of a *Rayleigh Distillation* (Chap. 6) process with gas exchange. The development is derived from the same water as the isotopes in the first calcite to be precipitated. That again causes a dependence on the calcite isotopes from soil pCO_2. Therefore, it is possible for the closed dissolution system to derive the soil pCO_2 from paired carbon isotopes (^{14}C and δ^{13}C) recorded in a stalagmite. For the open dissolution system this is not possible, because different pCO_2 values results in the same isotopic composition of the calcite.

In general real limestone dissolution systems will behave somewhere between the completely open and the completely closed system. Hence, the new aspects supposed to investigate in the PhD was to model intermediate limestone dissolution systems, and perform an inverse approach to estimate the soil pCO_2 of carbon isotopes recorded in stalagmites.

Thesis outline The thesis consists of six chapters. The introduction contains general facts about stalagmites (Sec. 1.1), information about uranium series dating and explains how different proxies are used as climate indicators. Additionally some general facts about radiocarbon (Sec. 1.2) are given. In Chapter 2 is presented how calcite samples of stalagmites were prepared for radiocarbon AMS measurements. Chapter 3 describes the chemical and isotopic changes of a solution (concentrations of ions and carbon isotopes of the carbon dissolved in the solution) during the penetration from the upper soil layers through the karst region into the cave.

Two time approaches were chosen for the ^{14}C analysis: the present-day situation (Chapters 4 and 5) and the late the Holocene (Chap. 6). The present day situation includes the investigation of annual cycles of cave drip water (Chap. 5) as well as the last 100 years of a stalagmite top (Chap. 4). Two Holocene stalagmites were analysed for the second approach.

The annual cycle of ^{14}C in drip water mirrors the processes in the soil above the cave. The measurements reveal a pronounced signal. Additionally the investigation of the present-day situation is supported by the measurements of the ^{14}C content of the calcite deposited in the last century on stalagmite ER-77. With this dataset the ages of a simple model of the soil reservoirs are estimated by using the approach of Genty and Massault (1999) and the recent soil air ^{14}C content is calculated. The Holocene time slices then give the possibility to apply the knowledge on stalagmites grown over several thousand of years.

Furthermore a drip water model (Chap. 5) is developed, which calculates the concentrations of carbon species during limestone dissolution and the ^{14}C and δ^{13}C isotopic composition of the solution. The model is tested by comparing the calculated carbon isotopes with the measurements. Two Holocene stalagmites are analysed on their ^{14}C content (Sec. 6.1). By applying a Rayleigh distillation process, described in Chapter 6, it is possible to determine the pCO_2 of the soil above the cave (Sec. 6.3) from paired ^{14}C and δ^{13}C values recorded in a stalagmite.

The last chapter (Chap. 7) gives a short summary of this work and an outlook about the potential of radiocarbon in speleothems in possible following studies.

1.1 Stalagmites as climate archives

For a better understanding of the present climate, for more exact forecasts of the future climate many people work in the field of geosciences to investigate the climate system in more detail. They gain more insights to processes, which occur in the climate system, build climate models for the earth system and test these models on present and past climate conditions. Only models, which reproduce the climate of the past and of the recent situation in reasonable patterns, are credible for modelling the future climate.

The present day climate is very well known and the model output can be easily compared to the measured data. For climate variables in the present day climate a worldwide network exist. However, for the past things looks different. The further one tries to look back, the sparser the data of the past climate become. To win a more complete view on past climate it is important to get more knowledge by investigation of climate archives.

Stalagmites are excellent climate archives. They are a relatively young tool for past climate interpretation and thus relatively unexplored compared to other climate archives like ice cores or deep-sea cores. Stalagmites offer huge advantages in time controlling by layer counting or the use of the accurate uranium-thorium clock. Other attractive reasons are that stalagmites can grow continuously for 1000 to 100000 years and that they show only little secondary alternations in general (Fairchild et al., 2006). Furthermore, they capture the caves response to the external environment, especially temperature and infiltration of precipitation into the soil. It is important to note, that the cave temperature is equivalent to the mean annual external temperature and drip water discharge reflects the amount of precipitation infiltration into the soil, albeit winter precipitation is most important.

Several elements and isotopes can be measured and give information on past climate conditions and about several properties of the cave system. For the time control of a stalagmite the uranium-thorium-dating is a powerful tool. After the age model is built, it is interesting to look for trace elements like magnesium, strontium and for stable oxygen and carbon isotopes (δ^{18}O and δ^{13}C [3]). In the case of this doctoral thesis it is especially interesting to investigate the unstable carbon isotope ^{14}C implemented in stalagmites.

The following subsections give a short overview about the investigation of elements and isotopes mentioned above.

1.1.1 ^{230}Th/U-dating of speleothems

The timing of climate changes is of prime interest for palaeoclimatology. Thus the dating is a key aspect of climate reconstruction and precise dating is necessary for stalagmites as well.

Carbonates of speleothems can be accurately and precisely dated using U-series disequilibrium methods (Scholz and Hoffmann, 2008). Uranium-thorium dating is based on the radioactive decay of radionuclides within the naturally occurring decay chains. There are three decay chains starting with ^{238}U, ^{235}U and ^{232}Th, respectively. The starting nuclide has the longest half life (4.47×10^9yr, 7.04×10^8yr and 1.41×10^{10}yr), which determines the equilibrium condition of the short living species arising by alpha and beta decay. In an undisturbed system all daughter nuclides reach a state of equilibrium with the parent nuclide after a few million years. Ultimately the chains end with a stable isotope of lead. Natural processes that separate the nuclides within a decay chain result in a disequilibrium between

[3] The delta notation for isotope samples (R=^{13}C/^{12}C, R=^{18}O/^{16}O) gives the normalised deviation to a standard ($\delta R = (R_{sample} - R_{standard})/R_{standard} \cdot 1000$ ‰).

the activity of the parent and the daughter isotope. The return to equilibrium then allows quantification of time and, thus, dating of the timing of separation (Bourdon et al., 2003).

The natural process of uranium and thorium separation in the cave is the dissolution of limestone above the cave. With the dissolution of calcite some minor and trace elements (i.e. Mg, K, Na, F, Cl, Br, and also U) are washed out of the host rock. The concentration of these trace elements in the drip water mainly depends on their concentration in the host rock and the corresponding partitioning coefficient. The elements in the water are then coprecipitated with speleothem $CaCO_3$ (Scholz and Hoffmann, 2008). Because thorium is (nearly) insoluble in natural waters no initial thorium is in the stalagmite. So the uranium-thorium clock is set to zero.

By measuring the ratios of $^{234}U/^{238}U$ and $^{230}Th/^{238}U$ one can calculate the time of the last complete isolation of uranium from thorium atoms. In the case of a cave the separation of both elements is the dissolution in the karst and the growth of the stalagmite. A crucial assumption is that the initial thorium content is zero and that the uranium incorporated in the calcite is not disturbed afterwards.

With those ages measured at different depths of the stalagmite a more[4] or less[5] sophisticated age model can be constructed. It is crucial to build a good age model because the exact determination of the timing and duration of specific events of course depend on the method used to calculate the age model. Then one can apply the age model on measured isotopes, trace elements or radiocarbon data.

1.1.2 Stable isotopes

Stable oxygen and carbon isotopes stored in speleothems are key indicators for past climate conditions. In each cave the question arises of how to interpret the $\delta^{18}O$ and $\delta^{13}C$ records. Interpretation of the stable isotopes can not be the same in all locations, because the soil above the cave and the climatic zone in which the cave is situated react differently on precipitation and temperature and alternate the isotope signal in different ways. The main source of oxygen is water. Minor oxygen sources are the CO_2 of soil air and $CaCO_3$ of the limestone dissolved in the water. The carbon originates mainly from soil respiration and from limestone dissolution. Through the mix of the different sources an isotopic signal is stored in the speleothem. Additionally one has to consider fractionation effects on $\delta^{13}C$ and $\delta^{18}O$. Much effort has been spent to determine the isotope fractionation factors (Deines et al., 1974; Friedman and O'Neil, 1977; Romanek et al., 1992; Kim and O'Neil, 1997; Mook and de Vries, 2000). The fractionation factors relate the oxygen isotopic composition of water and the carbon isotopic composition of dissolved inorganic carbon species to the $\delta^{18}O$ and $\delta^{13}C$ composition of $CaCO_3$ (Fairchild et al., 2006, and citations herein).

With prior calcite precipitation and kinetic fractionation the isotope signal becomes much more complicated. Prior calcite precipitation occurs in the karst above the cave before the drip water enters the cave. Here the solution gets heavier in oxygen and carbon isotopes. The process can lead to a correlation between $\delta^{13}C$ and Mg/Ca content (Verheyden et al., 2000; Fairchild et al., 2006). In addition, kinetic fractionation enlarges the parts of heavy isotopes in the calcite of the stalagmite and is caused by disequilibrium processes occurring in relation to degassing and evaporation on the speleothem surface. The kinetic fractionation is associated with Rayleigh fractionation processes (e.g. Hendy, 1971).

[4] E.g. some Bayesian approaches like Heegaard et al. (2005).
[5] E.g. linear interpolation or splines of data points.

Due to the huge amount of oxygen in the precipitation compared to that injected by CO_2 (mainly in the soil air) or calcite equilibration (during limestone dissolution) the $\delta^{18}O$ signal can be seen as a mixed temperature and precipitation signal. In special cases it is possible that the $\delta^{18}O$ signal can be attributed to a pure temperature or a pure precipitation signal. So e.g. Wang et al. (2001, 2005) interpret the oxygen record of a stalagmite from the Chinese Hulu and Dongge caves in terms of the strength of the East Asian monsoon. Even the amount of precipitation falling between Dongge and Heshang cave (China) can be derived by the difference in the $\delta^{18}O$ signal of stalagmites of both caves (Hu et al., 2008). On the other hand the $\delta^{18}O$ signal is interpreted as a pure temperature signal in the Austrian Spannagel cave by Mangini et al. (2005), who have even derived absolute temperatures.

The interpretation of the stable carbon isotope is much more difficult, because for that isotope not only temperature and precipitation are responsible for the $\delta^{13}C$ composition but also vegetation density and composition as well as the way of limestone dissolution. Because the carbon isotope interpretation is a very sophisticated matter a whole chapter (Chap. 3), is devoted on this topic in this thesis. Up to now there are no approaches to relate temperature or precipitation to the $\delta^{13}C$ signal of stalagmites. On the other hand there are some studies showing a clear relationship between the C3/C4 vegetation composition of the vegetation above the cave and the carbon isotope composition of the speleothem (Dorale et al., 1992, 1998; Denniston et al., 2000). In other cases, the vegetation amount has been hypothesized to control the speleothem $\delta^{13}C$ composition. For example one can take the heavy values of a New Zealand stalagmite from the late glacial (Hellstrom et al., 1998) or the observations of modern heavy values due to deforestation (Zhang et al., 2004).

1.1.3 Trace elements

The two most important ion sources in karst waters are calcite ($CaCO_3$) and dolomite ($CaMg(CO_3)_2$). So calcium and magnesium can be seen as major elements. Mg/Ca ratios in drip water are usually less than one (Morse and Arvidson, 2002) due to the fact that dolomite dissolves much more slowly than calcite. Elements, which are incorporated in the stalagmite more rarely than magnesium, are called trace elements. Examples are potassium, sodium, fluorine and chlorine. The amount of the trace elements depends on their occurrence in the karst system.

Like calcium and magnesium trace elements are dissolved by water charged with carbonic acid, and are incorporated in the stalagmite in the same manner as the major elements (Ca and Ma). The interpretation of trace elements is difficult and can vary between several caves.

Significant fluctuations of trace elements occur on an annual scale. So there is potential for unravelling cause and effect (Fairchild et al., 2006). There exist three basic idealized interpretative annual patterns, which are relevant to the transmission of climatic signals.

The fluid-dominated-pattern occurs by distinctive changes in fluid composition, where the equivalent signal is recorded in the speleothem. The second is termed crystal-dominated-pattern. That means some trace elements like P, Na, K and F show sinusoidal variations within annual laminae. The variations often display a broad peak antipathetic to the element Sr. Treble et al. (2003) described annual variations in U, Na, Sr and Ba and interpreted them in terms of a changing growth rate. The third phenomenon is the temperature-controlled-pattern. This pattern is the expected situation where significant temperature changes occur during the year. Since the Mg partition coefficient and those of other elements are temperature dependent, annual cycles of trace elements are likely in caves with temperature differences during summer and winter. One example is given by Roberts et al. (1998) who studied a

stalagmite of the Tartair cave in Scotland. Of course all three patterns can play a role by building annual variations of trace elements in stalagmites and can mask each other.

Further effects influencing the signal of trace elements occur by prior calcite precipitation. As mentioned in Section 1.1.2 the precipitation takes place in the limestone above the cave. The effect leads to increasing Mg/Ca and Sr/Ca ratios in cave waters. An example of increasing ratios due to prior calcite precipitation is given in Tooth and Fairchild (2003). The process occurs especially in dry weather periods.

1.2 Radiocarbon - ^{14}C

In Section 3.2 is described in detail how the radiocarbon behaves in stalagmites, in the soil and in the karst above the cave. For introductory purposes this section discusses about ^{14}C in the atmosphere and the effects which affect the atmospheric radiocarbon content.

There exist three carbon isotopes. The main isotopes are ^{12}C and ^{13}C with a relative occurrence in the atmosphere of 98.89 % and 1.11 %. Both isotopes are stable in contrast to the radioactive ^{14}C (radiocarbon), whose relative occurrence in the atmosphere is about 10^{-10} %.

Production and decay The overall ^{14}C equilibrium is maintained by production and decay of ^{14}C. Radiocarbon is produced by thermal neutrons (n), originating from spallation products of cosmic rays, reacting with ^{14}N under an emerging proton (p)

$$^{14}N + n \Rightarrow ^{14}C + p. \tag{1.1}$$

The production occurs mainly at an altitude of 12 km (Aitken, 1961) at the border between the troposphere and the stratosphere, where the folded intensity of nitrogen and neutrons is at maximum. Then the ^{14}C atom is oxidised to $^{14}CO_2$ and distributed to the whole troposphere within a short period compared to the 8033 year lifetime and to the lifetime in the atmosphere (Anderson and Libby, 1951). From the well-mixed atmosphere the carbon enters the earth's plant and animal life ways through photosynthesis and the food chain. In the worldwide mean, the probability for a ^{14}C atom to get dissolved in the ocean, is a multiple higher than to get assimilated by the vegetation (Münnich, 1963). Around 96 % of the whole carbon, which is thought to be able to exchange with atmospheric carbon dioxide[6], is dissolved as bicarbonate in the sea water. In the atmosphere and in the biosphere only 4 % of the exchangeable carbon are located. In consequence most of the ^{14}C atoms decay in the ocean (Münnich, 1963). Decaying ^{14}C atoms dissolved as carbonates in in ocean surface water were replaced within short time scales, because the ocean is in equilibrium with the atmosphere. On the other hand, the ^{14}C which decays in dead organic matter can be used to date.

Once living matter died, the ^{14}C decay overbalances carbon exchange processes with atmospheric CO_2 and the radiocarbon content decreases exponentially. The decay of radiocarbon results in a ^{14}N atom again and emits a beta particle (electron) with a maximum energy of 160 keV.

$$^{14}C \Rightarrow ^{14}N + \beta^{-}(160\,keV) \tag{1.2}$$

The decay of^{14}C follows an exponential law

$$R(t) = R(0) \cdot exp(-t/\tau) \tag{1.3}$$

[6]Limestone, for example, remains out of consideration.

with R = $^{14}C/^{12}C$ being the carbon isotope ratio at different times and $\tau = t_{1/2}/\ln 2$ being the lifetime. The half life $t_{1/2}$ of ^{14}C was determined by Willard F. Libby to 5568 ± 30 years (Libby et al., 1949). Later measurements, performed in Cambridge showed that the Libby half life was to small, they gave a more accurate and 3 % higher half life of 5730 ± 30 years (Godwin, 1962). Therefore, an age using the Libby half life has to be multiplied by 1.03 to convert to an age with respect to the so called Cambridge half life. Nevertheless, the Libby half life is usually still used in calculations in order to maintain consistency. After ten half-lives only a very small amount of radioactive carbon is left in a sample (the $1/2^{10}$ part of the initial value) and, thus, the limit of the ^{14}C dating technique is reached after 50000 - 60000 years.

Furthermore, the use of Libbys half life requires the assumption of a constant production rate. However, the production rate changed in the past, and hence the atmospheric ^{14}C concentration varied significantly. Nevertheless it is appropriate to use the Libby half life, because the variances of the ^{14}C level of the atmosphere get balanced by the use of the calibration curve (Reimer et al., 2004), which was as well calculated with the 3 % too low half life.

In this work the half life measured by Libby is used to be consistent with the community. So radiocarbon ages were calculated by

$$t = -8033 \cdot ln\left(\frac{R(t)}{R(0)}\right), \tag{1.4}$$

where $R(t)/R(0) \cdot 100$ is the ^{14}C activity of the sample ($a^{14}C$) in **p**ercent **m**odern **c**arbon (**pmC**). The time t refers to years before 1950 (according to the convention proposed by Stuiver and Polach (1977)). In this context the acronym BP stands for *before present*, which in fact means before 1950. If not mentioned otherwise the errors for ^{14}C measurements are given as the 1σ standard deviation.

Reservoir effects and human influence An important feature in radiocarbon age determination can be the reservoir effect. Due to this effect the sample seems to be older in its ^{14}C age than it really is, which generally happens if radiocarbon samples obtain their carbon not only from the atmosphere. One of the most commonly referenced reservoir effects concerns the ocean. Here the well mixed upper ocean layer exchanges the carbon (dissolved in water as $CO_{2(aq)}$, HCO_3^- and CO_3^{2-}) with the atmospheric CO_2. But additionally the upper ocean layer gets carbon from upwelling oceanic ^{14}C-depleted bottom water as well and the surface water seems to be older in the radiocarbon content than the atmosphere. A correction for the apparent age anomaly is possible when the reservoir-atmosphere offset in specific ^{14}C activity is known (Hughen et al., 2004). The offset (e.g. between ^{14}C age of marine sample and ^{14}C age of atmospheric sample) is expressed as a reservoir ^{14}C age, which is not necessarily constant in time (Stuiver and Braziunas, 1993).

Another reservoir effect is the *hard water effect*, which takes place in lakes and in ground water (e.g. Deevey et al., 1954; Münnich, 1957; Geyh, 2000; Olsson, 1979). Precipitation charged with carbon dioxide gas and the ^{14}C activity of the atmosphere dissolve calcium carbonate ($CaCO_3$) when the meteoric water comes into contact with limestone. Usually the limestone is a source of ^{14}C free carbon and shifts the ^{14}C activity of the water towards an apparently older age. In Section 3.2 the ^{14}C alternations of carbon dissolved in water within the soil and limestone zone will be described in more detail.

Since the beginning of the industrial revolution and more clearly since the 1890's the ^{14}C content of the atmosphere shows a decreasing trend. That effect is called *Suess-effect* (Suess,

1955). The predominant use of material of infinite geological age as industrial fuels (e.g. coal and petroleum, which are sources of ^{14}C free carbon dioxide), has lowered the radiocarbon activity of the atmosphere in the early part of the 20th century up until the 1950's.

An inverse effect, which increased the radiocarbon content of the atmosphere, were the extended test series of atomic weapons in the late 1950's to the mid 1960's. The effect was described first by de Vries (1958). This *bomb* ^{14}C is produced because nuclear bombs set free a huge number of thermal neutrons responsible for production of ^{14}C. So the ^{14}C concentration of the atmosphere almost doubled from 1950 to the year 1963 when in the northern hemisphere the maximum of atmospheric radiocarbon content due to nuclear bombs was reached. Since that time the amount has declined owing to exchange and dispersal of ^{14}C into the Earth's carbon cycle system and the *Suess-effect*. The presence of bomb carbon in the earth's biosphere has enabled radiocarbon studies to use ^{14}C as a tracer to investigate the mechanisms of carbon mixing and exchange processes.

Chapter 2

Sample preparation for radiocarbon measurements

Developments in the 1970s in **a**ccelerator **m**ass **s**pectroscopy (**AMS**) (Muller, 1977; Bennet et al., 1977; Nelson et al., 1977) opened a wide field of applications for radiocarbon measurements in recent years. For ^{14}C measurements of cave sinter it is a big advantage to use an AMS system, because the analysis requires less carbon compared to gas proportional counting. The slowly growing stalagmites offer only low amounts of calcite deposited within one year. Hence, it would be a big drawback to analyse large amounts of calcium carbonate, as needed for the conventional dating technique, by measure the mean ^{14}C activity of deposited calcite grown within several decades. But the low mass requirements for AMS need a careful handling of the samples during the preparation process. The danger of contamination is higher than for larger mass samples. A sophisticated procedure of sample preparation was developed over the years of radiocarbon analysis in order to eliminate all factors, which could be responsible for sample pollution.

This chapter describes the sample preparation procedure for AMS measurements focussing on the extraction of CO_2 and reduction to carbon atoms from inorganic carbon compounds (Sec. 2.1). Mainly the preparation steps given by the PhD thesis of Unkel (2006) were followed and improved with an additional heating step. The improvement, arisen under the comparison of the background sample measurements, is clearly visible in the results of background measurements (Sec. 2.2). The last part of this chapter presents the results of measured standard samples (Sec. 2.3).

2.1 Sample preparation

For measuring ^{14}C using the AMS technology solid carbon mixed with iron powder is required. The individual steps of the complete sample preparation from calcium carbonate of stalagmites to the carbon–iron mixture are sketched in the Figure 2.1. The flow chart includes all the working steps until the sample is pressed in an AMS cathode and is ready to be sent to an AMS facility. The measurements were done by external laboratories.

Drilling Calcite powder is obtained by using an dental drill under a glove box. The air in the glove box is CO_2 free, due CO_2 being absorbed in a NaOH base before entering the box. The CO_2 free atmosphere is considered to avoid carbon exchange during the drilling process and to keep the background as small as possible. At minimum 8 mg of calcite for each sample

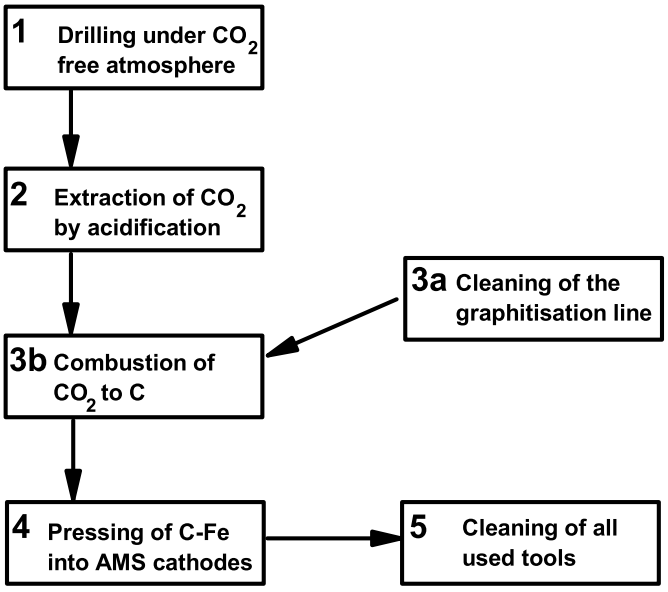

Figure 2.1: Flow chart of the work steps which are involved from the untreated stalagmite or drip water until the sample is ready for ^{14}C measurement. For drip water drilling is not necessary, of course.

were collected. That is enough for 1 mg of carbon, which is the necessary amount for AMS radiocarbon measurements.

Extraction The second step is the acidification of the calcite powder. From here the drip water undergoes the same treatment as the calcite to extract carbon dioxide from dissolved inorganic carbon in the water and to reduce it in the next step to pure carbon. The extraction line is built according to Dörr and Münnich (1980). The current system is described in the PhD thesis of Unkel (2006) in detail.

The acidification occurs under vacuum of around 10^{-2} mbar. First only the connecting passages, freezing finger and water trap are pumped. That means everything is evacuated except the sample space. In order to minimize the background of the ^{14}C measurements it is necessary to get rid of most of the water molecules sitting on the glass walls of the whole extraction line. In the water film carbon with atmospheric isotope composition is dissolved and tend to increase the ^{14}C content of a sample artificially. A heat gun heats up most of the glass materials to 350°C except those sections where an O-ring connects the different parts of the line. The heating lowers the water vapour pressure. Thus, the water evaporates and is pumped out of the line. It is satisfactory to heat the system (especially the water trap) for around five minutes under ongoing pumping. After this time no increase of the pressure in the extraction line is observed. Even a second heating step (two hours and roughly one day were applied under continuous pumping) after a sufficient cooling does not increase the water pressure notably over the basic pressure level of 10^{-2} mbar.

After the vacuum is established the sample and the acid are added to the line, which is then pumped again. Now the water trap is cooled by dry ice (frozen carbon dioxide with

a freezing temperature of -78°C) to freeze the water escaping from the acid (and the water sample) to avoid damage to the pump. Again a vacuum of around 10^{-2} mbar is established before the acid (e.g. HCl) is given upon the calcite or into the water and the resulting chemical reaction produces CO_2[1,2].

With the freed CO_2 molecules also some water vapour and other chemical bonds arise. To extract the pure CO_2, the molecules with a freezing point above -78°C, especially water vapour, are frozen out by the water trap, which is still cooled with dry ice.

To be as efficient as possible a part of the produced gas mixture is expanded from the reaction chamber to the volume of the water trap and stored there for some minutes. Then the next volume to the CO_2 freezing container is opened. There the CO_2 is frozen by cooling the container with liquid nitrogen (-196°C). The container is closed and remaining gas that is still present in the line after the CO_2 freezing is pumped out, because it is no CO_2 and extends the freezing time in the next step.

Then the next part of the CO_2-water vapour-mixture is expanded from the reaction chamber into the water trap and the steps described above are executed again. Then, this process is repeated several times until all CO_2 is frozen.

Reduction The CO_2 is then reduced to solid carbon. The Heidelberg graphitisation line, used here, is described in detail in the thesis of Unkel (2006). For the graphitisation step (reduction of carbon dioxide into carbon) in 5 mg of iron powder, which is placed in the heating finger of the reaction chamber, are prepared. The iron is used as a catalyst, where the carbon is supposed to precipitate. After evacuation of the whole system to lower than $4{\cdot}10^{-6}$ mbar the CO_2 is forced to freeze down in the freezing finger of the reaction chamber (cooled with liquid nitrogen). For 1 mg of carbon it is necessary to achieve a pressure of carbon dioxide of around 250 mbar in the reaction chamber. After freezing the 250 mbar again, an appropriate amount of hydrogen is filled into the reaction chamber. At 575°C in the heating chamber and -78°C in the freezing finger (a dewar filled with dry ice) the chemical reaction[3] starts to convert the CO_2 to pure carbon. The carbon precipitates on the iron and the dry ice freezes the generated water vapour. So the equilibrium of the reaction is on the product side and all CO_2 converts to solid carbon. For more details of the graphitisation step as well as about the prior cleaning procedure see Goslar and Czernik (2000) or the dissertation of Unkel (2006).

Pressing Now the carbon–iron mixture is pressed into AMS cathodes. The targets were then measured at the AMS facilities of Lund or Zurich.

Cleaning The last step in the process of sample preparation is the cleaning of all tools as the drill, tweezers, spatula or glass tubes. The different cleaning steps are washing with distilled water in an ultrasonic bath and washing with acetone afterwards. This procedure is also applied for the pressing devices. The glass tubes of the graphitisation line are heated to 900°C after mechanical cleaning with distilled water to get rid of all organic or inorganic carbon. For tweezers and spatula a cleaning with acetone is applied.

[1] For calcite: $CaCO_3 + 2HCl \rightarrow H_2O + CaCl_2 + CO_2$

[2] For dissolved inorganic carbon in water (consisting mainly of HCO_3^- and Ca^{2+} ions): $Ca^{2+} + 2HCO_3^- + 2HCl \rightarrow 2H_2O + CaCl_2 + 2CO_2$

[3] $CO_2 + 2\,H_2 \xrightleftharpoons{\text{iron catalyst}} 2\,H_2O + C$. Hence, the reaction needs an at least two times higher hydrogen pressure than the CO_2 gas.

2.2 Background

For ^{14}C dating it is necessary to measure the background to estimate sample radiocarbon ages and uncertainties. A background measurement shows the amount of modern carbon, which is introduced into the sample during the sample preparation, and the performance of the AMS system. A background analysis requires the preparation of a material, which is known to have an unlimited age (^{14}C activity = 0 pmC) and can be prepared for measurements similar to the samples. At the height of the background samples one can see how clean, with as less as possible recent carbon injection, the sample preparation is. In the case of calcite and water marble is a suitable background material. Usually marble is called "geologically old", which means in the case of radiocarbon that it is much older than the limit of ^{14}C measurements. Currently the measuring limit of unprocessed graphite, the best background available, is around until 60000 to 70000 years or 10 to 12 half lives (e.g. Scharf et al., 2007; Klein et al., 2007).

In AMS samples are usually measured in batches of 20 to 40 targets including several background and standard samples. The results of all measured background samples are listed in Table A.1 of Appendix A and plotted in Figure 2.2.

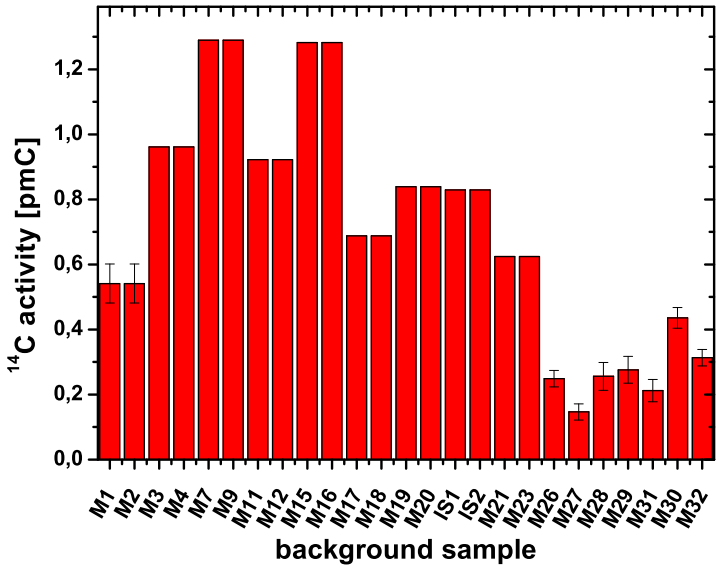

Figure 2.2: ^{14}C activity of marble (M1–M32) and Iceland spar (IS1,IS2) background samples. The lowest background is measured since sample M26, which goes conform with changing the AMS system (from Lund to Zurich facility). For some backgrounds no errors were given by the AMS facility.

During this thesis 34 background samples were prepared of which 25 were measured. Some of the background samples were used as "dummies", that means they were taken as samples to tune the AMS machine. The Lund facility used usually two background samples for the tuning while in the Zurich facility they tune their AMS machine with oxalic acid standard samples. In general marble is used for background determination, except the two Island spar calcite

background samples. These were drilled in Innsbruck in context of subsample micromilling of stalagmite ER-77 (Sec. 4). Thus the calcite samples (subsamples of ER77 and Island spar background) were the ones which were not drilled in a CO_2 free atmosphere, due to the use of an external laboratory and the sophisticated micromill construction there.

Until background sample M16 the heat gun was not used in the preparation of the extraction step, which explains the higher background of those samples. With the application of the heating step (from background sample M17 on) the background activities were reduced. As long as the samples were sent to the Lund AMS facility the background samples were hardly older than 40000 years. That is due to the fact that the system in Lund has a rather high chemical blank background of 48000 years or 0.25 pmC, and the background of processed anthracite is in the order of 44000 years or 0.4 pmC (Skog, 2007). The system is designed to measure ^{14}C as part of biomedical and environmental studies, where the ^{14}C activities are relatively high. The limit of the measured background samples is lower in Zurich (Fig. 2.2 from sample M26 on).

However, the height of the background is not relevant, as far as the activity is correctly subtracted from the unknown samples. Furthermore for this thesis only unknown samples of the Holocene and of modern composition were prepared and measured, which is far away from the background border.

The Lund single stage AMS system is the first AMS system based on a single stage and open-air insulated accelerator. The advantage of a single stage accelerator is that extra charge exchanges in the residual gas of the second acceleration step, which may result in molecular fragments with momentum equal to the rare isotope, are avoided. In Zurich a small 0.5 MV tandem accelerator was used to measure the samples. In both laboratories, Lund and Zurich, the AMS systems use the 1+ charge state, which can provide high precision radiocarbon measurements similar to the larger tandems that utilize the 3+ or 4+ charge states (Synal et al., 2000).

2.3 Standard

All ^{14}C (AMS-) measurements of unknown samples are measured relative to a standard. In the Heidelberg radiocarbon laboratory the oxalic acid II standard is used. The mean value of that standard is 1.2736 ± 0.001 times higher (Stuiver and Polach, 1977; Mann, 1983) than the first standard, oxalic acid I, which is not in use anymore. However, the oxalic acid I is still the international radiocarbon dating standard. Ninety-five percent of the activity of oxalic acid I from the year 1950 is equal to the measured activity of the absolute radiocarbon standard which is wood from the year 1890 and is defined to have 100 pmC. So the mean value of oxalic acid II is $100\,\mathrm{pmC} \cdot \frac{100\%}{95\%} \cdot 1.2736 \approx 134.04\,\mathrm{pmC}$.

All oxalic acid samples are listed in Table A.2 of Appendix A. The mean of all measured standards is 134.06 pmC with standard deviation of 0.5 pmC. So the mean agrees well with the expected value and the standard deviation is identical to statistical errors of single measurements.

Because measurements of unknown samples are made in relation to standards, many systematic errors cancel. Variations in the systematic errors contribute primarily to the final uncertainty (Finkel and Suter, 1993).

Chapter 3

^{14}C in cave systems

To evaluate radiocarbon measurements of stalagmites and drip water and to interpret variations in their ^{14}C content, it is necessary to understand the processes in soil-cave systems, which are responsible for the composition of the ^{14}C isotopes. Nevertheless, both carbon isotopes, ^{14}C and ^{13}C, are important to infer processes from which the variations originate.

To be able to interpret the carbon isotopes data in speleothem environment one has to follow the way of the water from the atmosphere through the soil and karst system to the cave and to understand processes occurring there. Before the water enters the cave, the ^{14}C content of the dissolved inorganic carbon changes in each region above the cave according to the radiocarbon composition of the carbon contributing matter. Small changes of the ^{14}C content of the carbon in the water occur in the soil due to fractionation and soil CO_2 enrichment. Large differences on the resulting ^{14}C in the drip water are depending on the way the calcium in the karst is dissolved. Finally, small changes occur in the cave on the stalagmite via fractionation effects.

In this chapter the way of the water from the atmosphere to the cave is explained (Sec. 3.1) and how the radiocarbon content of the drip water is changed in different stages of the penetration areas (Sec. 3.2). In Section 3.3 the different limestone dissolution behaviours are described, before the last part of this chapter (Sec. 3.4) gives an overview over the concept of the dead carbon fraction.

3.1 How stalagmites grow

A schematic view about how stalagmites grow is shown in Figure 3.1. The water, which finally will enter the cave, originates from the precipitation above the cave. During the contact with atmospheric carbon molecules the precipitation is in balance with the atmospheric CO_2 content. The pH-value of water in contact with 380 ppm of CO_2 (the pCO_2-value of the present atmosphere) is around 5.56. The balance could be described according to chemical Equation 3.1

$$CO_{2,g} + H_2O \leftrightharpoons H_2CO_3 \leftrightharpoons H^+ + HCO_3^- \leftrightharpoons 2H^+ + CO_3^{2-} \tag{3.1}$$

(see also Equations 5.1 – 5.4 in Sec. 5.2) and the temperature dependent equilibrium constants listed in Table 5.3 (Sec. 5.2).

Then the water enters the soil, where the partial pressure of CO_2 is enhanced due to root respiration and microbial induced oxidation of dead plant material. The partial pressure

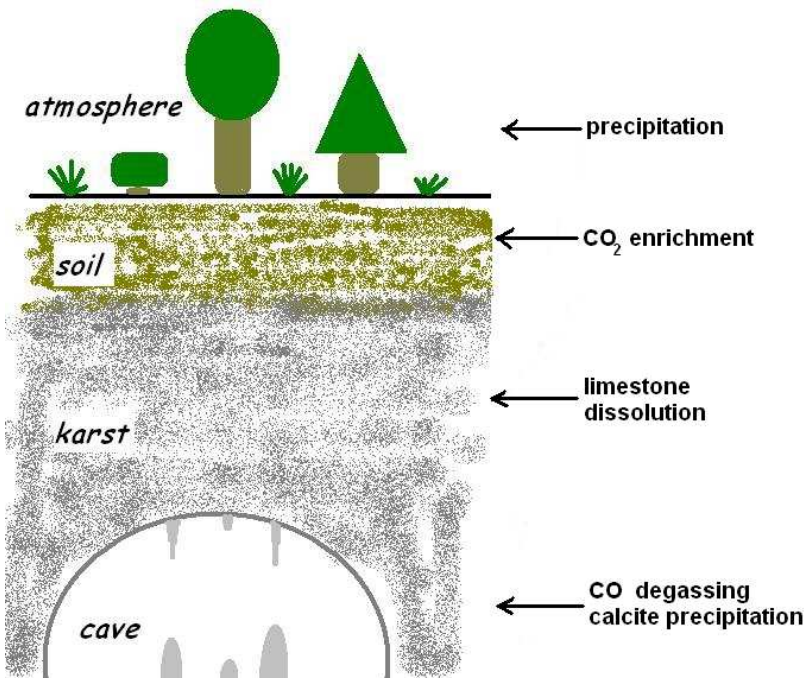

Figure 3.1: Schematic view on the growth of stalagmites. On the right hand side processes are indicated which are important for the growth of stalagmites. For more details see the text.

of CO_2 in the soil atmosphere ($CO_{2(g)}$) could be up to one hundred times of that in the bulk atmosphere. Therefore the chemical equilibrium changes and the soil water become more enriched in carbonic acid ($CO_{2(aq)} = H_2CO_3$), bicarbonate (HCO_3^-) and carbonate (CO_3^{2-}). For example: a solution in contact with a CO_2 partial pressure of one percent of the atmosphere ($pCO_2 = 1$ % atm = 10,000 ppm) has a pH-value of around 4.88, a concentration of carbonic acid of $5*10^{-4}$ mol/l and a concentration of bicarbonate ions of $1.3*10^{-5}$ mol/l. The amount of the carbonate ion concentration is negligible in this situation.

This happens under idealised conditions. In general the soil contains also minor and trace elements like magnesium, calcium, potassium, barium, sulphates and many others. These elements influence the calcite solubility of the solution. Due to generally low concentrations of minor and trace elements in the solution, which dissolve the limestone, they can be neglected in this work. Dreybrodt (1988), e.g., tried to include those minor and major elements, but the model procedure requires the known amount of each additional minor and trace element or molecule.

After the acidic solution leaves the upper soil it comes into contact with the limestone. This leads to the dissolution of calcium carbonate according to chemical Equation 3.2:

$$Ca^{2+} + 2HCO_3^- \leftrightharpoons CaCO_3 + H_2O + CO_2 \tag{3.2}$$

where Ca^{2+} is the calcium ion (see also Equations 5.1 – 5.5).

In two main processes the way of limestone dissolution can be distinguished: first the closed system, where the solution has no contact with the soil atmosphere and second the open system where the water stays always in contact with the soil atmosphere during the

process of limestone dissolution. In general these extreme cases occur very rarely and instead intermediate processes are common.

The solubility of the calcium carbonate depends on the partial pressure of soil CO_2 as Garrels and Christ (1965) and Hendy (1971) have already shown. If the solution is saturated no further chemical changes are supposed to occur. However, the karst is not homogeneous. Therefore, it is possible that there are voids, in which air of lower pCO_2 is trapped. When the water comes into contact to those soil irregularities, reprecipitation of calcite happens. Thus, the concentrations of the carbon species in the solution changes according to the pCO_2 existing in these voids.

As soon as the water leaves the karst and enters a cave, calcite precipitates from the water and can form stalactites, stalagmites or flowstones. These processes could occur if the cave atmosphere has a sufficiently low pCO_2 value compared to the infiltrating water. This pCO_2 difference leads to degassing of CO_2 from the water to the atmosphere and, hence, results in precipitation of $CaCO_3$, which forms a stalagmite. Another possible process is the evaporation of the drip water. In the rare case of low humidity in the cave the water is able to evaporate, the solution becomes supersaturated and the calcite deposits. However this process is very unlikely because in most caves the air humidity is very high, due to the low flow of air and the relatively large flow of water through most limestone caves.

For more details, see Hendy (1971), Salomons and Mook (1986), Dreybrodt (1988) Dulinsky and Rozanski (1990) or Romanov et al. (2008a).

3.2 Changing ^{14}C in soil, karst and cave water

During those processes described in Section 3.1 the carbon isotope composition of the water changes. Reasons for the change are that the carbon joining the solution has different origins (atmospheric carbon dioxide, carbon coming from plants and introduced by dissolution of the limestone). Table 3.1 shows the values for δ^{13}C and ^{14}C in different materials with which the water is in contact.

Table 3.1: The current isotope composition of carbon in materials, which supply the water on its way to the cave with carbon atoms (Data are taken from † Deines (1980) and ‡ Hendy (1971)).

material	^{14}C [pmC]	δ^{13}C [‰ vs. PDB]
atmosphere	106 (today)	−8 (today)
C3 vegetation	≈106	$-26^{\dagger}$
C4 vegetation	≈106	$-13^{\dagger}$
soil air derived by		
C3 vegetation	>106	$\geq -26^{\dagger}$
C4 vegetation	>106	$\geq -13^{\dagger}$
limestone	$0^{\ddagger}$	$+1^{\ddagger}$

No major variations of the ^{14}C level of the carbon in living vegetation is observed so far. So the carbon uptake via photosynthesis from the atmosphere does not show significant changes, when the carbon is stored in the plant. Hence, the soil air derived by vegetation should have the same ^{14}C composition as the atmosphere. At least this is true, if the soil CO_2 is only composed of root respiration. If organic decomposition is also important the soil air ^{14}C is

different from the atmosphere. The composition of the total carbon pool in the soil is then a mixture of recent and past atmospheric radiocarbon levels. Due to the nuclear weapon tests in the mid of the 20th century and the resulting strong atmospheric ^{14}C anomaly, nowadays in most areas the soil air has a higher radiocarbon value than the recent atmospheric ^{14}C level. How strong the difference is, depends on the impact of the dead organic material. On the other hand *pre-bomb soil* has a slightly lower ^{14}C content compared to the corresponding atmospheric ^{14}C level.

In contrast to ^{14}C the vegetation has a considerable influence on the $\delta^{13}C$ content via photosynthesis. Hereby one has to differentiate between plants using the Calvin photosynthetic cycle (C3 plants) or the Hatch-Slack photosynthetic pathway (C4 plants). In both pathways isotopic fractionation occurs during the uptake of atmospheric CO_2. C3 plants are depleted at about 13 ‰ and C4 plants at about 4 ‰ compared to the atmosphere. The same $\delta^{13}C$ composition which is stored in the plant is respired by the roots into the soil. Because the atmospheric $\delta^{13}C$ content was almost constant in time, the soil $\delta^{13}C$ content in the soil is also constant.

Additionally there are temperature dependent fractionation constants, which can change the isotopic composition significantly. The temperature dependent carbon fractionation constants are given in Section 5.2 in Table 5.5.

Especially for ^{14}C the changes of carbon in the solution follows a certain scheme (e.g. Genty and Massault, 1999). The dissolved carbon in the meteoric water has a ^{14}C value similar to the atmosphere, neglecting fractionation effects. The ^{14}C content of the soil atmosphere is in general lower than the radiocarbon content of the atmosphere[1], because of the dead carbon derived from old soil organic matter. When the water becomes enriched with carbon from the soil atmosphere the ^{14}C content in the water is decreasing. How much it decreases depends on how old the dead plants in the soil are and to which extent they give CO_2 to the soil atmosphere compared to the plant root respiration of living plants. It should be mentioned, that the ^{14}C content of dead organic material represents in general the ^{14}C activity of the atmosphere during the lifetime of the plants. The decay of ^{14}C has a negligible impact on the common time scales of plant decomposition. The fractionation from soil CO_2 to the dissolved inorganic carbon has the effect of enriching the radiocarbon content. An average enrichment of 2.6 pmC for a case study of some locations is given in Genty and Massault (1997). When the solution dissolves the limestone, which is completely depleted in radiocarbon, the ^{14}C activity declines up to 50 % of the value the water had before the limestone dissolution (for further explanations see Chapter 3.3). On the last step of speleothem formation the water saturated with calcite enters the cave and drips onto the stalagmite. Thereby the water looses some CO_2 molecules by degassing and some carbonate molecules by calcite deposition resulting in a relatively small ^{14}C enrichment of the calcite compared to the water. The sketch in Figure 3.2 illustrates these effects on the ^{14}C activity in the soil.

3.3 Open and closed dissolution system

The largest influence on the isotopic composition of the carbon in the solution comes from the condition of limestone dissolution. It can enrich the ^{14}C activity of the calciumless solution by 2 - 3 percent modern carbon or lower the activity to 50 % (see Section 5.3). So in the case of limestone dissolution it is very important to differentiate between the open and closed dissolution system or intermediate states.

[1]Except for time intervals of a fast degradation of the atmospheric ^{14}C level as for the *past-bomb* period.

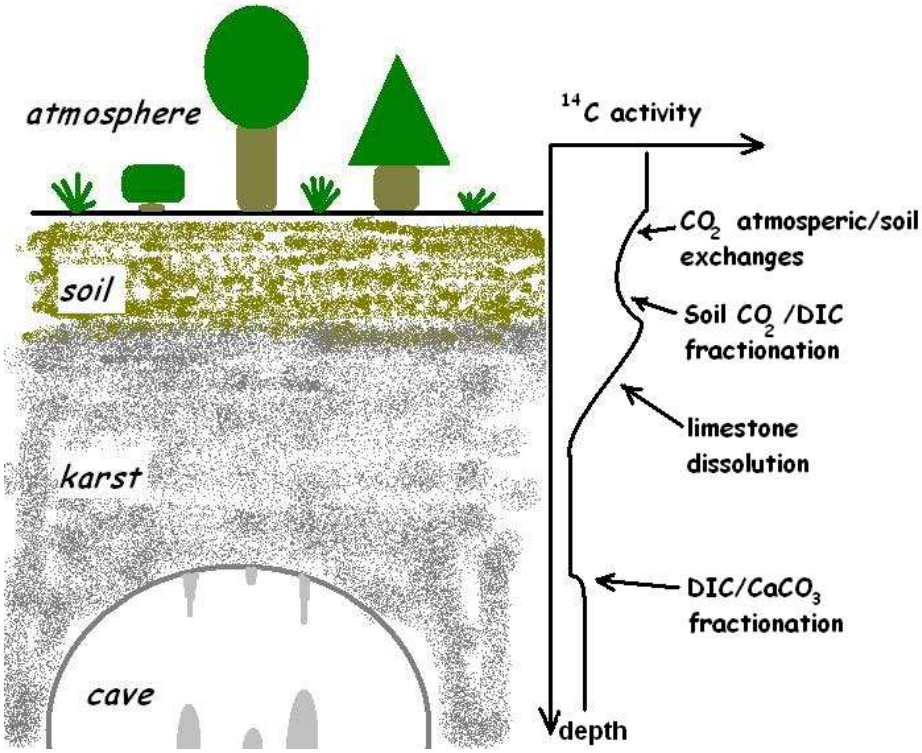

Figure 3.2: The schematic sketch shows the ^{14}C activity evolution of dissolved inorganic carbon in water. In each cave environment the extent of the different steps varies (redrawn after Genty and Massault (1999)).

Open limestone dissolution system If the dissolution takes place in an open system – in the presence of an unlimited excess of gaseous carbon dioxide – isotopic exchange between the carbon species in solution and the carbon dioxide in the soil atmosphere would maintain isotopic equilibrium between the gas and solution phase (Hendy, 1970, 1971). Since the amount of CO_2 produced in the soil is far greater than the amount that can leave the solution, the contribution of the limestone carbon to the total carbon in the solution and soil atmosphere system may be very small. Under these conditions the carbon species in solution would be close to carbon-isotopic equilibrium with the CO_2 produced in the soil. Then the carbon isotopes of the solution depend on the isotopic composition of soil atmospheric carbon (Tab. 3.1), the temperature-dependent isotope fractionation factors (Tab. 5.5) and on the partial pressure of CO_2, as it will be shown in Section 5.3.

Closed limestone dissolution system If, on the other hand, the limestone carbonate is dissolved in a closed system, the prediction of the isotopic ratios of the species in solution is more complicated. In a closed system the solution has no contact with soil pCO_2 during the dissolution of limestone. So it is approximately true, according to the chemical formulas (Eq. 5.1 – 5.5), that for every mole of limestone carbonate dissolved, one mole of aqueous carbon dioxide is converted to bicarbonate (Hendy, 1970). Thus, when the solution is saturated with respect to calcite, approximately half of the carbon in solution will have to come from the limestone and half from the soil carbon dioxide. The precise ratio of the contribution of the soil CO_2 to the total carbon in solution depends on the pCO_2 of the soil atmosphere. Besides

the pCO_2 the isotopic composition of the solution depends on the carbon isotopes of the soil atmosphere and the temperature-dependent isotope fractionation factors, as in the open case, and additionally on the isotopic composition of the limestone (Tab. 3.1).

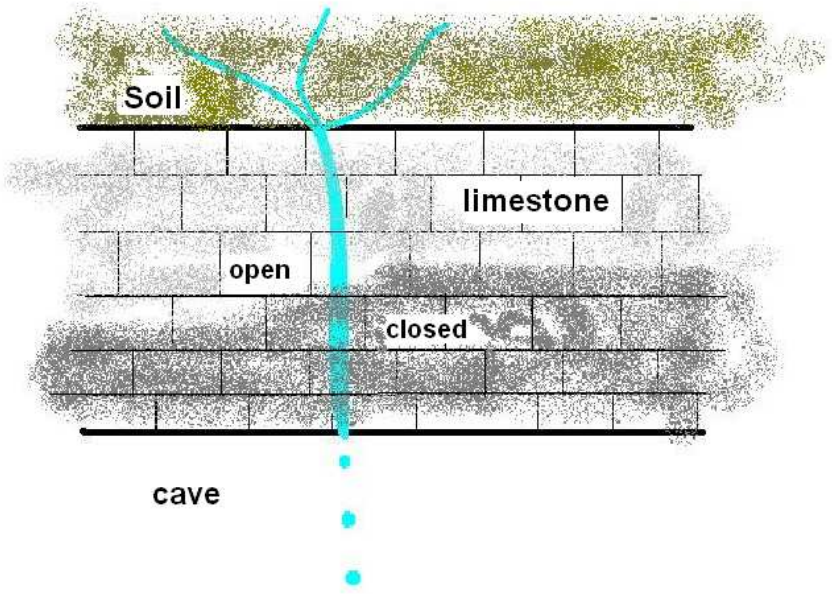

Figure 3.3: This sketch illustrates a possible limestone dissolution behaviour. The upper part shows the soil where the main part of the CO_2 in the solution is produced. The dissolution in the open system takes place in the upper part of the karst (the light grey background represents the limestone with gas filled voids). Below this horizon the dissolution occurs in the closed system (represented by the dark grey background with few washed out voids). In the last step the saturated solution enters the cave.

Intermediate limestone dissolution system The open and closed systems are the extreme cases of limestone dissolution. However, any real dissolution system will behave somewhere between the completely open and the completely closed one. The intermediate system will combine the characteristics of both extreme cases regarding the isotopic composition of the carbon in the solution. Usually the dissolution in the open system takes place in the upper part of the karst. In the lower part of the karst mostly the closed system is responsible for limestone dissolution. This behaviour is because the upper part of the karst is washed out by former stages of the limestone dissolution, resulting in free spaces filled with soil air, which can interact with the groundwater. Further down the water becomes isolated from the gas due to fewer free spaces. This scenario is visualised in Figure 3.3. Of course it is possible that the border between the open and the closed system decreases in depth with time due to dissolving processes in the upper karst.

Nevertheless there are several dissolution systems imaginable, but the simplest way to

deal with this topic is a stringent horizontal separation between the open and the closed system. In other situations the border could be situated in a vertical way (marked by **i** in Figure 3.4) or is somehow tilted (case **ii** in Figure 3.4) in the water flow. Or even more sophisticated is the case with a border of the open to the closed system, which is non linear with depth (case **iii** in Figure 3.4). But for those cases one has to assume a non mixing water flow, which is unrealistic in a turbulent fluid. Only if one does not assume that each molecule of the solution will come into contact to the surrounding soil atmosphere such scenarios makes sense. Else, in a well-mixed fluid, all molecules, dissolved under closed conditions, equilibrate with the soil atmosphere if they reach the side where the open condition is present. This is in general treated as a completely open system. The border of the dissolution system, marked as case **iv** in Figure 3.4 will lead to a resulting border like line **v**. With the explanations above it will be a horizontal border, as assumed for the model proposed in this work.

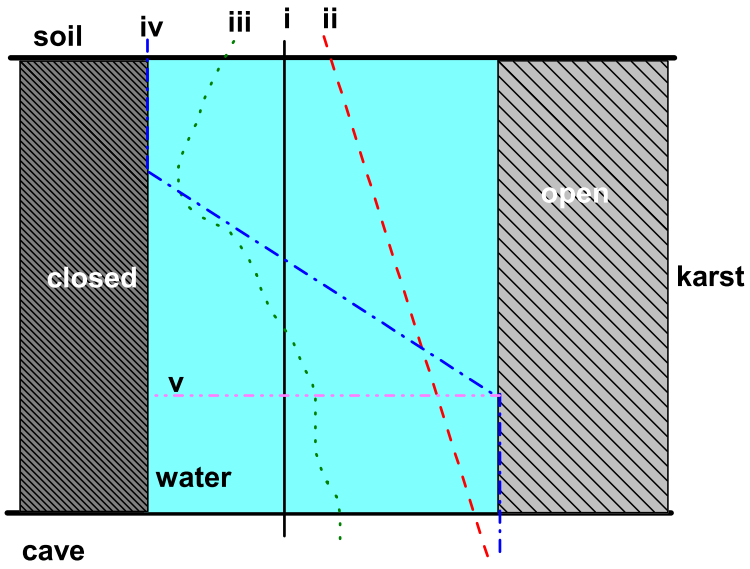

Figure 3.4: This sketch illustrates four possible limestone dissolution behaviours (**i** – **iv**), and the resulting open to closed system behaviour (**v**) from case **iv** (for more details see the text).

Further argumentations can be, that water mixing exists but is not complete in those systems, especially where the open limestone dissolution is only present for some less volume percent. Hence it is possible that only parts of the fluid, which dissolves the limestone in the closed way, exchange their isotopes with the gaseous phase. So intermediate very complex systems can be constructed. However, with this kind of complexity many artificial parameters have to be introduced. The fact, that the parameters are usually not known is the reason why to describe the dissolution system as simple as possible.

Another simple way of modelling the limestone dissolution is the attempt to treat the water as two single solutions in a certain volume ratio. One solution dissolves the limestone in an open system and the other of the two water parcels in the closed system. Both water

parcels mix[2] shortly before the water enters the cave. Such a model was written in the frame work of this PhD thesis as well, but this attempt showed no satisfying results compared with the model written after the illustrated scheme in Figure 3.3 (see further in Chapter 5).

3.4 Dead carbon fraction

Dead **c**arbon **f**raction[3] (**dcf**) describes approximately the part of carbon deposited on the stalagmite, which originates from the limestone above the cave. At a more detailed look into the problem of dcf it can be recognised that the determination of the dcf is more complex. The responsible processes for the complexity were already elucidated in Section 3.2 and summarised with Figure 3.2). Indeed the mean part of the dead carbon is introduced by the limestone. Nevertheless the other processes change the radiocarbon content in the solution and, hence, in the stalagmite as well. However, they influence the dcf only slightly in most cases.

Mathematically the dcf is defined by:

$$\mathrm{dcf} = \left(1 - \frac{\mathrm{a}^{14}\mathrm{C}_{stal}}{\mathrm{a}^{14}\mathrm{C}_{atm}}\right) \cdot 100\,\%, \tag{3.3}$$

with $\mathrm{a}^{14}\mathrm{C}_{stal}$ being the ^{14}C activity of the stalagmite and $\mathrm{a}^{14}\mathrm{C}_{atm}$ the ^{14}C activity of the atmosphere. Either both values belong to a time t where the calcite settled down or both values belong to measurements performed today on the stalagmite and on a parcel of the atmosphere originated from time t. The ^{14}C activity of the stalagmite is measured. For the past atmospheric ^{14}C activity one can take the IntCal04 calibration curve (Reimer et al., 2004). The absolute time t is provided by uranium series dating as e.g. in Genty et al. (1999, 2001); Beck et al. (2001) or, in some cases, by laminar counting (e.g. Genty and Massault, 1997; Genty et al., 1998; Scholz et al., in prep.).

The dcf determines the difference of the radiocarbon content between the atmosphere and the stalagmite normalised to the atmospheric radiocarbon content at time t and includes all ^{14}C changes, which occur in the soil above the cave. A more detailed look to ^{14}C changes due to single processes is not possible to stalagmites grown in the past, because only the difference between the radiocarbon content of the stalagmite and the atmosphere is measurable.

The determination of the dcf depends strongly on an exact age model. Where "exact" means in terms of small error bars on the timescale, which requires high precision U/Th measurements and in terms of the right gradient, which requires an adequate technique for building such an age model.

The dcf values published in literature are mostly between 10 to 20 %. A small selection is given in Table 3.2. Only two caves have a dcf value lower than 10 %.

In theory, changes in dcf result from at least two major and two minor causes. A first major cause is due to errors in the absolute chronology, especially if one has age errors in only some stalagmite sections. If for example the true age is overestimated one calculates a lower dcf than it would be with the correct age. Secondly, differences in the input of host rock carbon are very important, which means that a system switches its limestone dissolution system. Going from a more open to a more closed system would show increasing dcf values.

[2]Which results in a non saturated solution (Dreybrodt, 1988).

[3]The term **dead carbon** is used when no radioactive carbon is present in a material. The fraction says how much of the **dead carbon** material is mixed with/dissolved in an other material/solution.

Table 3.2: Published dcf of some stalagmites.

cave location	dcf [%]	paper
Sutherland (Scotland)	22 – 38	Genty et al. (2001)
Villard (France)	21.1±1.5	Genty and Massault (1997)
China	18	Hodge et al. (2006)
Browns Folley Mine (GB)	17.5	Genty et al. (2001)
Bahamas	16.5±4.7	Beck et al. (2001)
Han-sur-Lesse (Bel)	13.8±1.5	Genty and Massault (1997)
Postojna (Slovenia)	13 ±1.5	Genty and Massault (1999)
La Faurie (France)	12.2±1.5	Genty and Massault (1997)
Proumeyssac (France)	9.2±1.5	Genty and Massault (1997)
Timta (India)	2 – 6	Glynn et al. (2006)

A minor point, which could change the dcf, is a changing in the age/lifetime of the organic material in the soil. But it is very unlikely to explain large differences (above some percent[4]) with the organic material except in rare cases of peat layer forming above the cave (Genty et al., 2001). The last point is a change in the $CaCO_3$ precipitation rate. Especially a decreasing $CaCO_3$ precipitation rate would allow more CO_2 exchange between the solution and the cave atmosphere (Dulinsky and Rozanski, 1990). That would result in a decreasing dcf under the assumption that the cave air radiocarbon content mirrors the free atmosphere sufficiently.

[4]E.g. an increase in dcf of 5 % would mean that the soil organic matter would be older by around 450 years (Applying the ^{14}C lifetime of 8270 years leads in 80 years to a decrease of roughly 1 pmC in ^{14}C activity or 1 % in dcf). And that is very questionable.

Chapter 4

Determination and modelling of soil ^{14}C

For the interpretation of the ^{14}C variability in drip water it is important to investigate the ^{14}C content of the soil atmosphere. The soil radiocarbon content can be determined directly from the soil air (Warembourg and Paul, 1973; Dörr and Münnich, 1986; Tegen and Dörr, 1996). However, the disadvantage of this method is that the measurements are difficult to perform due to problems with the extraction of soil CO_2. Another way is to determine the soil air ^{14}C content by an indirect method. This approach derives the soil air ^{14}C content from the shape of the radiocarbon bomb peak, recorded in the calcite of a stalagmite.

This chapter contains information of the ^{14}C composition of the total carbon in the soil air, as well as explanations about the method to derive soil reservoir parameters from ^{14}C measurements on stalagmites (Sec. 4.1). Furthermore, in this chapter radiocarbon measurements of the top of stalagmite ER-77 are presented (Sec. 4.2). With the ^{14}C time series one can derive the age spectrum of a three soil reservoir model of soil organic matter above Ernesto cave. The known age spectrum allows to determine the recent soil air ^{14}C content, which will be used in Chapter 5 to model the ^{14}C isotopes in drip water.

4.1 Soil reservoir parameters

The method to estimate the soil reservoir parameters from radiocarbon data recorded in a stalagmite was developed in the late 1990s (Genty et al., 1998; Genty and Massault, 1999). The idea is based on the assumption of Dörr and Münnich (1986) that the age spectrum of the total carbon pool in the soil is determined by the lifetime and the CO_2 contribution of the soil reservoirs. Dörr and Münnich (1986) proposed at least two soil carbon reservoirs. With the simplified assumption that soil CO_2 is produced, first, by fast decomposition of organic matter and by root respiration (both processes with practically no difference in ^{14}C activity to atmospheric CO_2; young reservoir), and, second, by the decomposition of a long living soil organic matter component (old reservoir). The relative contribution of these reservoirs to the total soil respiration can be calculated with a two (or more) component mixing equation:

$$a^{14}C_{soil} = c_1 \cdot a^{14}C_1 + c_2 \cdot a^{14}C_2, \tag{4.1}$$

With $a^{14}C_{soil}$ being the soil ^{14}C activity and $a^{14}C_{1,2}$ being the ^{14}C activity of the young and the old reservoir. The young reservoir is thought to have atmospheric ^{14}C activity. $c_{1,2}$

are the relative contributions of the components to the total soil and $c_1 + c_2 = 1$.

For a beech/spruce forest with a sandy soil Dörr and Münnich (1986) found a $\Delta^{14}C$ [1] for the old reservoir of 110 ‰ with an annual cycle for the contribution of the components. The cycle reveals that the old reservoir contributes around 25 % in summer and 75 % in winter to the total soil carbon.

Tegen and Dörr (1996) found for deciduous forest soils that the young reservoir contributes 63 ± 17 % to the total carbon pool. In coniferous forest soils, however, they calculated the contribution of the young reservoir to be 37 ± 24 %.

Genty et al. (1998) and Genty and Massault (1999) used the soil reservoirs to explain radiocarbon measurements of stalagmites grown during the 20th century. They observed a shifted and attenuated bomb peak in the ^{14}C content of the stalagmite calcite. The modifications of the bomb peak in the stalagmite compared to the atmospheric radiocarbon bomb peak results from soil processes. For the estimation of the soil reservoir parameters such as the dcf, the lifetimes and contributions of the reservoirs, Genty et al. (1998) wrote a stalagmite model focussing on the ^{14}C isotopes. This model simulates the carbon isotope content of soil water during limestone dissolution and stalagmite growth and includes fractionation processes between the single carbon species. Then the isotopic composition of the stalagmite is calculated. All calculations, especially for the isotopic fractionation, are performed using the cave temperature, which is the mean annual temperature.

4.2 Soil reservoirs at Ernesto cave

In this thesis the model of Genty et al. (1998) is used to estimate the soil parameters for Ernesto cave, using stalagmite ER-77 (Frisia et al., 2003). 17 samples at the uppermost 11 mm (upper right panel in Figure 4.1), corresponding to the period 1890 AD to 1990 AD, were drilled and analysed. The calibrated age was determined from the date of collection ER-77 (1995 AD)[2] and lamina counting. It was not possible to drill the samples on the same track as the lamina counting was performed, because many holes were on this side of the stalagmite slice. Due to the convex stalagmite top this corresponds to an offset of 1.57 mm. Transferred to time it is a shift of ten years, leading to an age of the most recent sample to roughly 1980 (mean position of sample collection). The results for the 17 samples are given in Table A.3 and plotted in Figure 4.1.

Each subsample of ER-77 covers a time interval between 4 and 10 years, depending on the growth rate of the stalagmite. Until 1950 AD the ^{14}C level in the atmosphere was almost constant. Due to the nuclear bomb tests the radiocarbon content of the atmosphere increased very fast with a maximum in the mid 1960s (Levin and Kromer (2004), blue curve in Figure 4.1). The ^{14}C activity of ER-77 (black squares) reveals both the constant phase and the bomb peak. The bomb peak, stored in the stalagmite, is attenuated and slightly shifted. Both the delay and the attenuation are caused by carbon soil reservoirs.

For the estimation of the carbon soil reservoir parameters one has to determine the dcf coming from the limestone. The estimations of parameters, dcf and soil reservoirs, have to be performed simultaneously. In contrast to the total dcf (Eq. 3.3), the contribution of the limestone dead carbon is obviously not easy to calculate because of changes in the ^{14}C activity due to fractionation effects and CO_2 input of old organic matter in the soil. The

[1] $\Delta^{14}C = \left(\frac{^{14}C/^{12}C_{sample}}{^{14}C/^{12}C_{standard}} - 1\right) \cdot 1000$ ‰

[2] The zero point was chosen to be 1992 AD by Frisia et al. (2003), because the three topmost laminae had to be discarded due to damages on the top laminae during the thin section preparation.

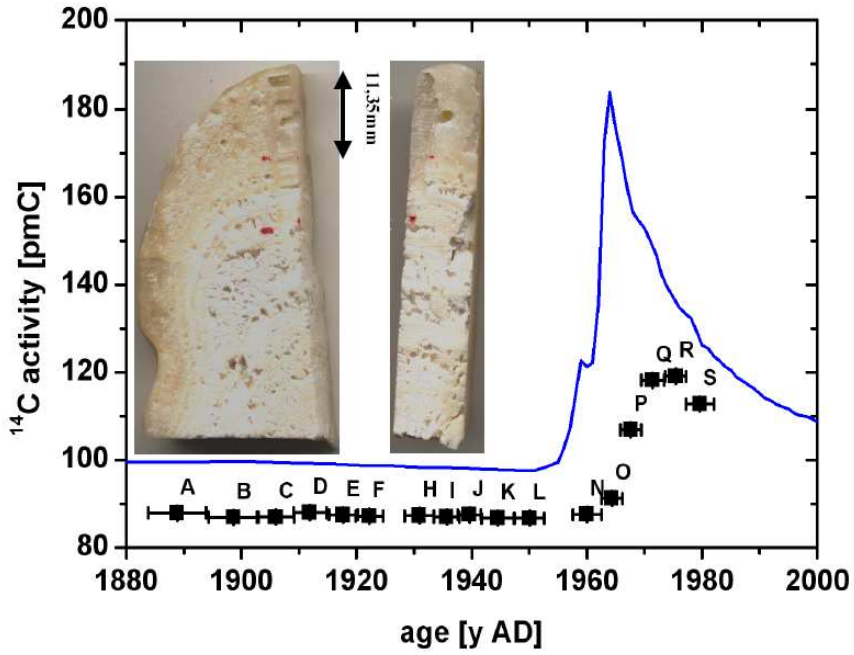

Figure 4.1: The top of stalagmite ER-77 is shown on the upper left part of this Figure. in the upper 11.35 mm 17 subsamples were drilled and analysed for their ^{14}C content. The measurements from the subsamples (black squares) reveal a shifted and attenuated ^{14}C peak, which results from the atmospheric radiocarbon content (blue line).

fractionation effect increases the ^{14}C of the solution. In the pre/past bomb peak period the soil CO_2 decrease/increase the ^{14}C activity of the solution. Hence the dead carbon proportion from the limestone has to be larger than the dcf calculated by Equation 3.3.

A convenient period to estimate dcf is during the interval of a relatively constant radiocarbon content in the atmosphere. The choice of a phase with a constant atmospheric ^{14}C level is important because the soil reservoir parameters have a minor and especially constant effect on the ^{14}C content of the soil atmosphere during those constant phases. The dead carbon originating from the limestone was estimated to 12.9 %. That finally results in a dead carbon fraction of 10.9 %, calculated from the pre-bomb interval (1810 – 1950 AD) by using the best fit (red line in Figure 4.2) through the measurements of subsamples ER-77 A to ER-77 L.

The model was applied using three soil reservoirs. The young reservoir is responsible for the delay of the ^{14}C increase in the stalagmite, while the old reservoir has the main influence on the attenuating signal. The timing of the maximum in stalagmite ^{14}C is due to the age of the intermediate soil reservoir. It is also possible to describe the signal with only two soil reservoirs, but then there are difficulties to describe maximum, offset and decrease of the ^{14}C anomaly with one set of parameters. Figure B.1 in Appendix B shows the best fit which is possible with two soil reservoirs. Especially the beginning of the ^{14}C increase is not well reproduced.

The reservoir ages were determined to 5, 11 and 100 years with a contribution to the total soil carbon of 7, 51 and 42 % (Fig. 4.2). The reservoir ages describe the duration for which the ^{14}C content of soil organic matter has been averaged. It is assumed that the annual input of new organic matter has a ^{14}C activity, which is equal to the atmospheric ^{14}C activity of

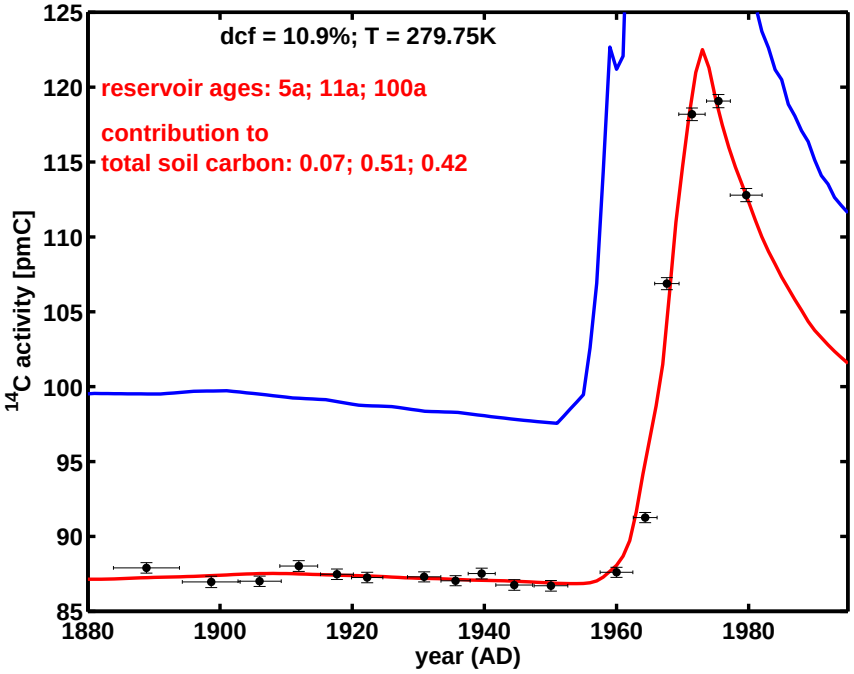

Figure 4.2: The plot shows how the atmospheric radiocarbon anomaly – bomb peak – (blue line) is recorded in the stalagmite top of ER-77 (black dots). The red line represents the best fit through the data calculated with the model according to Genty and Massault (1999). The model assumes a cave temperature of 6.6°C. The dcf is 10.9 % and three reservoirs were used to fit the data.

that year. The ^{14}C activity is corrected for radiocarbon decay. However, this correction is almost negligible for these short time scales.

The mean radiocarbon activity of the soil reservoirs is determined by calculating the mean ^{14}C activity of the atmosphere during the lifetime of that reservoir. The calculations of the activities are described by Equations 4.2 – 4.4:

$$a^{14}C_1 = \frac{1}{a_1} \sum_{i=n-a_1}^{n} a^{14}C_{atm}(i) \tag{4.2}$$

$$a^{14}C_2 = \frac{1}{a_2 - a_1} \sum_{i=n-a_2}^{n-a_1-1} a^{14}C_{atm}(i) \tag{4.3}$$

$$a^{14}C_3 = \frac{1}{a_3 - a_2} \sum_{i=n-a_3}^{n-a_2-1} a^{14}C_{atm}(i) \tag{4.4}$$

Here the $a^{14}C_{1,2,3}$ are the mean ^{14}C activities of the three reservoirs, $a_{1,2,3}$ are the corresponding ages, n is the year for which the calculation is performed and $a^{14}C_{atm}(i)$ is the atmospheric radiocarbon activity of year i.

The young reservoir can be considered as a combination of root respiration, decomposing leaves and the outer parts of dead branches and trunks growing within the determined age of the young reservoir. The intermediate reservoir can be understood as the most resistant

parts of the leaves, the older parts of the branches and the intermediate parts of the trunks. The old reservoir is composed similarly. Only material which is older than the age given by the intermediate one belongs to that reservoir.

The young reservoir contributes only a small amount of CO_2 to the total soil CO_2. Thus, soil respiration and fast decomposing leaves or needles do not play a major role for the total radiocarbon composition of the soil above Ernesto cave. This is at least valid for winter, the time of the year the stalagmite is supposed to grow fastest according to Frisia et al. (2003). During winter the vegetation does not produce important amounts of root respiration derived CO_2. Thus, the decomposition of old organic material is most important in winter. 51% of the total carbon is supposed to come from the intermediate reservoir. Organic matter, which is decomposed between 6 and 11 years after death, contributes to the second reservoir. Also the old reservoir, which includes organic matter decomposed between the years 12 and 100 after death, has a major contribution to total soil CO_2 (40%). The determined parameters agree well to the ranges given in the study of Trumbore (2000).

One should keep in mind that the old reservoir is not well constrained because only two measurements were performed in the decreasing part of the bomb peak. The decrease, calculated by the model, is mainly influenced by the age of the old reservoir (see Figure B.2).

The chosen parameters reveal a linear correlation coefficient of R = 0.991 between data and model showing that the model fits very well with the measured data. The correlation coefficient is a measure for the shape. For example, applying the same parameter set, except the dcf - let it be 8 % - the correlation has the same value as above. However, there is always an offset between the model and data. To keep the offset as small as possible another quantity is used to test for the goodness of the chosen parameters.

This quantity is the accumulated offset of single ^{14}C data points to the calculated radiocarbon curve of the stalagmite. The investigated stalagmite part was divided into two periods: the bomb phase includes six data points and the pre-bomb phase 11 data points. With the pre-bomb interval one can estimate the best dcf value, while the bomb phase reveals the best choice of the soil reservoir parameters. The parameters mentioned above fulfil the minimum condition. In the vicinity of the chosen values no other reservoir parameters are better than the proposed ones. It is unlikely that a completely other set of parameters can be applied to fit the data, because the soil parameters are responsible for the offset between the modelled and measured ^{14}C data (dcf), the onset of the ^{14}C increase (young reservoir), the timing of the maximum (intermediate reservoir) and the decrease (old reservoir) of the bomb peak. Hence they are decoupled from each other and can not be superimposed from another set of parameters.

With the determined parameters one can estimate the soil ^{14}C activity for each year, assuming the parameters are constant over time, and the atmospheric ^{14}C content is known. For the year 2006 this results in a soil ^{14}C activity of 110.7 pmC. This value is chosen in Section 5.3.2 as the mean ^{14}C activity of the soil above Ernesto cave.

Chapter 5

^{14}C in cave drip water

For the approach to investigate the present day situation in speleothems monthly collected drip water samples of Ernesto cave and Bunker cave were analysed. The samples were collected and sent by R. Miorandi and D. Riechelmann. Additional information like meteorological data, stable isotope and CO_2 measurements of soil and cave air were provided by D. Riechelmann and R. Miorandi as well. Stable isotopes were also measured in Innsbruck by C. Spötl. The measurements of anions and cations were performed by A. Schröder-Ritzrau at the Institute for Environmental Geochemistry of the University of Heidelberg.

In the first part of this chapter the radiocarbon measurements of the carbon in the drip water of both caves are presented. Then a drip water model is developed and the results are shown. In the last section of this chapter the carbon isotopes calculated by the model are compared with the drip water measurements.

5.1 Drip water measurements

For the drip water measurements the ^{14}C activity and the $\delta^{13}C$ content are of major interest, because with changes in both isotopes one can support or reject hypotheses of processes occurring in the soil and cave. With both carbon isotopes the present processes can be determined more clearly than with radiocarbon data alone.

5.1.1 Ernesto cave

Grotta di Ernesto is a shallow cave of around 20 m below surface in Northeast Italy (45°58'37" N, 11°39'28" E). The cave is situated at the northern slope of the Valsugana valley at 1167 m above sea level. Precipitation minus evapotranspiration has a bimodal distribution with maxima in autumn and spring. Snow lays usually between December and March with a following snow melt until April. The vegetation consists of C3 plants and the soil thickness is 1.5 m (Borsato, 1997; McDermott et al., 1999; Huang et al., 2001; Frisia et al., 2003).

The monthly sampling period of the drip water from two drip locations was between November 2005 and October 2007. The locations were ER-76 and ER-G1. ER-G1 is a fast drip with a high coefficient of variation in the discharge of water – a so-called seasonal drip (pers. com. R. Miorandi). ER-76 is a seasonal drip as well (Frisia et al., 2003) but has a longer drip interval than ER-G1. Due to the different drip intervals it was necessary to collect water of ER-76 during a whole month, while a sampling period of some hours during a cave visit was sufficient for ER-G1.

The water samples, which were prepared for radiocarbon AMS measurements, had a volume of around 80 to 90 ml. They were prepared and measured as explained in Chapter 2. The ^{14}C data of ER-G1 and ER-76 are given in Table A.4 and A.5 of appendix A. In Figure 5.1 the ^{14}C data are plotted over the two years of investigation.

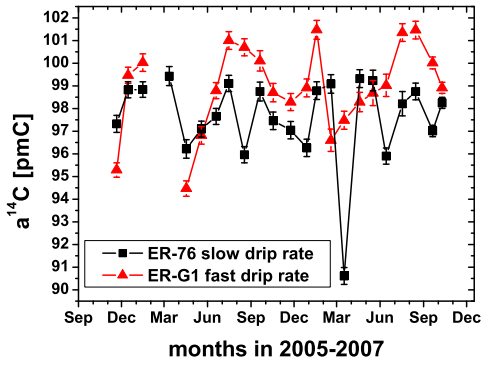

Figure 5.1: Monthly measured radiocarbon data of the drip water samples collected at drip locations ER-G1 (black squares) and ER-76 (red triangles).

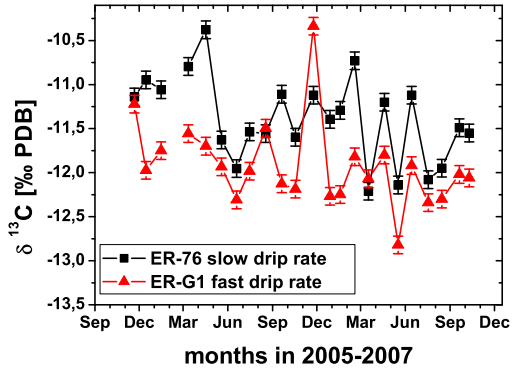

Figure 5.2: Monthly measured $\delta^{13}C$ data of the drip water samples collected at drip locations ER-G1 (black squares) and ER-76 (red triangles).

In the soil a strong seasonal signal in the soil air $\delta^{13}C$ is visible with differences of the $\delta^{13}C$ values during the maximum in winter and the minimum in summer of around 3.5 ‰ (Fig. B.3). However this variability is not detected in the drip water, where the variation of the $\delta^{13}C$ values is low (about 1 to 1.5 ‰) and does not represent the seasonal signal observed for soil air $\delta^{13}C$ (Fig. 5.2). The signal of the soil seems to be attenuated by processes occurring between the upper soil and the cave. According to the observed $\delta^{18}O$ signal of precipitation and drip water (Fig. B.4) it can be assumed that the attenuation is due to mixing processes in the ground water. Figure B.4 show the large range of $\delta^{18}O$ in precipitation ($\approx$ 10 ‰). In contrast to precipitation the $\delta^{18}O$ of the drip water is nearly constant. Only mixing processes of water can be responsible for attenuating the soil signals in both isotopes. This confirms the assumption of Frisia et al. (2003), who proposed a soil water reservoir above Ernesto cave with constant isotopic composition and ion concentrations on annual time scales.

Radiocarbon measurements over the two year sampling period reveal a pronounced annual cycle (Fig. 5.1). This is more significant for the ^{14}C values of the ER-G1 drip water (red) than for the radiocarbon content of drip water location ER-76 (black). Both years show an increasing trend between November and January, followed by a strong decrease in the ^{14}C activity in the next month. Between February and July a steady increase occurs until the radiocarbon content decreases slightly until November. This pattern is less pronounced in the ^{14}C activity of the ER-76 drip water in the second year.

Carbon from the soil and from the limestone can be responsible for a seasonal signal like shown in Figure 5.1. Both areas are the most important carbon sources for the carbon species in the drip water. Firstly the annual pattern can be explained by changes in the composition of the total soil CO_2, which is derived from different reservoirs of soil organic matter (Sec. 4). The percentages of the different reservoirs to total soil pCO_2 change the soil CO_2 composition throughout the year. But this is not the process driving the annual cycle in case of the Ernesto

cave. If one calculates the ^{14}C activity of the single soil reservoirs, determined in Section 4, it becomes obvious that the drip water ^{14}C range of roughly 8 pmC (drip location ER-G1) can not be explained by the different reservoirs. The mean activities of the short, middle and long organic matter reservoirs are 106.27 pmC, 109.42 pmC and 112.92 pmC, respectively. So the expected difference if only one of the three reservoirs provides the CO_2 to the total carbon is at maximum about 6.5 pmC. However, it is very unlikely that for example in winter all CO_2 is derived by the old reservoir and then in summer the CO_2 originates completely from the young reservoir.

Furthermore, the attenuating process visible in the $\delta^{13}C$ values (Fig. B.3) makes the difference in radiocarbon from the respired soil air to the drip water smaller. It can be assumed that the short reservoir delivers a dominant part to the total carbon pool in the spring and summer months due to a temperature induced growing vegetation and increased CO_2 root respiration. According to the activities of the different reservoirs in this soil system, this should result in a decreasing trend during that time which is not observed. Hence, the observed ^{14}C trend is not controlled by soil processes.

The second possibility is that the signal originates from the karst. A straight forward process which drives the radiocarbon annual signal is unlikely, because of the stationary water reservoir on annual scale. A more sophisticated reason seems to be responsible for a seasonal cycle in radiocarbon drip water. Important is the consideration that the water in the well mixed ground water is not saturated. This demand is satisfied, either by the non saturated solution joining the reservoir or by the fact that the mixing of two saturated solutions each in equilibrium with different pCO_2 generates a non saturated solution (Dreybrodt, 1988). This mixed solution is supposed to emerge from the open dissolution system, because the dissolution happens in the upper soil layers, where enough contact to soil air is possible.

If the second explanation is appropriate, a possible reason for the seasonal cycle in drip water ^{14}C activity is the correlation between seasonal drip water ^{14}C data and corresponding pH values (Fig. 5.3). Furthermore a correlation between the ^{14}C data and the drip rate (Fig. 5.4 upper inlet) should be established. Both correlation coefficients are above 0.6 and the probability that the correlation is by chance are lower than 0.003.

The process, which drives the radiocarbon value with the drip water pH, can be explained as follows. At first relatively low precipitation rates are assumed and a well-mixed water reservoir is present. Then the non-saturated, mixed soil reservoir water dissolves the limestone with contact to soil air filled voids. A relative strong gas exchange occurs, which is the definition for an open dissolution system. Hence, in times with less rain above Ernesto cave, resulting in a period of low drip rate[1], high ^{14}C values in the drip water are more likely. This is clearly shown in the upper panel of Figure 5.4, where the correlation between drip rate and precipitation is illustrated. The correlation calculation was performed without the samples, which were collected during or shortly after strong rain events (marked by the squares in brackets).

In the case of high precipitation, which brings undersaturated water to the reservoir, the voids in the soil are nearly completely filled with the solution. Now limestone dissolution in the reservoir water occurs in a closed system, because no (or not much) gas exchange with the soil atmosphere is possible. Especially the lower parts of the water reservoir, which get pushed into the cave first, can not equilibrate with soil air. Therefore, high precipitation rates result in high drip rates and low ^{14}C values in the drip water.

[1]ER-G1 drip rates are time delayed to precipitation by less than two weeks. The drip rate on ER-76 needs one or two month to react on precipitation events (Borsato, 1997). Exceptions are strong rain events (more than 12 mm/day) where the drip ER-G1 reacts within 12 hours.

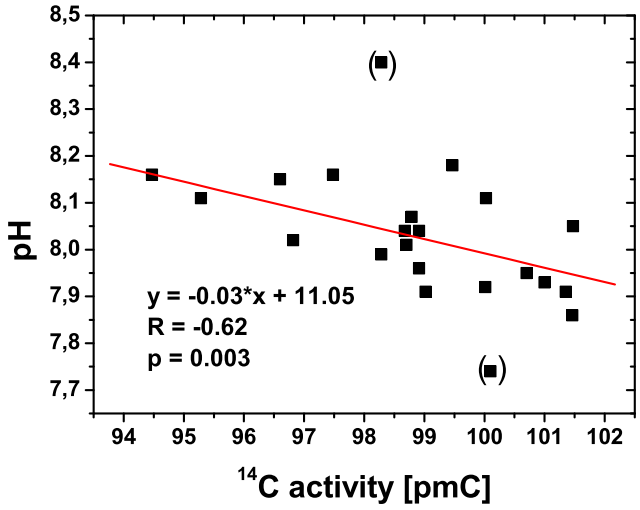

Figure 5.3: Monthly measured radiocarbon data of the drip water samples collected on drip location ER-G1 correlated with corresponding pH values (black squares). The red line represents the linear correlation without the points in brackets, which are erroneous in pH value due to technical measurement difficulties.

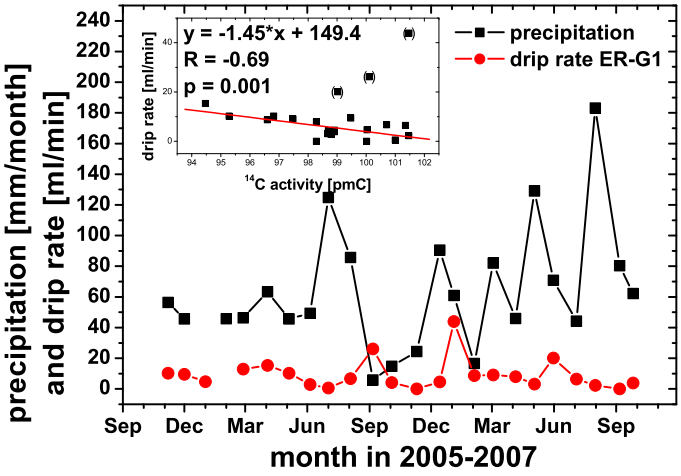

Figure 5.4: The monthly precipitation (black squares) and the monthly measured drip rate of location ER-G1 (red circles) show a time lag of up to one month. In the upper panel the correlation plot between ^{14}C activity and drip rate is shown. The points in brackets were left out for correlation calculations (see text).

If there is too much precipitation before or during the cave visit a threshold is crossed and the water penetrates the soil and the karst very fast (Borsato, 1997; Frisia et al., 2003). At very high precipitation rates the drip water, originated from the mixed reservoir, has probably no chance to reach the calcite saturation state. This is due to the existing undersaturation in the reservoir, as mentioned above, and the strong pressure from the additional rainwater, forcing the deeper situated water to penetrate very fast through the karst. This implies that the carbon in the drip water mainly derives from the open dissolution system, which results in high ^{14}C values of drip water carbon. At Ernesto the samples from January and June 2007 have experienced high precipitation rates during or some days before sample collection. Both months also show high drip rates. For September 2006 a high drip rate (Fig. 5.4) was measured but no high precipitation rates were observed. The reason for the behaviour in September 2006 is unknown. But at least the saturation indices[2] calculated by A. Schröder-Ritzrau show a lower saturation index for water collected in these tree months than in all the other month (Tab. 5.1).

Table 5.1: Saturation index (SI) of ER-G1 drip water. The SI is given with respect to cave atmosphere, meaning that the SI in the karst is lower due to a higher pCO_2. Hence the SI is only shifted and the tendency of calcium content does not depend on the medium the water has contact to. SI was calculated with PHREEQ-C using ion strength and pH values of the drip water.

date	sample name	SI	date	sample name	SI
20.04.2006	ER-G1 52	0.49	02.01.2007	ER-G1 60	0.42
22.05.2006	ER-G1 53	0.34	23.01.2007	ER-G1 61	0.22
22.06.2006	ER-G1 54	0.40	22.02.2007	ER-G1 62	0.48
18.07.2006	ER-G1 55	0.25	22.03.2007	ER-G1 63	0.57
21.08.2006	ER-G1 56	0.32	24.04.2007	ER-G1 64	0.43
19.09.2006	ER-G1 57	0.14	22.05.2007	ER-G1 65	0.53
23.10.2006	ER-G1 58	0.29	19.06.2007	ER-G1 66	0.24
27.11.2006	ER-G1 59	0.74			

So the three outliers in Figure 5.4, upper panel, can be explained. Without the outliers the correlation (red line in Figure 5.4, upper panel) is convincing (correlation coefficient R = 0.69, p = 0.001). Hence the observed ^{14}C trend in ER-G1 drip water (Fig. 5.1) appears to be controlled by this process.

Another reason, which can in principle be responsible for the radiocarbon drip water cycle, is the carbon exchange between limestone and water. However, the possibility that the ^{14}C signal is only due to carbon isotope exchange between limestone and water can be rejected for Ernesto cave. The initial pH value of soil water is throughout the year nearly constant, due to the well-mixed ground water reservoir. Exchange processes usually do not change the pH value of a solution. Hence a possible carbon isotope exchange of the solution with the limestone can not be responsible for the observed trend in drip water pH value and in the ^{14}C signal.

Very remarkable in Figure 5.1 is that the ^{14}C values of ER-76, the drip with the slower rate, are in general lower than for ER-G1. On the other hand the δ^{13}C values (Fig. 5.2) are in general higher. Assuming that the drip water of both drip locations is fed by the same

[2]The saturation index for calcium carbonate is a measure for the calcium-carbonic acid-equilibrium.

water reservoir with the same isotopic composition the difference between the carbon isotopes of both drip locations is due to processes in the karst or the cave. Degassing of the solution during the one month sampling duration is one possible process to explain the enhanced δ^{13}C values. This contradicts with the lower ^{14}C values in the carbon of the drip water. A higher value in the δ^{13}C measurements of 0.5 ‰ (as the observed mean of the two year time period) would result in a higher mean radiocarbon activity of roughly 1 pmC. However, a lower mean value of 1.3 pmC in ER-76 was measured. Hence, degassing of drip water is not responsible for the observation of higher δ^{13}C and lower ^{14}C values in ER-76 compared to ER-G1.

Lower ^{14}C activities and higher δ^{13}C contents can be explained by a more intense contact of water and limestone in the host rock. Intense contact means either the dissolution occurs under more closed conditions or carbon exchange processes between the solution and the limestone are present. For both drip locations, ER-76 and ER-G1, one has to assume similar processes influencing the isotope drip water signal, due to the same cave system, the nearby locations of both drips and the same discharge behaviour[3]. Only the amount of water discharge (roughly two orders of magnitude difference) and the time shift of water infiltration (around two month compared to two weeks for ER-G1) are different. Due to the same discharge behaviour, and a seasonal pH signal similar to ER-G1 (Fig. 5.5) one can assume that the same dissolution process as described above is present for ER-76.

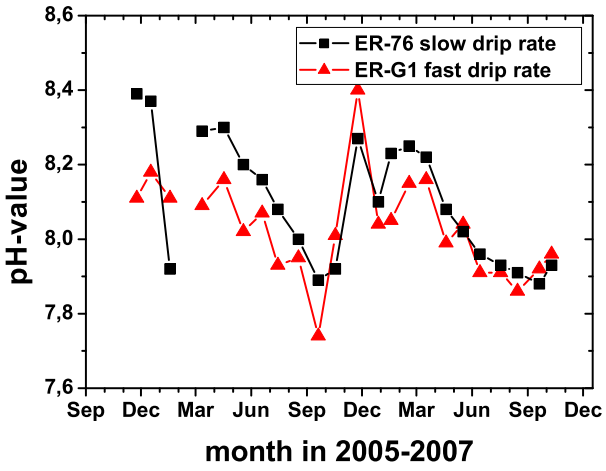

Figure 5.5: The monthly measured pH values of the drip water samples collected on drip location ER-G1 (red triangles) and ER-76 (black squares) reveal a synchronous behaviour. ER-76 is in general more alkaline than ER-G1.

The main difference in the pH value between both drip waters is the mostly more alkaline drip water of ER-76 compared to the ER-G1 drip water. Degassing of the solution can be clearly seen on the stable carbon and oxygen isotope composition. Thus, a degassing effect, due to a water collecting time of one month, is not very important for the pH difference because the δ^{13}C and δ^{18}O values of ER-76 and ER-G1 have similar values (Figs. 5.2 and B.4).

[3]Both drips are classified as seasonal drips reacting on seasonal precipitation changes.

Thus the difference is to be attributed to a more closed dissolution pathway for ER-76 than for ER-G1. The more closed conditions are only present below the water reservoir, which for both drip locations is the same. It is not excluded that isotopic exchange is present to a certain extend in the karst. This process would drive the isotopes of the solution in the same direction as a more closed limestone dissolution pathway. That will make the solution more heavier in the δ^{13}C isotopes and more lighter in the radiocarbon isotopes. The water-limestone isotope exchange is more likely for ER-76 than for ER-G1, because the water of ER-76 is thought to have a longer residence time in the soil (Borsato, 1997).

5.1.2 Bunker cave

Bunker cave is situated in Sauerland in central Germany. The Bunker cave has a length of 2000 m and is a part of the large cave system of Iserlohn. The rock thickness above the different cave chambers in Bunker cave is approximately 15 to 20 m (Grebe, 1993). The soil thickness is one meter with many stones inside. The vegetation consists of C3 plants. The drip water samples come from drip location two (Bu-TS2), which is situated in a large chamber with a many stalagmites.

Radiocarbon was measured in monthly collected drip water for one annual cycle, March 2007 – February 2008 (Tab. A.6). The data reveal a pronounced annual cycle (Fig. 5.6) similar to the Ernesto cave system. In contrary to Ernesto cave an annual cycle is visible also in the δ^{13}C content.

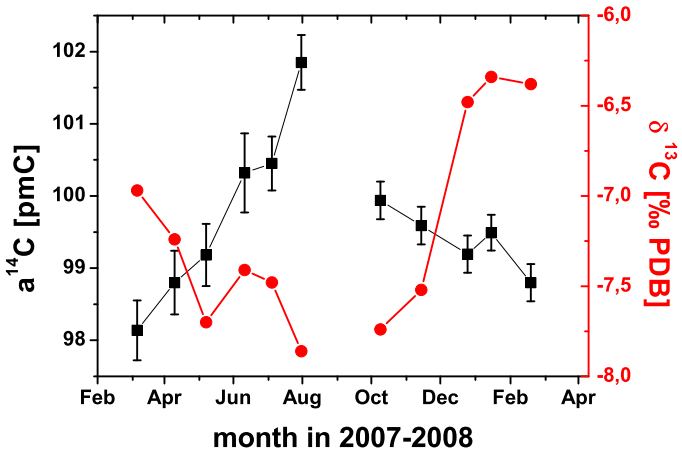

Figure 5.6: The monthly measured ^{14}C activity (black squares) and δ^{13}C content (red circles) of the drip water samples collected on drip location Bu-TS2 show a seasonal cycle. The radiocarbon measurements peak in summer and have a minimum in winter. The δ^{13}C values reveal an opposite trend.

It is more difficult to interpret the annual cycle of the carbon isotopes in drip water of Bunker cave (Fig. 5.6) than for the drip locations of Ernesto cave. Firstly, at Bunker cave the data series comprise only one year. While at Ernesto cave monitoring data are available from the late 1990s the measurements of cave and soil parameters at Bunker cave started in

2006. Data on radiocarbon content of soil air are not available. In addition there is no "tool" to determine the soil ^{14}C content with the ^{14}C bomb peak stored in a stalagmite.

Secondly, all the samples of Bu-TS2 are samples with water collected over one month due to low drip rates. Additionally, it was discovered that a degassing of the water in the cave is present, which strongly influences the isotopes in drip water (pers. comm. D. Scholz). In April 2008 two samples of Bu-TS2 were measured for $\delta^{13}C$ content. One was the usual monthly collected water and one was an instant sample with water collected in the time of the cave visit. The instant sample was around 1.3 ‰ lighter than the monthly collected sample. Assuming degassing is responsible[4] for the effect and that the deviation is constant over time the $\delta^{13}C$ difference can be used for correcting the radiocarbon results. So all measured radiocarbon samples would have been approximately two to three permil (0.2 to 0.3 pmC) lighter if they could have been sampled during a shorter time period.

Nevertheless, the offset is rather small and is in the range within the 2σ error bar of the ^{14}C measurements and can be neglected therefore. Furthermore, it is not known, if the strength of the degassing process is constant in time. Drip water samples collected during some hours of a cave visit and during the month before at drip locations Bu-TS5 and Bu-TS7 (Tab. 5.2) indicate that the degassing process vary. Thus, a radiocarbon correction of the measured data is not possible due to the unknown strength of the degassing.

Table 5.2: $\delta^{13}C$ content of Bu-TS5 and Bu-TS7 drip water samples. The results of the two samples of both months lead to the conclusion that the degassing process might not be constant.

location	date	sampling duration	$\delta^{13}C$ [‰]	sampling duration	$\delta^{13}C$ [‰]
Bu-TS5	04.03.2008	one month	-6.17	some hours	-9.63
Bu-TS5	22.04.2008	one month	-8.33	some hours	-9.6
Bu-TS7	04.03.2008	one month	-8.94	some hours	-9.97
Bu-TS7	22.04.2008	one month	-8.64	some hours	-10.92

Though it is not possible, yet, to explain the processes responsible for the radiocarbon signal in the drip water, it can be pointed out that the drip water carbon isotope variations can be due to changes in the carbon isotope composition of the soil atmosphere. In the Bunker cave no well mixed water reservoir like at Ernesto cave is present, which is obvious by comparing the measured $\delta^{13}C$ or $\delta^{18}O$ isotopic composition of the soil air/precipitation, soil water and drip water of Bu-TS1 and Bu-TS2 (Figs. B.6 and B.7).

Drip location Bu-TS1 is the only one, where it is possible to collect water during the cave visit, that means within some hours. Here possible degassing of the drip water can be neglected. The strong $\delta^{18}O$ signal of 6 ‰ (Fig. B.7) in the precipitation is attenuated by soil processes like evapotranspiration. So the soil water shows variations of 0.75 ‰. These variations are found in the drip water of Bu-TS1 as well (Fig. B.7), only shifted in time. It appears that the time the water needs from the soil into the cave is around four to six month, but the time series is only one year. The same is valid for the $\delta^{13}C$ data. Soil air measurements of the stable carbon isotope show no trend, but the water of the soil and of Bu-TS1 show

[4]Strong changes in the isotopic composition during the sampling time of one month do not seem to be responsible, because the $\delta^{13}C$ content of the water sample taken the month before was at the same $\delta^{13}C$ level like the April samples, that means there was no strong intermonthly trend observed. Also high intramonthly variabilities in $\delta^{13}C$ content are not supposed to occur.

variations of 2.5 ‰ (Fig. B.6). By neglecting the outlier of each time series[5] the time shift could be evaluated to four to six month again. However, this is rather speculative, yet.

The four to six month time shift is applicable for Bu-TS1, but it seems that the time shift is not valid for Bu-TS2. This is a typical case of different soil-karst-cave behaviour in even the same cave. Figure B.6 compares the carbon isotopes of soil air, soil water and drip water of Bu-TS2. The δ^{13}C soil signal is seen in the drip water of Bu-TS2 and no time shift between soil air and drip water δ^{13}C content is detected. For ^{18}O a time shift of four to six month can not be excluded (Fig. B.7). This contradiction is indeed a bit puzzling.

Strong changes of the drip water δ^{13}C signal are not expected to originate from changing limestone dissolution ratios (Secs. 5.3.1 and 5.3.2, drip location ER-G1). So it is unlikely that a changing dissolution system is responsible for the δ^{13}C pattern. Hence the δ^{13}C signal of the soil is visible in the drip water of Bu-TS2 it is likely that the radiocarbon seasonal cycle can be caused by soil air ^{14}C changes. So the ^{14}C increase during spring and summer months can be explained by a growing influence of root respiration compared to the decomposed dead organic matter. The contribution is reversed in the autumn and winter months where the influence of the dead organic matter grows, leading to a decreased radiocarbon activity in the drip water during this time. If the ^{14}C content of the solution is composed like explained, it would mean that there is no large time lag between soil and drip water, as shown by the stable carbon isotope measurements.

If the ^{14}C content of the solution depends on the soil ^{14}C, it would have a large impact on the ages of the soil reservoirs. As seen for the soil above Ernesto cave the old reservoir has a higher ^{14}C activity than the young one. Assuming the explanation of the composition of the total soil ^{14}C content is correct, the ^{14}C activities of the soil reservoirs of Bunker cave should show higher values for the young reservoir than for the old reservoir. Hence it is an inverse behaviour compared to the soil composition at Ernesto cave. This can be archived by an increased age of the old reservoir. The influence of the bomb peak would decrease and hence the ^{14}C level of the old reservoir decreases as well. A further possibility to change the ^{14}C ratio between the old and the young reservoir is to increase the age of the young reservoir, in order to increase the influence of the bomb peak to that reservoir.

Another interesting fact of the drip water is that the water in the cave has lower Ca^{2+} values than the soil water. So it is likely that prior calcite precipitation occurs at Bunker cave. That finding is supported by magnesium to calcium ratios of Bu-TS2 (pers. comm. A. Schröder-Ritzrau). The process of prior calcite precipitation can also contribute to changes in the carbon isotopes. With prior calcite precipitation the solution is expected to get heavier.

Furthermore, the calcium differences between soil water and drip water indicate that the soil water is already saturated in the upper soil layers. This is not necessarily the fact at the depth the soil water comes from (ca. 0.5 m), but maybe not far away from this depth. If the limestone dissolution occurs mainly in the upper parts of the soil, it is very likely that the calcite is dissolved near the open system. The results of the stalagmite Bu1 support the implication (Sec. 6.3.2).

5.2 Drip water model

For the aim of calculating the pCO_2 value of the soil above the cave in the way it was described in the introductory part, a model was developed. It is based on the model used in Hendy (1971). It contains the solubility of soil CO_2 and the solubility of calcite in meteoric

[5] March 2007 for Bu-TS1 and July 2007 for soil water.

water, degassing of CO_2 and precipitation of $CaCO_3$ in the cave and fractionation of carbon within these processes. With help of the description of the chemical reactions and isotopic fractionation effects the ^{14}C and $\delta^{13}C$ values of the stalagmite are calculated.

To invert the model the version described above was repeated with different initial conditions until the ^{14}C and $\delta^{13}C$ values, measured in the stalagmite, were found. This procedure is necessary because the model used much iteration for calculating the concentrations and activities of the solution. Therefore, it is not possible to develop a real inverse model. In this Section only the limestone dissolution part is explained – the drip water model. In Section 6.2 the Rayleigh distillation model for calculating the carbon isotopes on stalagmites will be discussed.

5.2.1 Concentration calculations

The dissolution of limestone carbonates and the precipitation of calcite on speleothems can be summarised by the chemical reaction: $CaCO_3 + H_2O + CO_2 \rightarrow Ca(HCO_3)_2$. Or split in single steps of calcite dissolution, the process reads like in equations 5.1 to 5.5. This is valid under ideal conditions, where no other minor elements (e.g. Mg, Na, K) participate on the dissolution process and the contribution of ion pairs like $CaOH^+$ or $CaHCO_3^+$ is negligible. The equations for the temperature dependent equilibrium constants the model uses are given in Table 5.3.

Table 5.3: Temperature dependence of mass action constants as used in Dreybrodt (1988). T = t(°C) + 273.15 Kelvin

$\log(k_{CO_2})$	=	$108.3865 + 0.01985076 \cdot T - 6919.53/T$ $+40.45154 \cdot \log(T) + 669365/T^2$
$\log(k_1)$	=	$-356.3094 - 0.06091964 \cdot T + 21834.37/T$ $+126.8339 \cdot \log(T) - 1684915.0/T^2$
$\log(k_2)$	=	$-107.8871 - 0.03252849 \cdot T + 5151.79/T$ $+38.92561 \cdot \log(T) - 563713.9/T^2$
$\log(k_w)$	=	$22.801 - 0.010365 \cdot T - 4787.3/T$ $-7.1321 \cdot \log(T)$
$\log(k_c)$	=	$-171.9065 - 0.077993 \cdot T + 2839.319/T$ $+71.595 \cdot \log(T)$

$$CO_{2(g)} \overset{k_{CO_2}}{\leftrightharpoons} CO_{2(aq)} \tag{5.1}$$

$$CO_{2(aq)} + H_2O \overset{k_1}{\leftrightharpoons} HCO_3^- + H^+ \tag{5.2}$$

$$HCO_3^- \overset{k_2}{\leftrightharpoons} CO_3^{2-} + H^+ \tag{5.3}$$

$$H_2O \overset{k_w}{\leftrightharpoons} OH^- + H^+ \tag{5.4}$$

$$CaCO_3 \overset{k_c}{\leftrightharpoons} Ca^{2+} + CO_3^{2-} \tag{5.5}$$

The equations for the single concentrations of the participating species are derived from the equilibrium of the chemical reactions, which read (For Equations 5.7 and 5.9 the activity of water is assumed to remain unity.):

$$k_{CO_2} = \frac{(CO_{2(g)})}{(CO_{2(aq)})} \tag{5.6}$$

$$k_1 = \frac{(HCO_3^-) \cdot (H^+)}{(CO_{2(aq)})} \tag{5.7}$$

$$k_2 = \frac{(CO_3^{2-}) \cdot (H^+)}{(HCO_3^-)} \tag{5.8}$$

$$k_w = (OH^-) \cdot (H^+) \tag{5.9}$$

$$k_c = (Ca^{2+}) \cdot (CO_3^{2-}) \tag{5.10}$$

Where the molecule in brackets, (i), representing the activity of species i which are related to concentrations c_i by $(i) = \gamma_i \cdot c_i$ (e.g. Garrels and Christ, 1965) with γ_i being the activity coefficient. For uncharged species such as H_2O and CO_2 the activity coefficients are given by $\gamma_i = 10^{0.1I} \approx 1$, if $I < 0.1$ (Plummer and Mackenzie, 1974). I is the ionic strength and is calculated by the sum of the product of charge (Z_i) and concentration of all species in the solution:

$$I = \frac{1}{2} \sum_i Z_i^2 \cdot c_i. \tag{5.11}$$

For charged species the activity coefficients are usually calculated by the extended Debye-Hückel equation:

$$log_{10}\gamma_i = -A \cdot Z_i^2 \cdot \frac{\sqrt{I}}{1 + B \cdot a_i \cdot \sqrt{I}} \tag{5.12}$$

A and B are values which depend on temperature ($A = 0.4883 + 8.074 \cdot 10^{-4} \cdot T; B = 0.3241 + 1.6 \cdot 10^{-4} \cdot T$ with temperature T in °C (Dreybrodt, 1988)) and the a_i represent the ionic radii of species i. The corresponding ionic radii for the species in the solution are given in Table 5.4.

Table 5.4: Ionic radii of species participating in the dissolution process of calcite. Values are taken from Dreybrodt (1988).

ion	H^+	OH^-	HCO_3^-	CO_3^{2-}	Ca^{2+}
ionic radius [$\mathring{A}$]	9	3	4	4.5	6

Additionally the concentrations of the different molecules have to fulfil the condition of electroneutrality:

$$c_{H^+} + 2c_{Ca^{2+}} - c_{OH^-} - c_{HCO_3^-} - 2c_{CO_3^{2-}} = 0. \tag{5.13}$$

With formulas 5.6 to 5.9 and 5.13 one can determine the equations for the concentration of c_{CO_2}:

$$c_{CO_{2(aq)}} = \begin{cases} \dfrac{c_{H^+}\left((c_{H^+})^2 - \frac{k_w}{\gamma_{H^+}\gamma_{OH^-}}\right)}{\frac{k_1\gamma_{CO_{2(aq)}}}{\gamma_{H^+}} \cdot \left(\frac{c_{H^+}}{\gamma_{HCO_3^-}} + \frac{2k_2}{\gamma_{H^+}\gamma_{CO_3^{2-}}}\right)} & \text{for no calcite in the solution} \\ \dfrac{\frac{k_w}{c_{H^+}\gamma_{H^+}\gamma_{OH^-}} - c_{H^+} + 2Z}{2 + \frac{k_1\gamma_{CO_{2(aq)}}}{c_{H^+}\gamma_{H^+}\gamma_{HCO_3^-}}} & \text{closed dissolution system} \\ c_{CO_{2(aq),soil}} & \text{open dissolution system} \end{cases} \tag{5.14}$$

For a solution without any calcium in the equation of electroneutrality, $c_{Ca^{2+}}$ is set to 0 moles/l. The third case of Equation 5.14 is also the definition of the open system. Z represents the sum of the concentrations of all carbon species before any limestone dissolution, i.e.

$$Z = c_{CO_{2(aq),soil}} + c_{HCO_{3,soil}^-} + c_{CO_{3,soil}^{2-}} \tag{5.15}$$

The equations for all participating ions can be transferred from equations 5.7 to 5.9 to:

$$c_{OH^-} = \frac{k_w}{c_{H^+}\gamma_{H^+}\gamma_{OH^-}} \tag{5.16}$$

$$c_{HCO_3^-} = \frac{k_1 c_{CO_{2(aq)}}\gamma_{CO_{2(aq)}}}{c_{H^+}\gamma_{H^+}\gamma_{HCO_3^-}} \tag{5.17}$$

$$c_{CO_3^{2-}} = \frac{k_1 k_2 c_{CO_{2(aq)}}\gamma_{CO_{2(aq)}}}{(c_{H^+})^2(\gamma_{H^+})^2\gamma_{CO_3^{2-}}} \tag{5.18}$$

With knowledge of the concentrations of the carbon containing species and the hydroxide ions the concentration of calcite can be calculated with the equation of electroneutrality (Eq. 5.13).

The calculations follow a certain algorithm: At first the pH value is to set andc_{H^+} can be determined. For the first step the concentration calculation assumes no calcium in the solution. An iterative process is applied because all concentrations depend, besides the hydrogen ion concentration, on several activities. Primarily all activity coefficients are set to one and are used to calculate the concentrations according to the above equations. On the other hand the concentrations, calculated with $\gamma_i = 1$, are used to determine the single activity coefficients by taking equation 5.12. The activity coefficients in turn are used to calculate the concentrations again. This loop is repeated until changes of successive values of activity coefficients and concentrations were sufficiently low.

This procedure is executed for successively higher pH values. In contrary to the first step the calcium concentration has to be considered. Higher pH values simulate a more alkaline solution and describe in this case the dissolution of limestone. Here the second or the third

case of equation 5.14 is applied. The whole dissolution process stops when the pH value is large enough so that the calcite saturation is achieved. The condition of saturation is described by equation 5.10.

In the cases of coupling the open and closed dissolution system the model calculates the concentrations to a defined point of the open system, first. At that point, defined by a number smaller than the equilibrium constant k_c, $x \cdot k_c, x \in [0,1]$[6], the model switches to the closed system. The last values of the carbon species in solution ($c_{i,last}$ with i = $CO_{2(aq)}$, HCO_3^-, CO_3^{2-}) calculated by the open system are treated as the first values of the closed dissolution system. The model uses the dissolved calcite at this point to reduce the molecule number of the carbon containing species, which are supposed to be acidic, by $c_{ca^{2+}_{open,last}}$ of the last dissolution step, performed in the open system. So Z from equation 5.14 is defined now as:

$$Z = c_{CO_{2(aq),open}} + c_{HCO^-_{3,open,last}} + c_{CO^{2-}_{3,open,last}} - c_{Ca^{2+}_{open,last}}. \tag{5.19}$$

In other words Z gives the sum of concentrations of carbon containing species, which is still available for more calcite dissolution.

5.2.2 Carbon isotope calculations

With the known concentrations it is easy to calculate the carbon isotopes in the solution at each step of the dissolution process. For the calculation the model uses the temperature dependent isotope fractionation factors listed in Table 5.5.

Table 5.5: Carbon isotope fractionation factors in the equilibrium system of pure karst waters $CO_2 \Longleftrightarrow HCO_3^- \Longleftrightarrow CO_3^{2-} \Longleftrightarrow CaCO_3$ for δ^{13}C. The ^{14}C fractionation factors are by a factor of 2.3 higher than for δ^{13}C according to measurements by Salièges and Fontes (1984). Temperature T = t(°C) + 273.15 Kelvin. The data are adapted from Mook and de Vries (2000).

$\epsilon_{CO_{2(aq)}-g}$	=	$-373/T + 0.19$ ‰
$\epsilon_{HCO_3^- - g}$	=	$9483/T - 23.89$ ‰
$\epsilon_{CO_3^{2-} - g}$	=	$8616/T - 21.37$ ‰
$\epsilon_{CaCO_3 - g}$	=	$5380/T - 9.15$ ‰

The isotope fractionation factors ϵ_{j-i} are to understand in the direction when the carbon atom in a molecule i (e.g. gaseous phase - g) changed into molecule j. For the transition into the other direction the signs reverse. Assuming a known value for $\delta^{13}C_{CO_{2,(g)}}$ the isotopic composition of the other species can be determined by:

$$\delta^{13}C_i \cong \delta^{13}C_{CO_{2,(g)}} + \epsilon_{i-g} \tag{5.20}$$

with i = ($CO_{2(aq)}$, HCO_3^-, CO_3^{2-}, $CaCO_3$) and using the common δ notation. In a soil covered by C3 plants $\delta^{13}C_{CO_{2,(g)}}$ is in general between -21 and -25 ‰ (e.g. Mook and de Vries, 2000), depending on the vegetation density and the time of the year. In the open system the isotopic exchange between dissolved inorganic carbon and soil CO_2 is the main factor for

[6] In this model x = 0 represents the closed dissolution system and x = 1 the open case.

calculating the isotopic composition of the water. Hence the $\delta^{13}C_t$ value of the total carbon in the solution can be determined by simple mixing calculations:

$$\delta^{13}C_t = \frac{(c_{CO_{2,(aq)}} \cdot \delta^{13}C_{CO_{2,(aq)}} + c_{HCO_3^-} \cdot \delta^{13}C_{HCO_3^-} + c_{CO_3^{2-}} \cdot \delta^{13}C_{CO_3^{2-}})}{(c_{CO_{2,(aq)}} + c_{HCO_3^-} + c_{CO_3^{2-}})} \text{‰}. \quad (5.21)$$

This is valid for the open system and for the initial step where no calcite is dissolved. In the closed system on the other hand the calcite plays an important role. The isotopic composition of dissolution step n could be calculated as:

$$\begin{aligned} \delta^{13}C_t(n) &= \frac{\delta^{13}C_t(n-1) \cdot (c_{CO_{2,(aq)}}(n-1) + c_{HCO_3^-}(n-1) + c_{CO_3^{2-}}(n-1))}{(c_{CO_{2,(aq)}}(n) + c_{HCO_3^-}(n) + c_{CO_3^{2-}}(n))} \\ &+ \frac{\delta^{13}C_l \cdot (c_{Ca^{2+}}(n) - c_{Ca^{2+}}(n-1))}{(c_{CO_{2,(aq)}}(n) + c_{HCO_3^-}(n) + c_{CO_3^{2-}}(n))} \text{‰}. \end{aligned} \quad (5.22)$$

$\delta^{13}C_l$ is the $\delta^{13}C$ isotopic composition of the limestone carbonate and has a value of around +1 ‰ (e.g. Mook and de Vries, 2000). Formulas 5.21 and 5.22 for the $\delta^{13}C$ isotopes can be applied to the ^{14}C calculations as well. The $^{14}C_{CO_{2,(g)}}$ activity is around the value of the atmosphere, depending on the dead organic content in the soil, and the $^{14}C_l$ activity is the ^{14}C activity of the limestone carbonate and is in general zero.

5.2.3 Limits of the model

The model does not include minor or trace elements because the concentrations of them in karst waters are usually low. Nevertheless, karst waters are rarely derived from the pure system H_2O – $CaCO_3$ – CO_2 (Dreybrodt, 1988). Mostly due to dolomite or magnesia calcites and due to gypsum and anhydrite, which usually are also encountered in karst areas, one finds Mg^{2+}, NO_3^{2-} and SO_4^{2-} in quite considerable amounts. In many cases one also observes Na^+, K^+, Cl^- and other trace elements (Fairchild et al., 2000; Treble et al., 2003). All these ions change the ionic strength of the solution, affecting the ionic equilibria. Further the equilibria are changed by the common-ion effect, which occurs if minerals are dissolved which have one ion in common with $CaCO_3$ (e.g. $MgCO_3$ or $CaSO_4$).

Therefore also the solubility of calcite is changed in the presence of foreign ions. Especially in the presence of sulphate and magnesium (ion pair effect) and of a acid like HCl (acid effect) the solubility is increased quite considerably (Dreybrodt, 1988). Of course there are effects which reduce the calcite solubility as well, like the base effect and the before mentioned common-ion effect, but in sum the calcite solubility is increased.

Due to the neglected foreign ions one expects more calcite in the samples than the model predicts. The influence of the trace elements on the carbon isotopes of the carbon in the water via the enhanced calcite solubility is difficult to estimate. For the open system the influence of foreign ions on carbon isotopes is negligible since the reservoir of soil CO_2 is much more important for the isotopic composition of the carbon in the water than the dissolved limestone carbonate[7]. Therefore, the isotopic composition of the water should not be changed here, even in presence of the foreign ions, which increase the calcium solubility. In addition, in the closed system increasing calcite dissolution is supposed due to the foreign ions. This effect under

[7]Also the overall pCO_2 is not remarkably increased with an ongoing limestone dissolution.

closed conditions will tend to decrease the ^{14}C activity and to increase the δ^{13}C content of the carbon in the solution.

Secondly the model does not include prior calcite precipitation. Prior calcite precipitation occurs in the karst area before the saturated solution penetrates into the cave. In gas filled voids of the karst pCO_2 is lower than that of the equilibrium state of the saturated water. Therefore some CO_2 degas from the water and calcite precipitates before the water enters the cave. This degassing leads to an increased δ^{13}C and ^{14}C content. If this process is present in a cave system, the model will predict (slightly) lower values for the carbon isotopes in the drip water.

The third point is the choice of the open to closed dissolution system ratio. Other successions of open to closed system behaviours, than explained in Section 3.3, are imaginable. Calculations of the case of the volume divided water flow reconnecting before the water enters the cave leads to a significantly too low ^{14}C model output compared to measurements on drip water. For the other proposed limestone dissolution behaviours the impact on the carbon isotopes can not be estimated.

Furthermore, processes like additional carbon exchange between the karst and the solution due to longer residence times in the karst or degassing of drip water in the cave are not included. The model is kept as simple as possible, because with a more sophisticated model, a larger number of parameters have to be introduced, which are not known.

5.2.4 Model description

The drip water model consists of plenty of small functions to keep the whole model as clearly arranged as possible. In Figure 5.7 all functions are shown in a flow chart. The single functions in the chart are connected in the right order of use.

The model consists of four major paths, which represent different purposes. They use the same functions for the calculation of the limestone dissolution but in slightly different arrangements. In the *main1* function[8] the calculation modus is split into the four modes. The modes represent a demonstration mode (**pCO_2** and the corresponding string of Figure 5.7), a calculation of carbon isotopes in drip water mode (**datasearch** and the corresponding string of Figure 5.7), an inverse method to calculate the soil pCO_2 from measured carbon isotopes in cave drip water (**invers** and the corresponding string of Figure 5.7) and an inverse method to determine the soil pCO_2 from measured carbon isotopes in stalagmites (**inverskalk** and the corresponding string of Figure 5.7). A short, single function description is given in the following items.

- **main1** This functions starts the whole program. The function reads the *parameter.txt* file to set the major options, e.g. temperature of the cave, open to closed ratio or mode of calculation. Then the function *temperatur* is called with the following decision of the mode the model is supposed to run.

- **temperatur** Calculation of carbon isotope fractionation factors, equilibrium constants and parameters A and B for the Debye-Hückel equation (Eq. 5.12) are calculated at the temperature of the cave. The function is able to use temperature dependent values published in different papers (Hendy, 1971; Mook and de Vries, 2000; Dreybrodt, 1988).

[8] *main1* is to call in the Matlab command window to run the model. Paths selections and other options are to set in the concerning functions or text files.

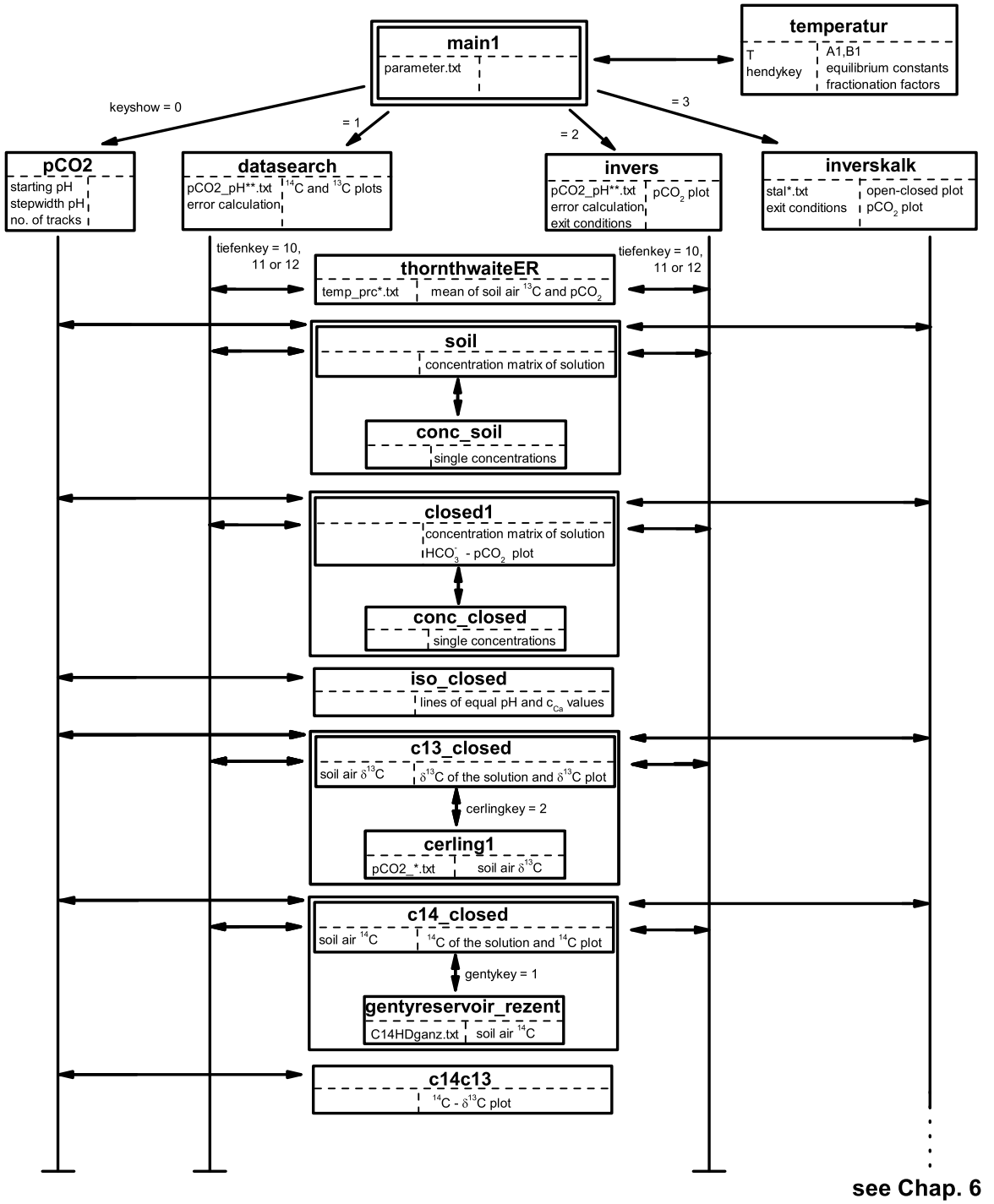

Figure 5.7: Flow chart of the drip water model. Only the limestone dissolution functions are shown here. Each rectangle symbolises one function (name of the function in bold type) and its input data (in the left dashed "sub-rectangle"). The input data are given by extern text files or by parameters defined in the code like limits of the search algorithms or resolution declarations. It is possible to use the pre-set values or to change them according to values of the different cave systems. The output of the function or its purpose is written in the right dashed "sub-rectangle" of each major rectangle. Arrows indicate how the functions are connected and in which order a function calls another one. In Chapter 6 the model for the stalagmite is proposed, which complete the "inversekalk" module path.

- **pCO$_2$** Prepares everything to run the model in the demonstration mode. Here the number of limestone dissolution tracks, which shall be calculated, and the starting pH value of the solution with highest pCO$_2$ are defined. The other "water packages" charged with less pCO$_2$ are calculated automatically by the chosen pH step width.

- **datasearch** Orders the subfunctions to calculate the carbon isotopes of a water parcel with a definite amount of soil air CO$_2$ and a pH value of the saturated water entering the cave. Additionally, an error estimation can be applied. A text file (in Fig. 5.7 the name is *pCO2_pH**.txt*) with information about the carbon isotope measurements, soil pCO$_2$ and soil δ^{13}C as well as the drip water pH value is read, to allow the model to start the calculations. In comparison with the drip water measurements the results of the carbon isotope simulation are plotted in graphs.

- **invers** Reverse of *datasearch* by applying a search algorithm. Orders the subfunctions to calculate the soil air pCO$_2$ of given ^{14}C, δ^{13}C data pairs of drip water. The function needs the same file of data as function *datasearch*. The exit conditions are determined and an error estimation can be executed.

- **inverskalk** The first part is the same as the *invers* function. The module orders the subfunctions to calculate the soil air pCO$_2$ of measured ^{14}C, δ^{13}C data pairs of a stalagmite. Then *pco2band* is called and the results for pCO$_2$ are saved and plotted. For more information see Section 6.2.

- **thornthwaiteER** The subfunction needs a monthly resolved temperature-precipitation-pCO$_2$-δ^{13}C text file to calculate the water amount resisting in the soil. For that purpose the formula of Thornthwaite (1948) is used. Then an annual weighted mean for soil pCO$_2$ and δ^{13}C is calculated. This subfunction is only necessary for the drip water modes (*datasearch* and *invers*) and can be disabled by not choosing "1" for the cerlingkey in *parameter.txt*.

- **soil** Prepares variables for the concentration calculation in *conc_soil* and saves the results of this subfunction.

- **conc_soil** Calculates the chemical equilibrium of the participating ions in the soil water under the assumption that no calcium is available. An iterative process between the concentrations and the activities is applied here. If necessary it is possible to change the accuracy by redefining the break-off condition (the pCO$_2$ difference of two successive steps).

- **closed1** Prepares variables (for a successive increasing pH value) for the concentration calculation in *conc_closed* and saves the results of *conc_closed* until calcium saturation is reached. Further a HCO_3^-–pCO$_2$ plot is drawn here.

- **conc_closed** Calculates the chemical equilibrium of the participating ions in the karst water under the assumption of an open or closed dissolution system (choosing "0" or "1" for "dcf" in *parameter.txt*). An iterative process between the concentrations and the activities is applied. If necessary, it is possible to change the accuracy by redefining the break-off condition (the calcium concentration difference of two successive steps).

- **iso_closed** This subfunction works only in demonstration mode of *pCO2*. The module searches for values of equal pH values and calcium concentrations among the different

water parcels during the limestone dissolution, and plots the resulting line into the HCO_3^-–pCO_2 graphic made by *closed1*.

- **c13_closed** After determining the soil $\delta^{13}C$ content (via cerlingkey in *parameter.txt*), the $\overline{\delta}^{13}C$ content of the carbon in the solution of each dissolution step is calculated. A plot of the $\delta^{13}C$ content over pCO_2 of the saturated solution is drawn.

- **cerling1** If cerlingkey is equal to "2" in *parameter.txt* the soil $\delta^{13}C$ content, needed in *c13_ closed*, is calculated after Cerling (1984). For this function it is necessary to know the CO_2 content of the atmosphere and pCO_2 value at a certain depth in the soil.

- **c14_closed** After determining the soil ^{14}C activity (via gentykey in *parameter.txt*), the ^{14}C activity of the carbon in the solution of each dissolution step is calculated. A plot of the ^{14}C activity over pCO_2 of the saturated solution is drawn.

- **gentyreservoir_rezent** The soil ^{14}C activity is determined with the calculated soil reservoir parameters (Sec. 4). It is necessary to provide the atmospheric radiocarbon content (e.g. the combined records of Reimer et al., 2004; Levin and Kromer, 2004) from at least two centuries before the stalagmite starts to grow (for *inverskalk*) until 2007 AD (for the drip water modules).

- **c14c13** This subfunction is needed in the demonstration mode to plot the ^{14}C activity over the $\delta^{13}C$ content of the carbon in the saturated solution.

The functions describing the carbon isotopes during calcite precipitation, additionally included in *inverskalk*, are explained in Section 6.2. In the following all main variables used in the program are introduced.

- **c(k,i,l)** contains the data for the concentration of all participating ions during the limestone dissolution.
  - k ∈ [1,2,3,4,5,6] stands for the different ions
    - k=1 → pH value [ ];
    - k=2 → pCO_2 [% atm];
    - k=3 → concentration of OH^- [mol/l];
    - k=4 → concentration of HCO_3^- [mol/l];
    - k=5 → concentration of CO_3^{2-} [mol/l];
    - k=6 → concentration of Ca^{2+} [mol/l];
  - i ∈ [1,2,...,imax] gives the number of dissolution steps the model simulates until saturation is reached. imax depends on the pH step width, the ratio of the open to closed dissolution system and the soil pCO_2. The soil pCO_2 is the reason why the matrix is filled up with zeros in the demonstration mode.
  - l ∈ [1,2,...,lmax] gives the number of the water parcels for which the limestone dissolution is calculated (only for the demonstration mode, l is 1 for all other modes).

- **z(k,m,l)** contains the data for the concentration of all participating ions during the precipitation of calcite (only for *inverskalk*). k, l are the same as in c(k,i,l) and m gives the number of degassing steps until the solution is in equilibrium with the pCO_2 value of the cave atmosphere.

- **c13_t(i,l)** is the δ^{13}C content of the solution.
- **c13_caco3(i,l)** is the δ^{13}C content of the first calcite to be precipitated of a solution with a δ^{13}C content of c13_t(i,l).
- **c14_t(i,l)** is the ^{14}C activity of the solution.
- **c14_caco3(i,l)** is the ^{14}C activity of the first calcite to be precipitated of a solution with a ^{14}C activity of c14_t(i,l).

5.3 Results of the drip water model

This section documents the application of the model. It is described how the model performs in the "demonstration" mode. A further application is to real drip water samples and the comparison of the modelled carbon isotope values with the measurements. The last application is the "inverse" method. With this approach it is possible to calculate the pCO_2 value of the soil above the cave using the measured carbon isotopes. It is not a real inverse method, because the model simulates all processes in a forward manner until the measured drip water values are reproduced.

5.3.1 Performance of the model in "demonstration" mode

To demonstrate the connection between ^{14}C and ^{13}C of the saturated solution in different open to closed system ratios it is necessary to calculate the concentrations participating in the calcite dissolution process under different soil pCO_2 values. In Figure 5.8 the bicarbonate ion concentration over the soil pCO_2 is shown. For seven water parcels charged with a different soil pCO_2 value the behaviour of the closed dissolution condition (the curved grey lines) is redrawn after Hendy (1971) while using more recent equilibrium constants mentioned in Section 5.2. Additionally the pathway of the limestone dissolution behaviour in the open system (the straight grey lines) is plotted. The starting pCO_2 values are the same as for the closed system. The graphic shows in the bottom part of each grey and blue line the pure water charged with carbonic acid without any calcite. The grey lines represent the calcite dissolution process of the limestone until saturation with respect to calcite is reached. This state is represented by the upper part of the grey lines, which can be connected through one straight line. The red lines, going from down left to up right, show the "iso-pH-lines" of the dissolution process. Some corresponding pH values can be found on the left end of each red line. Additionally the concentration of calcite (0.1 mmoles/l and 1 mmoles/l) dissolved in the solution is plotted, shown by the dashed black horizontal lines. The dashed blue lines represent the case for dissolution in the open system for 50 % of the saturation index following by 50 % of limestone dissolution in the closed system.

The behaviour of an open dissolution system followed by a closed one defines a border with a matrix change. Above the border there are enough voids in the limestone, which exist maybe due to advanced limestone dissolution in the past, to allow a steady gas exchange with the soil. Below the border such voids do not exist, which would allow contact to the soil air.

The isotopic composition of the carbon of the solution can be calculated at any single pH-value on each blue or grey line (open system: Equation 5.21 and closed system: Equation 5.22 for δ^{13}C and ^{14}C). In particular that means that the isotopic carbon composition of the saturated solution in any dissolution system is known. The δ^{13}C and ^{14}C values of the saturated solution of different pCO_2 are plotted in Figure 5.9.

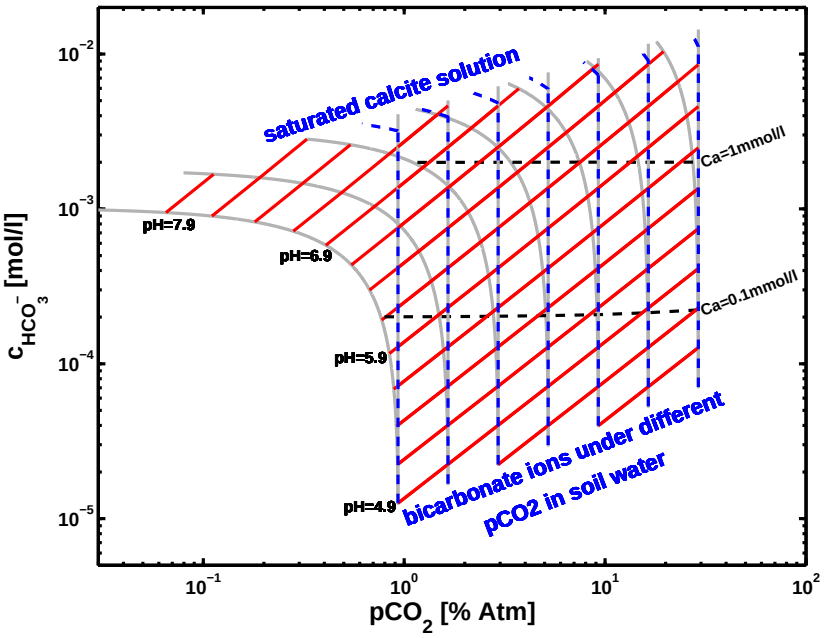

Figure 5.8: Pathways of bicarbonate concentration and partial pressure of pCO_2 during the limestone dissolution (T = 10°C). For demonstration purposes a wide range of soil pCO_2 was applied.

The open and the closed system behaviours are similar to the ones published by Hendy (1970). The upper blue line shows the isotopic composition of a calcite saturated solution in an open system and the lowest blue line the one of the closed system. Cases, situated between the completely closed and completely open condition, are labelled with the open to closed system ratio on the right of each line. For demonstration purposes the model uses following parameters: a temperature of 10°C, a soil air ^{14}C activity of 106 pmC and a soil air $\delta^{13}C$ content of -25 ‰.

Toward the right of each line, the isotopes are calculated with higher soil pCO_2 values. The more heavier the $\delta^{13}C$ isotopic composition is the less pCO_2 is in the soil. The isotopes in the open system show a linear trend with a decreasing behaviour in ^{14}C and $\delta^{13}C$ with increasing pCO_2, caused by the different composition of the participating concentrations and the isotopic fractionation factors. The ^{14}C and $\delta^{13}C$ relationship in the closed system is linear as well. ^{14}C increases with higher pCO_2 values whereas $\delta^{13}C$ decreases at the same time.

In all intermediate dissolution ratios the behaviour of ^{14}C and $\delta^{13}C$ is not linear, which goes conform with a ground water study by Wendt et al. (1967). It is suspect that the cases with a high open dissolution part (from 50 up to 100 %) do not show a big difference in the carbon isotope composition compared to cases with a low open dissolution part. The difference between a complete open to a 50 % open system is in ^{14}C around 8 pmC and in $\delta^{13}C$ around 0.5 ‰. On the other hand the difference between a 50 % open system to a complete closed one is higher than 2.5 ‰ in $\delta^{13}C$ and between 25 and 45 pmC in ^{14}C depending on pCO_2.

The carbon isotope values calculated for intermediate dissolution systems are higher compared to a linear interpolation between the carbon isotopes of the open and the closed system. The effect is due to the dominating isotopic composition derived in the open system, which is characterised by carbon exchange between fluid and gaseous CO_2. This can be understood

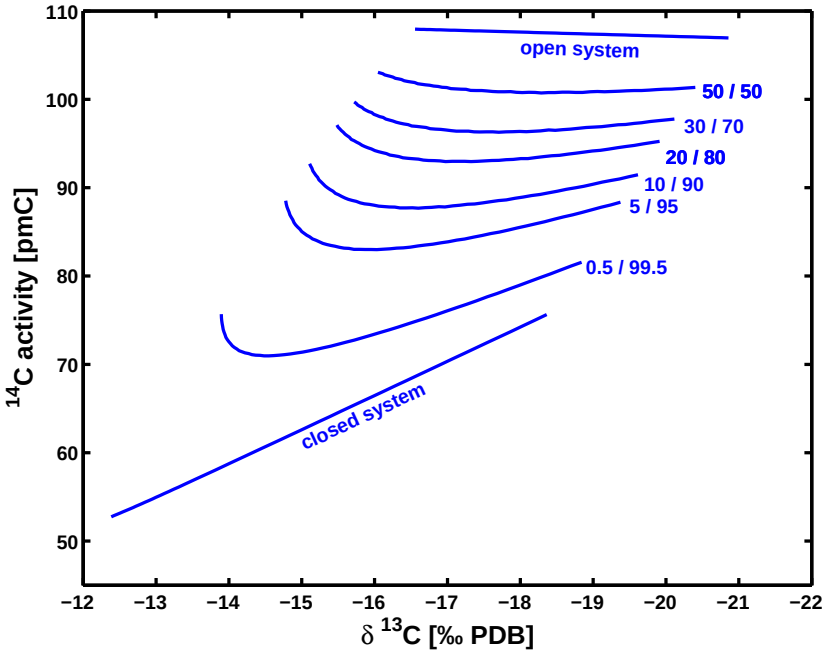

Figure 5.9: Isotopic carbon composition of saturated water with respect to calcite. Plotted are the open and the closed system as well as some intermediate states of the dissolution system (numbers at the right of the corresponding lines, where "30/70" means a 30 % open dissolution system followed by a 70 % closed one). Input parameters: T = 10°C, $^{14}C_{soilair}$ = 106 pmC, $\delta^{13}C_{soilair} = -25$ ‰.

by looking at the pH values and the calcium and carbonate concentration during a pH step. Furthermore, it is important, that for each dissolved calcium ion one carbonate ion is released. During the open dissolution system, occurring at low pH, more carbonate of the calcite will be transferred to bicarbonate, to aqueous dissolved CO_2 or to gaseous CO_2 according to the equilibrium status (described by equations 5.1 to 5.5) than at high pH values, as for example reached during the closed dissolution system. On the one hand in the beginning of the dissolution process the carbonate concentration rises very slowly compared to the calcite concentration. On the other hand the model treats the change between the open to closed dissolution system ratio with respect to the saturation index $k_c = c_{Ca^{2+}} \cdot c_{CO_3^{2-}} \cdot \gamma_{CO_3^{2-}} \cdot \gamma_{Ca^{2+}}$ (see equation 5.10). That means in the 50/50 ratio case, the model jumps from the open to closed dissolution system after 50 % of k_c are reached. So at 50 % of k_c the $c_{Ca^{2+}}$ is bigger than 50 % of the saturated solution and $c_{CO_3^{2-}}$ is smaller than 50 % of the saturated solution. Hereby the activity coefficients are neglected, because their changes are very small. Due to both facts the limit between open to closed system, even in the 50/50 case, is reached when the majority of the calcium is already dissolved. So the light ^{14}C and heavy δ^{13}C values coming from the limestone are exchanged with the carbon isotopes of the soil air. Only the small amount of carbon coming from the limestone into the solution in the closed dissolution system decreases the ^{14}C and increases the δ^{13}C values of the carbon in the solution.

The non-linearity of ^{14}C and δ^{13}C of saturated water derived by intermediate dissolution systems can be explained by the sum of the concentrations of the carbon containing species shortly prior the switch from open to closed dissolution and the amount of calcite dissolved in the closed system. The carbon species of the open system have the typical open case isotope

concentration and the calcium dissolved in the closed system represents the carbon which comes from the limestone which typically has no radiocarbon and $\delta^{13}C$ values around +1 ‰. The ratio of both, calculated for the seven water parcels shown in Figure 5.8, give parable like lines as shown in Figure 5.9.

5.3.2 Performance of the model in "datasearch" mode

In the following the model will be applied to water samples in order to calculate the carbon isotopes and to compare the model output with the measurements.

To apply the model it is necessary to use suitable boundary conditions. The conditions will only define a start point and an end point of the water under investigation. In this case soil pCO_2 is used as the start point and the pH of the drip water, measured in the cave, defines the end point. Figure 5.10 illustrates the working process of the model to simulate the correct isotopic composition of the drip water.

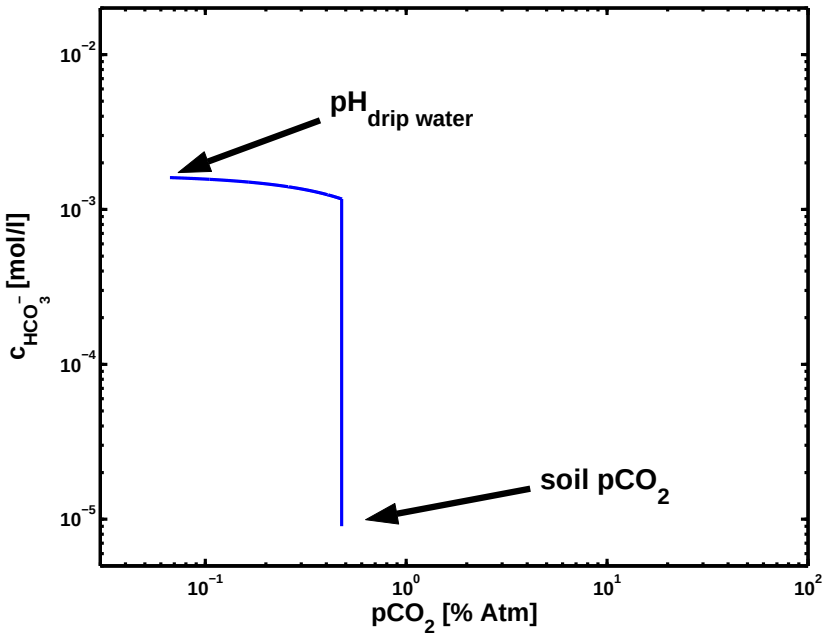

Figure 5.10: The start point for the simulation is given by the soil pCO_2, the end point is marked by the pH of the drip water. The blue line represents the unique solution for the open to closed dissolution system ratio, which joins both significant points. This example represents the condition for drip location ER-G1 in November 2005. For that month a soil pCO_2 of 0.477 % atm (4,770 ppm) and a pH of 8.11 were measured. The model calculates a dissolution system which is to 5.6 % open.

The model first defines the right soil pCO_2 by calculating the concentrations without any calcite in the solution. This is done by varying the starting pH value. Once the pH value is found, which corresponds to the applied soil pCO_2, the program calculates the limestone dissolution by a stepwise increase in pH until the saturation state is reached. First that is done for a certain open to closed dissolution system ratio. If the drip water pH of the simulated solution is not consistent with the measured drip water pH the model changes the open to closed system ratio and calculates the limestone dissolution again with the new ratio. This process is repeated until the pH of the saturated modelled solution fits the measured pH.

It is easy to see, that only one track of limestone dissolution between start and end point is possible (Fig. 5.10). The open part of the dissolution is the same for each chosen open to closed system ratio. However the condition (e.g. pH, concentrations), with which the closed dissolution begins, is different with a changing open to closed system ratio. The condition that only one track can connect the start and the end point is then given by the fact that the closed dissolution system tracks are parallel and do not cross each other.

If the track of limestone dissolution is fixed it is possible to calculate the carbon isotopes (^{14}C and δ^{13}C) along the track. First this is done by using the open isotope calculation (Eq. 5.21) and after the dissolution system switches the closed isotope calculation is applied (Eq. 5.22). Therefore, it is possible to simulate the isotopic composition of the saturated solution. Then these values can be compared to the measured isotopic composition of the drip water.

Before comparing data and model results one constrain has to be mentioned. Soil water, taken at a depth similar to the depth were the pCO_2 is measured, contains already dissolved calcite. This is not considered in the model. If the soil pCO_2 is given to the model, the model is forced to calculate all concentrations in the solution without calcium in the first step. Thereafter it calculates the limestone dissolution.

Since the measurements of soil pCO_2 are performed in the upper part of the soil, one can assume that all calcite, already in the soil water, was dissolved under open dissolution condition. Then the calcite in the soil water does not matter for the simulation, because the condition measured in the soil water will be simulated later within the calculations as long as the open condition, where the soil pCO_2 is meant to be constant, is present.

Drip location ER-G1 For application of the model to drip location ER-G1 an end point given by the pH value of the drip water (Figs. 5.5 and B.5, red triangles) was used. The soil pCO_2 signal (Fig. B.5, blue circles) was weighted by precipitation and evapotranspiration, due to the well mixed water reservoir which is supposed to be in the soil (Sec. 5.1.1). The weighting was done for a three year time period (November 2004 – October 2007), where measurements on soil pCO_2 were performed. The calculated weighted mean is $pCO_{2,soil}$ = 0.477 % atm. This value is used as a starting point throughout the two years of drip water analysis from November 2005 to October 2007.

In addition it is necessary to define the isotopic composition of the soil air. For radiocarbon the mean value is 110.7 pmC (Sec. 4). The δ^{13}C value is determined by weighting monthly soil air δ^{13}C data with precipitation and evapotranspiration as for pCO_2. The mean value is -22.48 ‰.

Figure 5.11 shows the comparison for ^{14}C content between the model output (blue) and the measurements (red). The annual cycle of the measured ^{14}C activity is well reproduced by the model. The two outliers in September and November 2006 are supposed to be due to erroneous determination of drip water pH.

The comparison of the δ^{13}C measurements with the corresponding model output reveals that the model does not perform the calculations as convincingly as for the ^{14}C isotopes. Anyway, the range is well reproduced, an indication for the well-chosen soil δ^{13}C value. The observed small underestimation of the model compared to the measurements can be the result of CO_2 degassing and calcite precipitation occurring when the solution runs downwards the stalactite. It is unlikely that the degassing process is constant during the investigated time interval and therefore single variations of the measurements can not be reproduced by the model. Nevertheless the large trend is visible. The mean difference between the modelled and the measured δ^{13}C values is about 0.5 ‰. Thus the degassing of the water would result in an enrichment in ^{14}C of 0.1 pmC and, thus, is negligible.

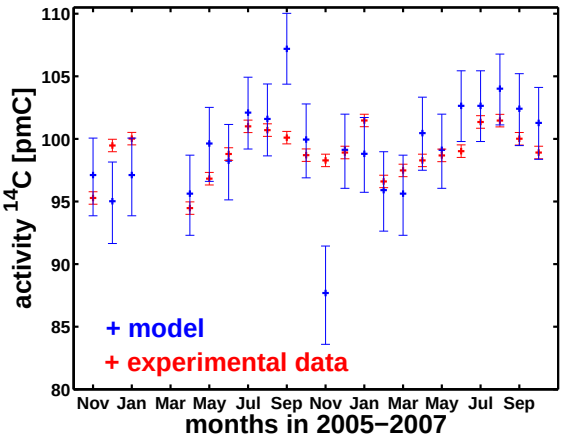

Figure 5.11: Monthly measured ^{14}C data of drip water samples (red) collected on drip place ER-G1 compared to the modelled radiocarbon content of the drip water (blue).

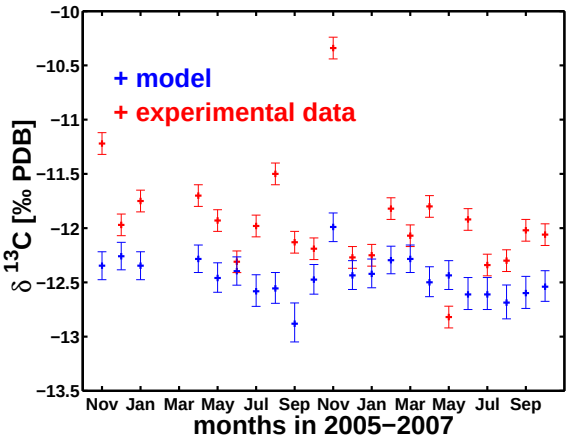

Figure 5.12: Monthly measured δ^{13}C data of drip water samples (red) collected on drip place ER-G1 compared to the modelled δ^{13}C content of the drip water (blue).

Another advantage of the model is the fact that the annual cycle in ^{14}C measurements is reproduced by the model, but the model does not show a seasonal signal in the stable carbon isotope – like in reality. Therefore, the model seems to depict the soil processes well.

A reason why the large annual cycle is seen in ^{14}C and not in the δ^{13}C, is the difference in the isotope content between the single major carbon reservoirs, responsible for the isotopic composition of the drip water. While for radiocarbon the isotopic compositions between the soil air ($\approx$ 108 pmC) and the limestone (= 0 pmC) is rather large ($\approx$ 108 pmC), the difference in δ^{13}C is $\approx$ 12 ‰. This value originates from the limestone (0 to 1 ‰) and the soil air δ^{13}C of roughly -22 to -24 ‰ plus a fraction effect of $\approx$ 10 to 11 ‰ (Mook and de Vries, 2000), due to the transition of gaseous CO_2 to dissolved inorganic carbon. Furthermore, the δ^{13}C isotope is more influenced by degassing processes than the radiocarbon isotope, and hence the annual cycle of the stable carbon isotope originating from the limestone dissolution process is more easyly to disturb.

So even small variations in the open to closed limestone dissolution ratio show clear signals in the radiocarbon, but not in the stable carbon isotope composition. Assuming a mixing system, which changes the contribution of the two participating materials only slightly in two successive months (e.g. from a ratio of 90/10 % to 85/15 %), simple equations for the resulting isotopic composition can be applied (similar to the mixing equation 4.1). The results are shown in Table 5.6.

The ^{14}C values calculated by the model cover the measurements with respect to the estimated uncertainties (Fig. 5.11). For the November sample of 2005 a comparison of the errors introduced by uncertainties of pH, pCO_2 and soil ^{14}C is shown in Figure 5.13. The errors of the model (Fig. 5.11) are calculated under the assumption that the pH measurements of the drip water cause the main error and the error coming from pCO_2 measurement uncertainties is negligible (Fig. 5.13)

The mean estimated error of pH measurements is 0.1, which leads to an uncertainty of drip water ^{14}C of $97.11^{+3.02}_{-2.84}$ pmC. Additionally to that error a typical measurement uncertainty of 0.005 % atm soil pCO_2 results in an error of $97.11^{+0.22}_{-0.17}$ pmC. Combining both error sources, an uncertainty of $97.11^{+3.25}_{-2.95}$ pmC is calculated for the example of November 2005. The fourth

Table 5.6: The calculation results for mixing processes, with the values shown in the table, reveal a rather large difference in the ^{14}C content compared to the small difference seen in the δ^{13}C content. The relative change is approximately the same.

Month	isotope	mixing factor 1	isotopes in soil air	mixing factor 2	isotopes in limestone	mixing composition	difference
1	^{14}C	0.9	108 pmC	0.1	0 pmC	97.2 pmC	5.4 pmC
2	^{14}C	0.85	108 pmC	0.15	0 pmC	91.8 pmC	
1	δ^{13}C	0.9	-13 ‰	0.1	+1 ‰	-11.8‰	0.6 ‰
2	δ^{13}C	0.85	-13 ‰	0.15	+1 ‰	-11.2 ‰	

label in Figure 5.13 concerns the error which arises, in case the absolute soil ^{14}C error is estimated to be 2 pmC. However, due to the assumption of constant soil water conditions, this will lead only to a constant offset of all modelled results. Hence the soil ^{14}C uncertainties were not considered in the calculations.

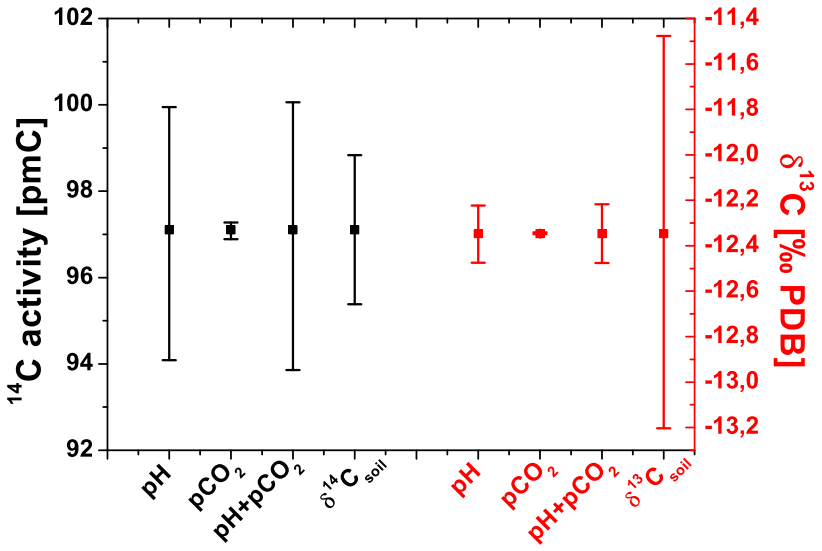

Figure 5.13: The error estimation of single error sources for ^{14}C (black) and δ^{13}C (red). The errors shown in the plot are due to uncertainties of pH of 0.1, of soil pCO_2 of 0.005 % atm (50 ppm), of both combined and of a soil ^{14}C of 2 pmC or soil δ^{13}C of 1 ‰, respectively.

The error estimation for the δ^{13}C values gives -12.35$^{+0.12}_{-0.13}$ ‰, due to pH uncertainty and -12.35$^{+0.01}_{-0.01}$ ‰, due to pCO_2 uncertainties. Combining both uncertainties results in an error of -12.35$^{+0.13}_{-0.13}$ ‰. The error which arises, if the absolute soil δ^{13}C uncertainty is estimated to 1 ‰ is represented by the fourth red label in Figure 5.13. Again this will lead to a constant offset and is not considered in the calculations.

If one also considers errors in the evapotranspiration function and the weighting of pCO_2,

a higher deviation in pCO_2 ($\approx$ 0.1 % atm) is introduced, and hence the errors in the ^{14}C increase. In fact the error introduced by pCO_2 is now comparable to the pH one. The error variation is $97.11^{+3.75}_{-3.75}$ pmC. Combining both error sources, pH and pCO_2, an uncertainty of $96.93^{+7.25}_{-6.11}$ pmC is calculated. A version of the comparison between model and measurements with the more uncertain assumption of mean soil pCO_2 is plotted in Figure B.8 in the appendix.

The model also calculates the open to closed system ratio, in which the water dissolves the limestone. For the investigated two year time period the open to closed system ratio is plotted in Figure 5.14.

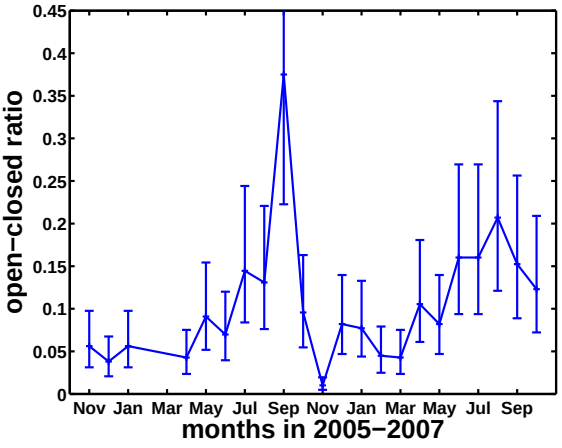

Figure 5.14: The figure represents the open to closed dissolution system of the limestone carbonate derived by the model for drip location ER-G1, using the mean weighted soil pCO_2 of 0.47 % atm and the measured pH of the drip water. Zero in the open-closed ratio means that the system is completely closed and one represents a completely open system.

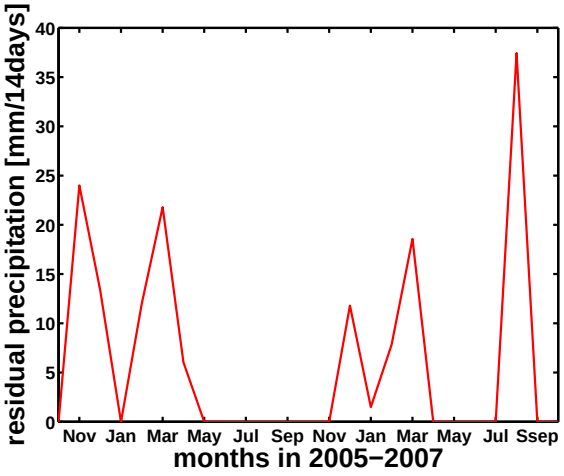

Figure 5.15: The calculation results of the available water (residual precipitation) in the soil within two weeks before sample collection reveals dry summers and autumns and wet winters and springs. August 2007 seems to be an exception due to high precipitation rates in the two weeks before sample collection.

The errors for the single points correspond to the above-mentioned uncertainties of drip water pH and soil pCO_2. The winter and spring months in both years show more closed conditions than the summer and autumn months. As in Figure 5.11 the points for September and November 2006 are supposed to be outliers due to the unusual values of drip water pH. More closed conditions would mean for the Ernesto soil-cave system, that the voids in the soil and karst are more clogged by water than in the other time of the year.

This result in Figure 5.14 indicates, in the context of limestone dissolution in the Ernesto soil-cave system (Sec. 5.1.1), that in the winter and spring months the soil contains more water than in the summer and autumn months. Figure 5.15 shows the available water in the soil over the sampling period. The water in the soil is calculated by precipitation minus evaporation calculated after Thornthwaite (1948). Due to the study of Borsato (1997), who found that the soil residence time of meteoric water, feeding drip location ER-G1, is supposed to be less than two weeks, the water content in the soil is calculated only with the rain amount fallen within the two weeks before sample collection.

Comparing Figures 5.14 and 5.15 confirms the assertion that a more open system goes conform with dryer conditions in the soil. On the contrary a more wet soil is responsible for a limestone dissolution occurring in a more closed system. Of course Figure 5.15 is only a rough approximation of the soil water availability. Evaporation is difficult to calculate and a many evaporation formulas exists (e.g. Thornthwaite, 1948; Penman, 1948; Haude, 1954; Hamon, 1961). For this thesis the Thornthwaite formula is used, because it is an empirical technique, which does not require amounts of data. Despite uncertainties in evaporation calculations the general relation in Figures 5.14 and 5.15 is correct.

Additionally it is possible to compare the calcium concentration of measurements on drip water with the model output. The problems in calculating the calcium concentration are foreign ions introduced in the solution by minor and trace elements. Depending on the foreign ion composition this results most likely in increased calcium solubility. Hence the negligence of foreign ions in the model can explain the offset observed in the comparison between measurements and model output (Fig. 5.16).

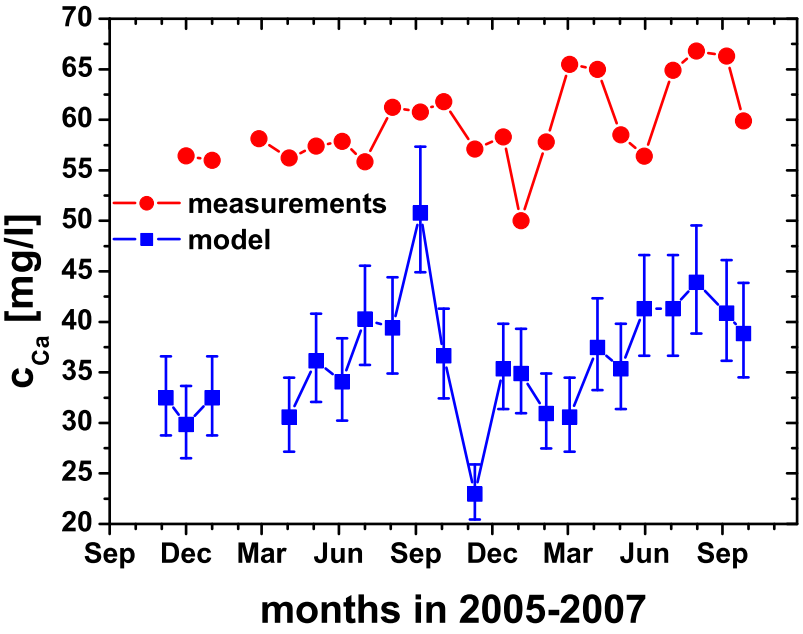

Figure 5.16: The model results for the calcium concentration (blue) are around 25 mg/l lower compared to the measurements (red). Furthermore, the comparison shows that the short-term trend (single points, from month to month) is not reproduced. Nevertheless the long-term trend seems to fit. Therefore, a correlation of R = 0.42 (p = 0.08) between both time series exists – excluding the two model outliers of September and November 2006.

The magnitude of calcium concentration is not reproduced well (Fig. 5.16). However, this is expected, because minor and trace elements are thought to change the solubility of the solution. The short-trend is not seen in both time series in Figure 5.16 as well. The fact, that the concentrations of trace and minor elements vary around a mean value within the

two years of investigation (Figure B.10 in Appendix B) explains that finding. Nevertheless, the overall trend is seen in both calcium concentration time series in Figure 5.16. Thus even with the negligence of foreign ions, the reproduced long-term trend shows how well the model works for ER-G1.

Drip location ER-76 In contrast to ER-G1 interpreting of model results from drip water of location ER-76, which corresponds to the stalactite feeding stalagmite ER-76, is more complex. The drip rate of ER-76 is much lower than the rate of ER-G1 and hence the drip water was collected over a whole month to get enough water for ^{14}C analysis. Further, Borsato (1997) found that the water feeding ER-76 has a soil residence time of about two month. The boundary conditions used for the carbon isotope simulations of ER-76 are the same ($^{14}C_{soilair}$, $\delta^{13}C_{soilair}$, $pCO_{2,soilair}$). Only the drip water pH is changed according to the measured values for ER-76 (Figs. 5.5 and B.5, black squares). The comparison of the carbon isotopes in the drip water with the model results and the measurements are shown in Figures 5.17 and 5.18.

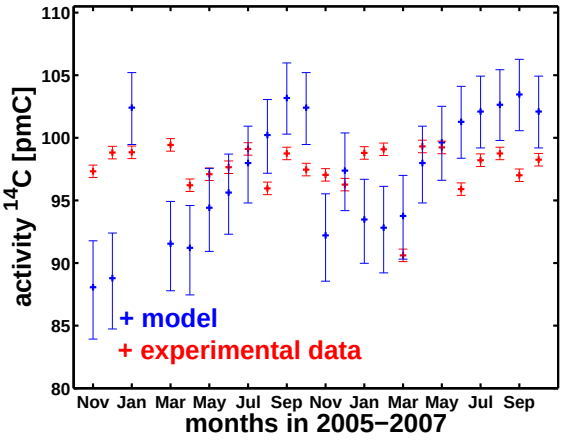

Figure 5.17: Monthly measured ^{14}C data of drip water samples (red) collected on drip location ER-76 compared to the modelled radiocarbon content of the drip water (blue). The calculated range of the model is consistent with the measurements but the amplitude of the annual cycle is overestimated.

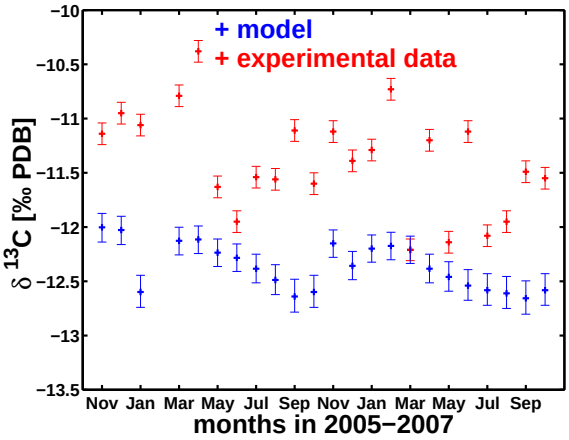

Figure 5.18: Monthly measured $\delta^{13}C$ data of drip water samples (red) collected on drip location ER-76 compared to the modelled $\delta^{13}C$ content of the drip water (blue). The calculated values are more underestimated than in the case of ER-G1. As for ER-G1 single data points do not fit.

The error calculation for Figures 5.17 and 5.18 is equal to those explained for ER-G1. The errors, arising by soil air isotope uncertainties, are not included.

Although the model simulates a well-pronounced annual signal for the ^{14}C isotopes, the cycle is not convincingly developed in the radiocarbon measurements. In general the range of the values, the model calculates, is correct, but the difference from maxima to minima is to large compared to the measurements.

Figure 5.1, where the radiocarbon measurements of the drip water of both drip locations, ER-G1 and ER-76, are plotted, shows that the annual cycle of the ^{14}C activities for ER-76 is more attenuated than the values for ER-G1. The attenuation of the ^{14}C signal in ER-76 drip water compared to the model and to ER-G1 drip water is very likely due to the enlarged residence time of the water in the soil and karst system. Nevertheless the responsible process is not clearly defined. The limestone dissolution occurs as described in Section 5.1.1 and

creates a pronounced seasonal signal. It is proposed that isotope exchange of the saturated solution with dead carbon of the karst is very likely present, due to the enlarged residence time. Alternatively, if the isotopic exchange occurs mainly in the soil, the exchange takes place with an almost atmospheric ^{14}C composition. So the isotopic exchange is superimposed on the seasonal signal in a way that the range of the ^{14}C signal is attenuated.

A possible approach to explain the attenuation by the enhanced soil residence time could be that during dry periods in summer and autumn (Fig. 5.15) the isotope exchange between solution and limestone is more important than during wet conditions. That would decrease the ^{14}C content of the drip water. In wet seasons the isotope exchange between solution and soil CO_2 is assumed to be more important (although carbon exchange between solution and limestone is also present) at large residence times of the soil water. Under these conditions the expected ^{14}C values of the drip water are higher.

This would be in agreement with the assumption of the emerging ^{14}C signal. Drier conditions are responsible for higher ^{14}C values in the carbon of the drip water (more open conditions). If the soil residence time of water is large enough, dry conditions are also responsible for enhanced carbon exchange in the karst and hence for a lowered ^{14}C value. For wet conditions it is inverse. Under wet conditions a more closed system is responsible for low ^{14}C values in the drip water. On the other hand, the water in a filled reservoir, due to much precipitation, has more time to exchange carbon within the upper soil layers. Hence, the low values were enriched in radiocarbon again. Therefore, the signal is attenuated.

The drip water model does not include an extra isotope exchange module. Hence, it can not simulate the right carbon isotope values. Nevertheless the model calculates a seasonal cycle, which is contributed to the fact, that the pH value stays constant during exchange processes. Therefore one can argue, that the model calculates the carbon isotopes in the solution, if no exchange processes occur.

The isotope exchange has some consequences for the δ^{13}C content as well. Assuming isotope exchange is responsible for variations of the carbon isotopes an increase in the δ^{13}C content should occur during dry periods, when exchange happens in the karst. A decrease should occur during wet periods with a more important exchange in the soil area. The measured δ^{13}C values scatter and no clear annual cycle is observed (Fig. 5.18) like for ^{14}C (Fig. 5.17) due to the fact that δ^{13}C values are easier to change by degassing effects in the cave than ^{14}C activities.

The δ^{13}C content of the drip water measurements is underestimated by the model (Fig. 5.18). As for drip location ER-G1 single data points can not be reproduced by the model for ER-76. The reasons here are the same as given for ER-G1. For ER-76 the underestimation of the δ^{13}C values is even higher than for ER-G1 due the enlarged sampling time and additional degassing. This effect does not have large impacts on the ^{14}C content.

A comparison of the calcium concentration in drip water and measurements is not possible, because on this drip location no measurements of anions and cations were performed. The model again calculated the open to closed system ratio of drip location ER-76 and, hence, it is possible to compare the dissolution system ratios of ER-G1 and ER-76 (Figs. 5.14 and 5.19).

For both drip locations, ER-76 and ER-G1, a more open dissolution system is simulated in summer and autumn months and a more closed situation in winter and spring. So the open to closed dissolution ratio of both drip locations goes conform with each other and to the calculation of the available water in the soil. That is an encouraging result, because in the same cave system similar processes are assumed to occur in the soil above the cave. The open to closed system ratio is not exact the same in both simulations, because the water takes

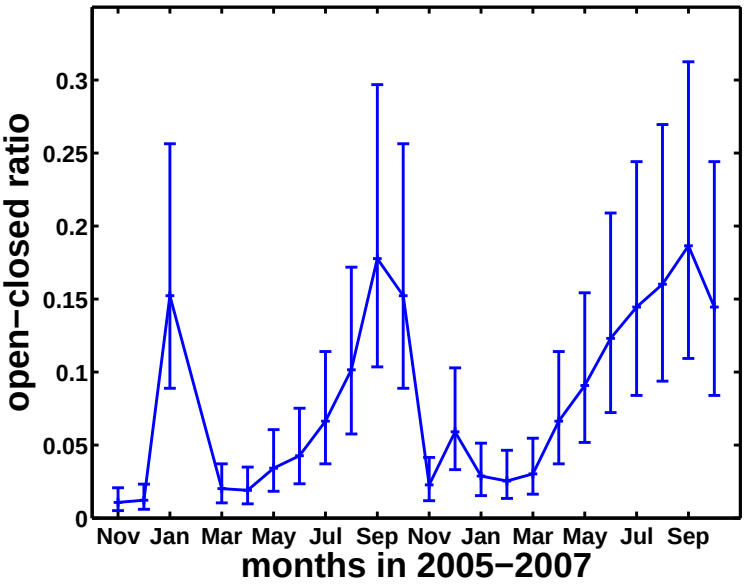

Figure 5.19: This figure represents the open to closed dissolution system of the limestone carbonate derived by the model for drip location ER-76, using the mean weighted soil pCO_2 of 0.47 % atm and the measured pH of the drip water. The value "0" in the open-closed ratio means that the system is completely closed and "1" represents a completely open system. Error calculation as for ER-G1.

different pathways through the soil. Therefore, it can be noticed that the open to closed ratio is in winter and spring more closed in ER-76 than in ER-G1 and in summer and winter the ratio is comparable in both simulations.

In summary the deviations in ^{14}C and $\delta^{13}C$ between the model and the measurements seem to be due to the two month residence time in the soil of the water feeding ER-76 and due to degassing effects in the cave during the one month of sampling collection. Both processes are not included in the drip water model. This results in deviations between measured carbon isotopes and those calculated by the model. The coherence in the open to closed dissolution system ratios between ER-G1 and ER-76 shows that the model performs well in this respect.

Drip location Bu-TS2 In Bunker cave other processes are responsible for the carbon composition of the drip water. Drip location Bu-TS2 is thought to include a prior precipitation effect (pers. comm. A. Schröder-Ritzrau) and a strong CO_2 degassing process is present there (pers. comm. D. Scholz, Tab. 5.2). This degassing process is especially important for the drip water isotope composition due to a sample collection during a whole month.

Because for drip location Bu-TS2 it is supposed that the soil signal is maintained by processes occurring in the karst, variable soil air $\delta^{13}C$ (Fig. B.6) and soil pCO_2 were applied to the model, as well as the monthly measured drip water pH values (Fig. 5.20).

If soil air $\delta^{13}C$ and soil pCO_2 vary throughout the year and hence the corresponding $\delta^{13}C$ values in the water as well (Fig. B.6), the soil radiocarbon content is supposed to vary, too. No data are available on the soil ^{14}C content above the Bunker cave. No analysis was performed for soil air ^{14}C. A "tool" for estimating soil air ^{14}C from a stalagmite as for Ernesto cave is missing. Hence for soil ^{14}C a constant value of 108.6 pmC is chosen. Further the ^{14}C activity

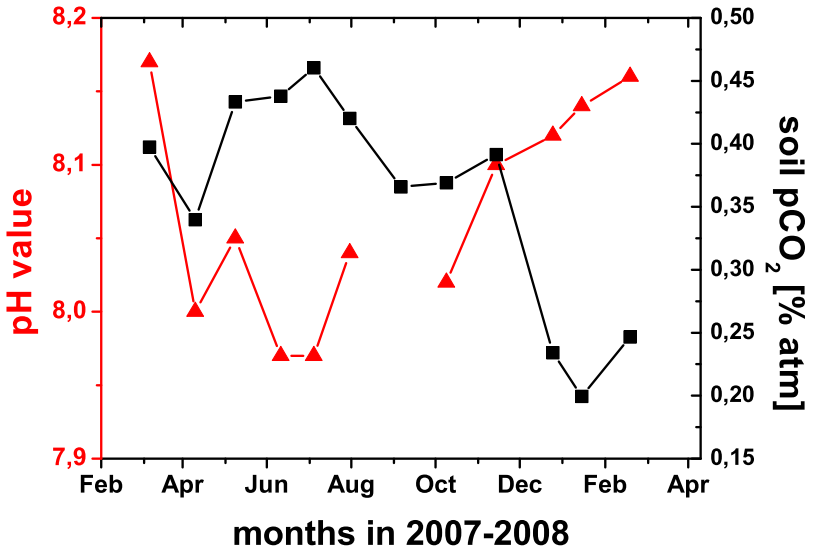

Figure 5.20: Soil pCO_2 of 25 cm soil depth (black squares) and drip water pH values (red triangles) used as input parameters for the simulation of carbon isotopes in the drip water of location Bu-TS2.

is certainly not constant over a full year. The contribution to the total soil CO_2 differs in each season. In winter, for example, it is very likely that most of the total soil CO_2 comes from the old reservoir due to dormant vegetation. In summer the vegetation is active and the root respiration is high. Hence the CO_2 coming from the young reservoir is more important.

Figures 5.21 and 5.22 show the comparison between the measured ^{14}C activity and δ^{13}C content with the modelled values. The modelled ^{14}C activities of each month are near the measured values. Even the trend seems to fit from March to November 2007. The modelled ^{14}C values of the three winter months (Dec, Jan, Feb) are around 5 pmC to high compared with the measurements. The offset could arise, if the soil ^{14}C content is significant lower in winter than in the other months. But even within these three samples the trend fits. If the soil air ^{14}C has two rather constant levels, one winter level and one for the rest of the year, the model reproduces small variations of drip water ^{14}C by the applied boundary conditions for soil pCO_2 and drip water pH. So maybe it is sufficient to describe the soil air ^{14}C throughout the year by two levels. One for the winter months, when the soil ^{14}C level is around 103 - 104 pmC and one level for the rest of the year at around 108.6 pmC. The last value is applied for the simulations for the whole year (Fig. 5.21). If that is the case, it can be supposed that the limestone dissolution system supports the two level soil air ^{14}C content.

Though degassing and prior precipitation effects are present, they have only minor consequences for ^{14}C but are clearly observable for δ^{13}C. The modelled drip water δ^{13}C content follows the trend of the measured samples (Fig. 5.22). Both time series show higher values in the cold months and more negative values in the warm months. The large offset of 4 - 5 ‰ is very likely due to prior calcite precipitation and degassing effects as already mentioned in Section 5.1. Both processes can differ in their strength on an intermonthly time scale result-

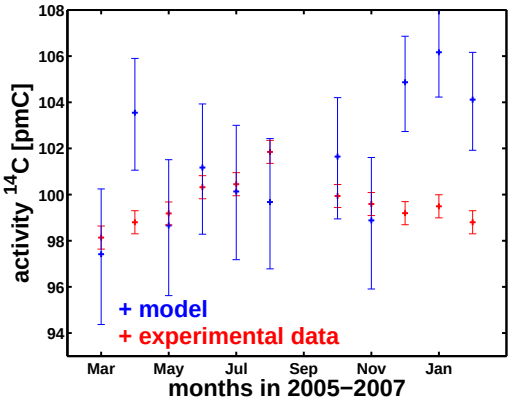

Figure 5.21: Monthly measured ^{14}C data of drip water samples (red) collected on drip location Bu-TS2 compared to the modelled radiocarbon content of the drip water (blue).

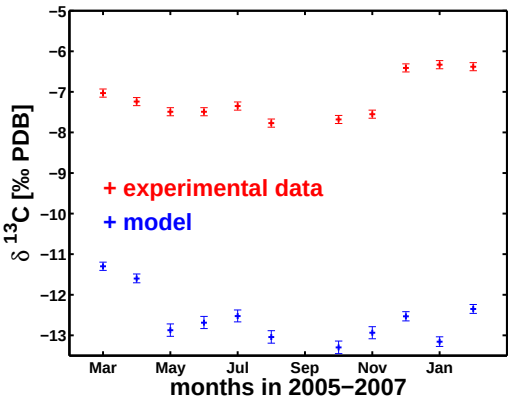

Figure 5.22: Monthly measured δ^{13}C data of drip water samples (red) collected on drip location Bu-TS2 compared to the modelled δ^{13}C content of the drip water (blue).

ing in different varying drip water δ^{13}C. Nevertheless the stable carbon isotope modelling of this drip location shows how well the model simulates the limestone dissolution process. The time shift for water from the soil to the cave of this drip location seems to be smaller than one month and the offset introduced by prior calcite precipitation and degassing is roughly constant within the year of investigation.

The errors of the modelled carbon isotopes are calculated as explained for drip location ER-G1. In this example the uncertainty introduced by the soil carbon isotopes is not included as well.

Furthermore, the open to closed system ratio is studied within the year of investigation at this drip location. Figure 5.23 shows the simulated ratio of drip location Bu-TS2.

In the limits of the errors there is no trend visible. It seems that the open to closed dissolution behaviour is nearly the same within the year of data collection only in December to February a slightly more open system is present. That explains the high ^{14}C values during that time. Unfortunately it is not possible to compare the open to closed ratio with the available water in the soil, because up to now there are not enough precipitation and temperature data available to build a time series.

The last point in the comparison part for this location is the comparison with the calcium dissolved in the saturated solution (Fig. 5.24). The comparison of the calcium concentration reveals a large offset of about 40 mg/l. The offset is in the order of the values calculated by the model and is, as for drip location ER-G1, not constant with time. That is due to the fact, that other elements in the solution change the concentration as well (Fig. B.11). Especially the most important ion sulphate, besides calcium, varies with time. Nevertheless, a certain parallelism is observed in both time series of the calcium concentration.

The offset of calcium concentration in Bunker cave is much larger than the one observed at Ernesto cave because the amount of ions, thought to increase the solubility of the solution is much higher than for ER-G1 (compare also Figures B.10 and B.11). Especially the SO_4 content is very high with a concentration comparable to the calcium content. Because SO_4 is supposed to increase the solubility the high sulphate concentration explains the large offset between calcium measurements and model output.

In summary the limestone dissolution model can be well applied for this drip location as

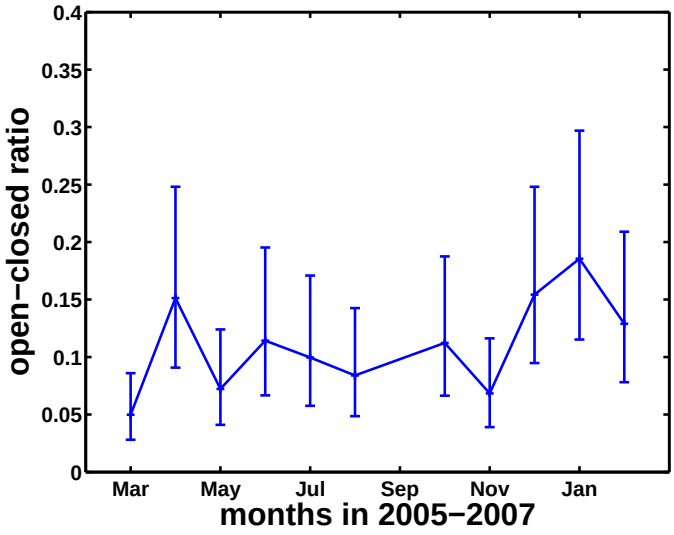

Figure 5.23: This Figure represents the open to closed dissolution system of the limestone carbonate derived by the model for drip location Bu-TS2, using the soil pCO_2 values and the measured pH of the drip water as shown in Figure 5.20. The value "0" in the open-closed ratio means that the system is completely closed and "1" stands for a completely open system. The errors for the single points correspond to the mentioned uncertainties of drip water pH and soil pCO_2 already explained for ER-G1.

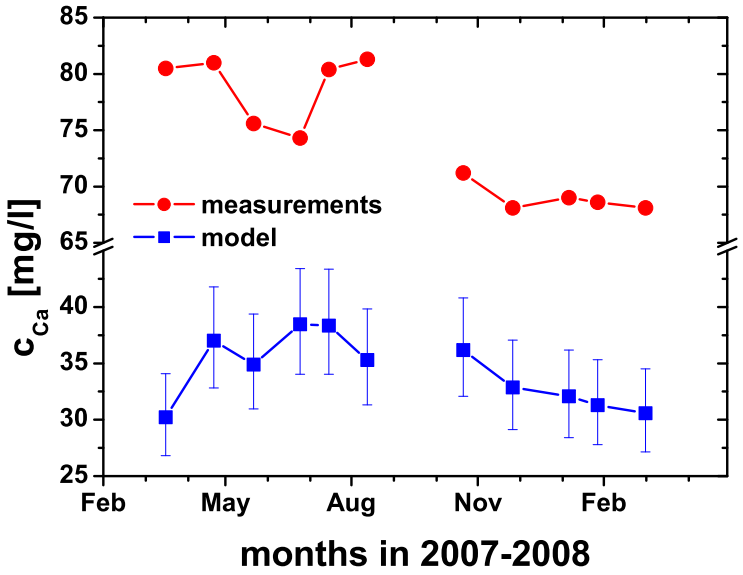

Figure 5.24: The comparison of the calcium concentrations in the drip water of location Bu-TS2 (red circles) and the corresponding model output (blue squares) reveals a large offset (about double the amount of the simulated calcium concentration).

for ER-G1. However, one has to consider the additional effects, which are not included in the model. The change of the limestone dissolution system has a much lower influence on this drip location than on the drip sides of the Ernesto cave.

5.3.3 Performance of the model in "inverse" mode

The model can also be used in inverse mode. With the measured carbon isotope data of the carbon dissolved in the drip water it is possible to derive the soil pCO_2 above the cave. The uniqueness is given by the carbon isotope behaviour of saturated drip water (Fig. 5.9). The blue lines in Figure 5.9, which represent different open to closed ratios, do not cross.

The measured carbon isotope data pairs of the drip water represent exactly one open to closed dissolution system ratio. The ^{14}C and $\delta^{13}C$ pair can be attributed to concentrations of the ion species dissolved in the water. Therefore the concentrations can be traced back from the calcite saturated solution to the initial conditions and, hence, to the soil pCO_2. So for paired ^{14}C and $\delta^{13}C$ values, only one solution for the soil pCO_2 is possible. The drip water model is no inverse model. Therefore, a computationally intensive search algorithm was applied, running the forward model with successive changing open to closed system ratios and soil pCO_2 values until the measured carbon isotopes values agreed with the measured ones.

Figures 5.25, 5.26 and 5.27 show the results of the modelled soil pCO_2 for the three investigated drip locations in comparison to the measured soil pCO_2 values.

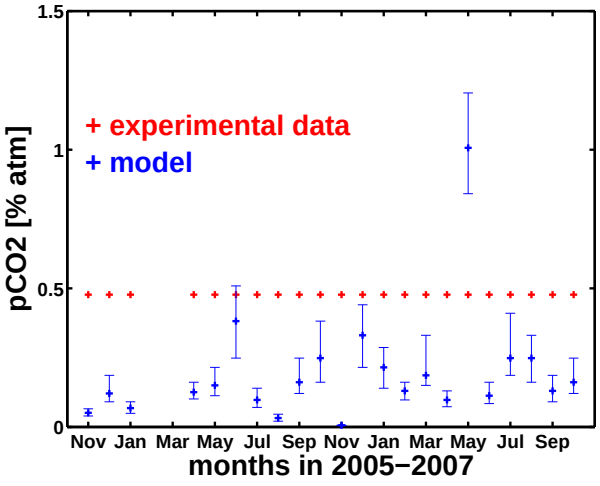

Figure 5.25: The comparison of mean weighted (red) and modelled (blue) soil pCO_2 for ER-G1 reveals an underestimation of the modelled values. The application of the weighting of soil pCO_2 was necessary due to the constant water reservoir. For the error bar estimation typical measurement uncertainties of 0.5 pmC and 0.1 ‰ were applied to the carbon isotopes of the drip water. Input parameters: T = 6.6°C, $^{14}C_{soilair} = 110.7\,\text{pmC}$, $\delta^{13}C_{soilair} = -22.48$ ‰

The measured values are not well reproduced by the model. Thus, the inverse approach seems to be insufficient for the determination of pCO_2 values. That is due to effects, which are not involved in the model, like degassing of drip water during the one month drip water collecting time or prior calcite precipitation that occur at the drip locations.

The exception is drip location ER-G1, where only CO_2 degassing and calcite precipitation occur when the solution runs downwards the stalactite. The degassing causes an increase of the carbon isotope values (compare the modelled and the measured $\delta^{13}C$ values in Figure

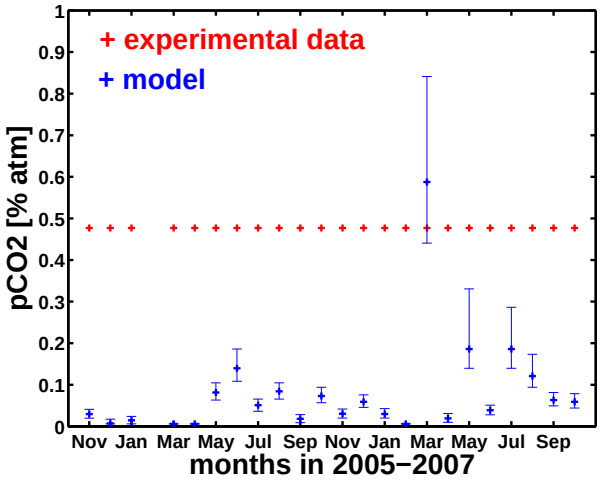

Figure 5.26: The comparison of mean weighted (red) and modelled (blue) soil pCO_2 for ER-76 reveals a stronger underestimation of the modelled values compared to the ER-G1 drip location. The application of the weighting of soil pCO_2 was necessary due to the constant water reservoir. For the error bar estimation typical measurement uncertainties of 0.5 pmC and 0.1 ‰ were applied to the carbon isotopes of the drip water. Input parameters: T = 6.6°C, $^{14}C_{soilair} = 110.7\,\text{pmC}$, $\delta^{13}C_{soilair} = -22.48$ ‰

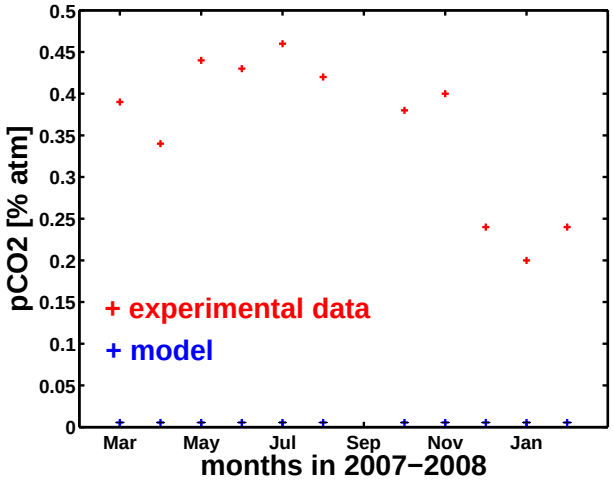

Figure 5.27: Comparison of measured (red) and modelled (blue) soil pCO_2 for Bu-TS2. The modelled values do not fit the data. Error bars of the model are within the sign size. Input parameters: T = 10°C, $^{14}C_{soilair} = 108.6\,\text{pmC}$, $\delta^{13}C_{soilair}$ = variable according to Figure 5.6

5.12), which is the reason for the deviation of modelled and mean soil pCO_2 at ER-G1.

Degassing and prior calcite precipitation are not included in the model because the corresponding parameters introduced by these processes are not known. Examples for these unknown variables are the extend of prior calcite precipitation and the concentration and isotopic composition of the solution before prior calcite precipitation and degassing started.

Chapter 6

^{14}C in stalagmites

After the investigation of the present day situation using a stalagmite top (ER-77) grown during the last 100 years and the drip water approach, in this chapter stalagmites, which grew within the Holocene, are investigated. The obtained knowledge of the present day situation helps to understand the soil-karst-cave system of Ernesto and Bunker cave. This knowledge contributes to improve the understanding of the carbon isotope measurements of stalagmites from both caves.

In Section 6.1 the measurements of the two Holocene stalagmites ER-76 and Bu1 are shown and discussed. Additionally, the dead carbon fraction is calculated for both stalagmites. Thereafter a Rayleigh distillation model for carbon isotope fractionation during drip water CO_2 degassing is introduced (Sec. 6.2). With the Rayleigh distillation model and the drip water model a method is developed to infer the soil pCO_2 content from the measured stalagmite carbon isotope values. The application of the method to the Holocene stalagmites ER-76 and Bu1 is presented in the last section of this chapter.

6.1 Two Holocene stalagmites

The investigated Holocene samples are stalagmite ER-76 from Ernesto cave and stalagmite Bu1 from Bunker cave. Stalagmite ER-76 was also studied under several objectives by McDermott et al. (1999); Huang et al. (2001); Frisia et al. (2003); Scholz et al. (in prep.). For this study subsamples were drilled from both stalagmites (13 in ER-76 and 17 in Bu1) and analysed for their ^{14}C content. The corresponding δ^{13}C values were measured at the University of Innsbruck by the group of C. Spötl. Additionally, U/Th measurements were performed, and an age model was determined for each stalagmite in order to relate the subsamples to an age (performed by D. Scholz).

6.1.1 Stalagmite ER-76

Stalagmite ER-76 is about 366 mm long and covers a time interval from roughly 8000 years BP to 1995 AD, when the specimen was removed from the cave (McDermott et al., 1999). In this study only the top 170 mm are investigated corresponding to a growth time of 4850 years. Figure 6.1 shows the measured ^{14}C and U/Th ages of the top 200 mm of ER-76. The best age model is plotted including the 2σ uncertainty range. Between 20 and 27 mm distance from top several small hiati were detected (Scholz et al., in prep.). Thus, it is not possible to establish an age model for this part either by lamina counting or by uranium series dating. The hiati cover a time period of roughly 1900 years (2313 – 413 years BP).

Two of the radiocarbon ages were determined at the locations of the hiati. The radiocarbon measurements and corresponding calibrated ages from the age model are can be found in Table A.7 in Appendix A.

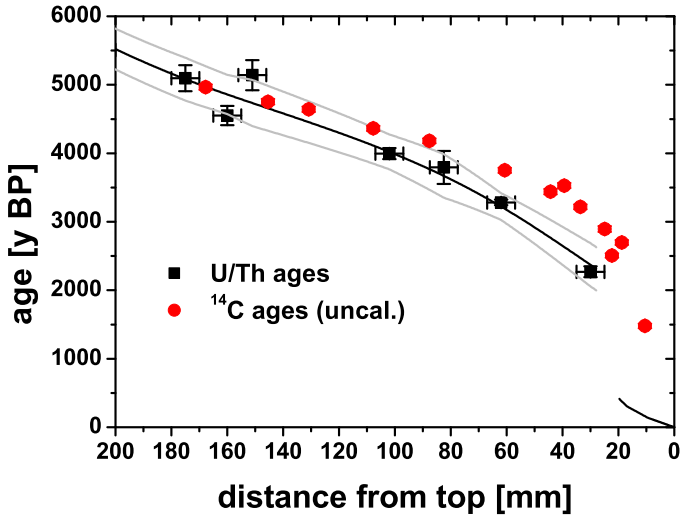

Figure 6.1: The figure shows the measured U/Th ages (black squares) of ER-76 and the 13 radiocarbon ages (red circles, error bars are smaller than the plot symbols) for the top 200 mm. The black line represents the best age model with the 2σ uncertainty range in grey. In the top section it was possible to determine an age model lamina counting (Frisia et al., 2003). No uncertainty is given there. Several hiati were detected between 20 and 27 mm distance from top.

The stalagmite ^{14}C ages show a higher radiocarbon age in the past than the calibrated age of the stalagmite. Since the radiocarbon content of the atmosphere was higher in the past than today the atmosphere seems to be younger in the ^{14}C content than the calibrated age. If the radiocarbon calibration curve is plotted over the distance from top of this stalagmite it would result in a line below the black line of the stalagmite age model. Hence the stalagmite ^{14}C ages are also higher than those of the atmosphere. This effect results from the dead carbon injection from the limestone. The mixing of dead carbon in a solution with approximately atmospheric ^{14}C composition leads to an apparent ageing of the solution and, hence, to an apparent ageing of the stalagmite.

With U/Th dates it is possible to determine the dcf, as already explained in Section 3.4. The calculation of the dcf was slightly modified in order to account for the uncertainties of the age model. The atmospheric ^{14}C activity at the time, when the calcite was deposited, was determined using a Monte Carlo simulation. The mean value of the age and its 1σ uncertainty was used to produce randomly a Gaussian probability distribution. For each age of this function the IntCal04 calibration curve was used to determine the corresponding atmospheric ^{14}C activity. The mean value and the standard deviation of the simulated ^{14}C values were calculated. The mean radiocarbon value was used as the atmospheric ^{14}C value in equation 3.3. The dcf uncertainty was calculated with Equation 6.1.

$$\Delta dcf = \left| \frac{\delta\, dcf}{\delta\, a^{14}C_{stal}} \right| \cdot \Delta\, a^{14}C_{stal} + \left| \frac{\delta\, dcf}{\delta\, a^{14}C_{atm}} \right| \cdot \Delta\, a^{14}C_{atm} \tag{6.1}$$

With the age model and the radiocarbon values shown in Figure 6.1 the dcf and corresponding errors were calculated. The result is presented in Figure 6.2.

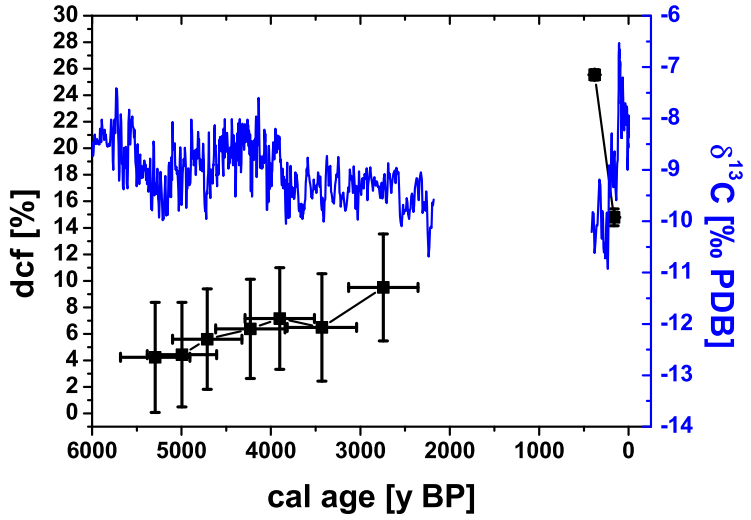

Figure 6.2: The Figure illustrates the trend of the dead carbon fraction (black squares) in stalagmite ER-76. The dcf increases with time. It is not possible to calculate the dcf for the ^{14}C ages in the section of the hiati. The blue line represents the measured δ^{13}C content of the stalagmite.

The calculated dcf shows an increase with time. The sample with a dcf of around 25 % at 400 y BP seems to be too high, because the point does not fit in the trend of the other samples. Such a high dcf value can be explained by an underestimation of the calibrated age. Maybe a growth stop occurred already before this sample depth and was not detected by lamina counting. Without that point the trend in dcf is nearly linear. The youngest data point has a dcf of 14.8 ± 0.7 % which is only slightly higher than the dcf of ER-77 (Fig. 4.2).

As explained in Section 3.4 there are several reasons, which can cause an increase in dcf. Using the δ^{13}C signal in the stalagmite, also shown in Figure 6.2, it is possible to exclude some effects. Assuming that the age model is correct, an increasing dcf would indicate to a more closed dissolution system or ageing of soil organic matter or increasing $CaCO_3$ precipitation rate.

With the last two points, ageing of soil organic matter and increasing $CaCO_3$ precipitation rate, it is hardly possible to obtain large differences such as the observed 5 % in dcf from 5000 to 2500 years BP. The decreasing trend of δ^{13}C does not exclude either an increase in $CaCO_3$ precipitation rate nor an aging of soil organic matter. Faster $CaCO_3$ precipitation would lead to a shorter time of CO_2 exchange between cave air and drip water and less atmospheric ^{14}C and δ^{13}C entering the solution on the stalagmite. This results in trends as observed in Figure

6.2. An aging of soil organic matter can also lead to a lower soil $\delta^{13}C$ and hence to lower stalagmite $\delta^{13}C$ if vegetation is not only aging but also becomes more dense.

As shown in Section 5.3.2 strong ^{14}C changes can occur in drip water, and hence in stalagmites, without being accompanied by large changes in $\delta^{13}C$. Thus, if the dissolution system is changed to more closed conditions, the observed strong $\delta^{13}C$ changes (≈ 2 ‰) can not originate from this effect alone. Furthermore, the trend in ^{14}C and $\delta^{13}C$ go to contradicting directions for dissolution system changes. Hence, it is supposed that several things changed in the cave system. There is not only a more closed dissolution system today than in the past, but also a more dense vegetation in the late Holocene was build up (Scholz et al., in prep.). It can be nearly excluded that $CaCO_3$ precipitation rate was enlarged in this period due to the decreasing lamina thickness from the 6000 to 2000 years BP. With both processes, dissolution system and vegetation change, overlapping each other, the carbon isotope signal seen in Figure 6.2 can be explained.

6.1.2 Stalagmite Bu1

Stalagmite Bu1 was also analysed by ^{14}C dating. The stalagmite is nearly 70 cm long and grew mainly in the Holocene. Only the bottom part shows an Eemian growth period. 17 ^{14}C samples between the top millimetre and the oldest part of the Holocene were analysed. U/Th ages, the derived age model and the uncalibrated ^{14}C ages are shown in Figure 6.3. The data are also shown in Table A.8 (Appendix A).

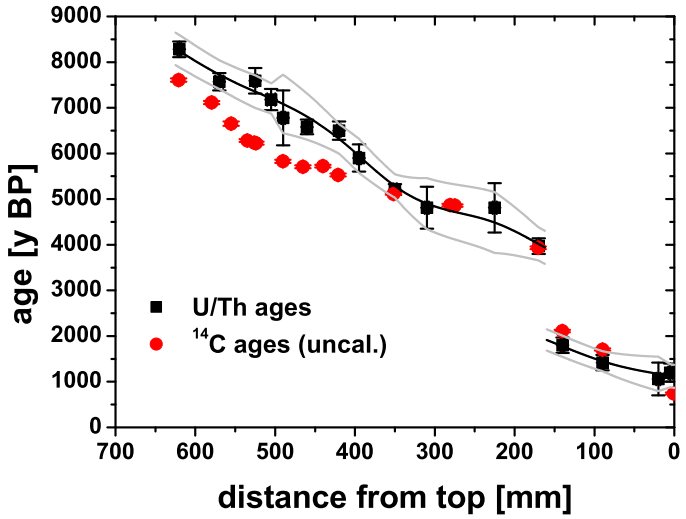

Figure 6.3: The figure shows the measured U/Th ages (black squares, depth errors are smaller than the plot symbols) for the top 620 mm of Bu1 and the 17 measured radiocarbon ages (red circles, error bars are smaller than plot symbols). At 525 mm distance from top two radiocarbon measurements, resulting in the same ^{14}C age, were performed. The black line represents the age model with the 2σ uncertainty range in grey. A hiatus is detected at 160 mm distance from top lasting about 2000 years.

In the upper 400 mm of the stalagmite the radiocarbon ages are higher than the U-series age model. This is caused by the dead carbon injection. In deeper parts of the stalagmite, however, the radiocarbon age is younger than the age model, and in some parts of the stalagmite (from 421 to 555 mm distance from top) the ^{14}C age is even younger than the atmospheric ^{14}C age. This unusual result is also evident in the dcf plot in Figure 6.4.

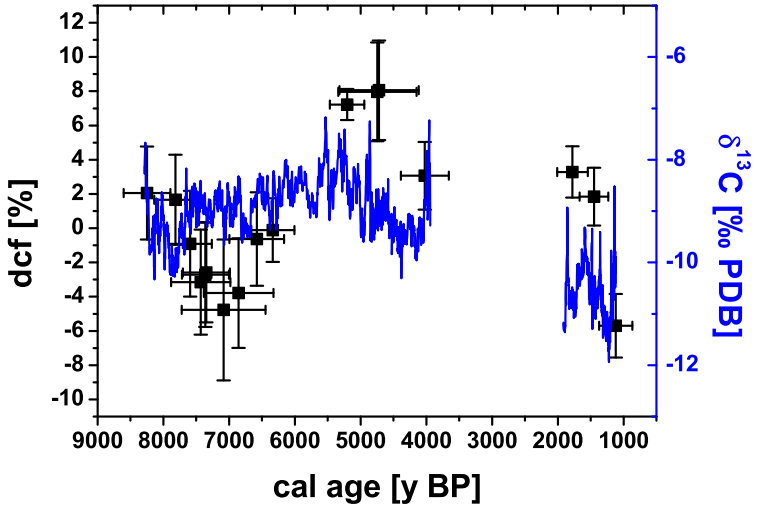

Figure 6.4: The figure illustrates the trend of the dead carbon fraction (black squares) of stalagmite Bu1. The dcf show negative values from 7600 to 6300 years BP. At other times the dcf is very low and varies considerably by about 13 %. The low dcf indicates a nearly completely open system. The blue curve represents the measured δ^{13}C content of the stalagmite.

Prior 7600 years BP a low dcf is observed, indicating a more open limestone dissolution system. Between 7600 and 6300 years BP the dcf is negative and, hence, by definition, the stalagmite has higher radiocarbon values than the atmosphere. Nevertheless, a negative dcf is possible. If the limestone dissolution system is completely open, the saturated drip water is supposed to have more ^{14}C than the soil atmosphere. According to Figure 5.9 up to two or three pmC, depending on pCO_2, are reasonable. Additionally, by precipitation of calcite a slight ^{14}C increase must be taken into account, due to the fractionation effect between the dissolved inorganic matter of the solution and the stalagmite. Hence, a 3 pmC higher stalagmite ^{14}C value compared to the atmosphere is possible, if the limestone dissolution occurs in a completely open system. That would result, with an atmosphere of around 100 pmC, in a dcf of approximately -3%. However, U-series dating errors can not be excluded and can be responsible for dcf values lower than -3 %.

After 6300 years BP the dcf increases again to positive values with a maximum of about 8 % at 4700 years BP. Then the dcf decrease until the top of the stalagmite, which shows a negative dcf. At the top the U/Th measurements are associated with some uncertainties, due to low uranium content and the young age (pers. comm. D. Scholz). Thus, the real age is possibly younger, resulting in higher dcf value.

Assuming the age model is correct, the dcf is very low in most growth periods of the

stalagmite. Furthermore, the dcf varies strongly, which is only possible due to changes in the dissolution system. This is supported by the $\delta^{13}C$ values (Fig. 6.4, blue curve), which are rather constant in the long term trend. In the period of the hiatus some changes in the cave environment must have been occurred resulting in lower $\delta^{13}C$.

The very low dcf values mostly found in the stalagmite were indirectly confirmed by recent calcium concentration analysis of drip and soil water. The data show that the calcium content of soil water is higher than that of the drip water, suggesting major limestone dissolution in the upper part of the soil, where an open dissolution system is more likely due to many soil air filled voids. In addition, the simulation for Bu-TS2 (Sec. 5.3.2, Fig. 5.23) of the Bunker cave system show more open conditions throughout the year than simulations for Ernesto cave in winter (Figs. 5.14 and 5.19). For Ernesto cave Frisia et al. (2003) assume that stalagmites grow mainly in winter. Thus, only comparisons of the open to closed system ratios for the winter months are meaningful. Hence, for stalagmite Bu1 a nearly completely open limestone dissolution system is most likely throughout the Holocene.

6.2 Rayleigh distillation model

In Section 5.2 the drip water model including soil conditions and limestone dissolution was explained. Dissolution occurs until the solution is saturated with respect to calcite. Now a Rayleigh distillation model is shortly presented, including degassing of CO_2 and precipitation of calcite, which form the stalagmite.

6.2.1 Quantitative description of concentrations and carbon isotopes

When the solution seeping into the cave comes into contact with the cave atmosphere, two processes affect the isotopic ratio. Firstly, there is a progressive enrichment in $\delta^{13}C$ and ^{14}C of the carbon species remaining in the solution due to the combined removal of CO_2 and $CaCO_3$ from the solution. Secondly, isotopic exchange occurs between the carbon dioxide in the cave atmosphere and the carbon species in solution.

The first of these processes can be described as a Rayleigh Distillation process. Hereby gaseous CO_2 and $CaCO_3$ of different isotopic composition compared to the species remaining in solution are progressively removed. The removal of the molecules occurs in such quantities that the solution stays saturated in calcite.

The calculation of the Rayleigh Distillation process is performed as explained in Hendy (1971). The calculation of the concentrations was performed until the solution had a equal pCO_2 like the cave atmosphere. Using the concentrations during the degassing process allows calculating the isotopic composition of the solution. In addition, the carbon isotopes of the solution influence the isotopic composition of the precipitated calcite. The calculation of the carbon isotopes was performed including isotopic exchange processes between the carbon in the solution and the CO_2 of the cave atmosphere.

The following assumptions are made: The rate of CO_2 transport across the solution – gas interface from the solution to the cave atmosphere, is proportional to the partial pressure of carbon dioxide in solution. Similarly, the rate of transport from the cave atmosphere to the solution has to be proportional to the partial pressure of CO_2 in the cave atmosphere. A detailed description is given by Hendy (1971).

6.2.2 Model description

The model includes five subfunctions, which describe CO_2 degassing and calcite precipitation of the solution seeping into the cave. These functions also include the calculation of the carbon isotopes in the solution. In Figure 6.5 the arrangement of the subfunctions is shown.

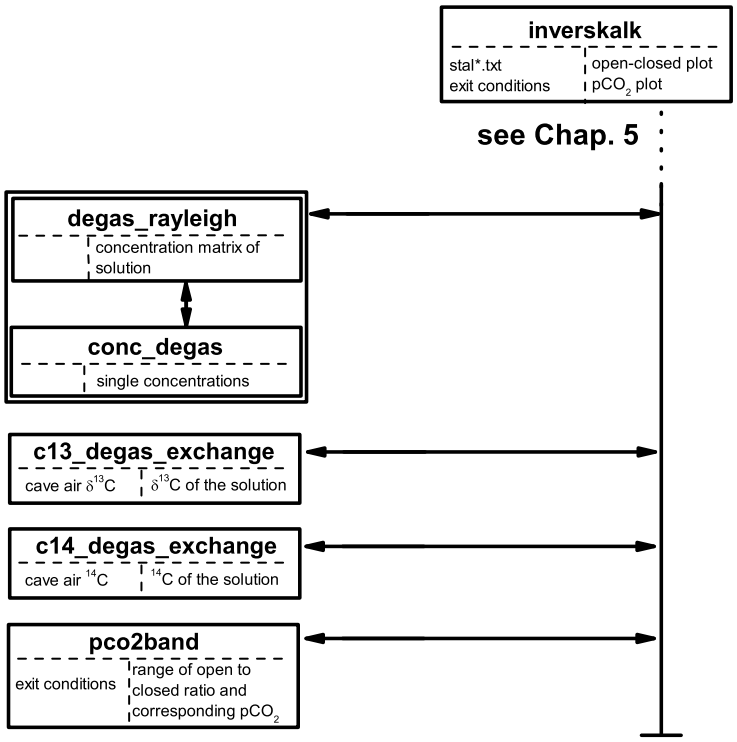

Figure 6.5: Flow chart of the calcite precipitation model. The sketch is the completion of *inversekalk* as shown in Figure 5.7. CO_2 degassing and calcite precipitation are simulated under the condition of a permanently saturated solution. The carbon isotopes of the solution and hence of the calcite is modelled under gas exchange between the dissolved inorganic carbon of the solution and gaseous CO_2.

- **inverskalk** This module orders the subfunctions to calculate soil air pCO_2 of measured ^{14}C - δ^{13}C data pairs of a stalagmite. Several soil pCO_2 values can be derived from one ^{14}C - δ^{13}C data pair (see below and Fig. 6.8). Thus *inversekalk* solves for only **one** possible solution, determined by **one** open to closed limestone dissolution ratio. Then *pco2band* is called, and the results for soil pCO_2 of this subfunction and the corresponding open to closed ratios are saved and plotted.

- **degas_rayleigh** Prepares variables (for a successively decreasing calcium concentration) for the concentration calculation in *conc_degas* and saves the results of *conc_degas* until the carbon species in the water are in equilibrium with the cave atmosphere. Furthermore, the HCO_3^-–pCO_2 plot already created in function *closed1* is completed here.

- **conc_degas** Calculates the chemical equilibrium of the participating ions in the solution under the assumption of a Rayleigh Distillation process. An iterative process between the concentrations and the activities is applied here. If necessary, it is possible to vary the accuracy by redefining the break-off condition (the pCO_2 difference of two successive steps). The iterative process is repeated until successive changes in pCO_2 are less than 10^{-10} moles/l.

- **c13_degas_rayleigh** After determining the cave CO_2 and $\delta^{13}C$ content, the $\delta^{13}C$ content of the carbon in the solution for each degassing step is calculated. Gas exchange processes are considered in the calculations. Also the $\delta^{13}C$ content of the precipitated calcite is determined.

- **c14_degas_rayleigh** After determining the CO_2 content and the ^{14}C activity of the cave atmosphere, the ^{14}C activity of the carbon in the solution for each degassing step is calculated. Gas exchange processes are considered in the calculations. Also the ^{14}C activity of the precipitated calcite is determined.

- **pco2band** This subfunction is similar to *inverskalk*. It seeks for **all** possible soil CO_2 values, which can be derived by a single ^{14}C - $\delta^{13}C$ data pair. The results are given back to *inverskalk*.

6.2.3 Method to estimate soil pCO_2

The method of how to calculate the soil pCO_2 from stalagmite carbon isotope pairs (^{14}C, $\delta^{13}C$) was already shortly summarized in the introduction part. Here a more detailed description is given.

Using the limestone dissolution model introduced in Section 5.2 and the calcite precipitation part introduced above, it is possible to calculate the ion concentrations in the drip water during limestone dissolution in the karst and the degassing of the solution in the cave. Figure 6.6 shows the bicarbonate ion concentration during both processes. Limestone dissolution is performed both under open (straight blue lines) and closed (curved blue lines) dissolution conditions. The resulting degassing of CO_2 in the cave (red line) is performed under saturated conditions, which means that for each carbon atom leaving the solution as a CO_2 molecule one atom is bound in a $CaCO_3$ molecule.

As explained for the limestone dissolution model (Sec. 5.2), it is also possible to calculate the carbon isotopes for the degassing process. The carbon isotopes are plotted in Figure 6.7 for the open and closed limestone dissolution process and the isotopic enrichment during the degassing of the solution in the cave. Water parcels of different soil pCO_2 values were used to draw the solid lines in Figure 6.7, representing the carbon isotopes of saturated solutions (solid blue) and the first calcite to be precipitated (solid red line). The dashed red lines show the behaviour of the carbon isotopes during degassing.

The principles of determining soil pCO_2 are easy to explain using Figure 6.7. Assuming measured carbon isotope values at one section of a stalagmite of $^{14}C_{stal}$ = 65.5 pmC (initial value) and $\delta^{13}C_{stal}$ = -10 ‰ (black "+" in Figure 6.7), it is easy to trace back to the soil values. Going back the red dashed line in Figure 6.7, from the black "+" leads to the first calcite to be precipitated and to appropriate values for the saturated drip water. For both, first calcite and saturated drip water, exactly one concentration state can be determined. From the saturated drip water, in turn, the soil conditions are easy to trace back (Sec. 5.3.3). Thus, the soil pCO_2 that causes the measured carbon isotopes can be determined.

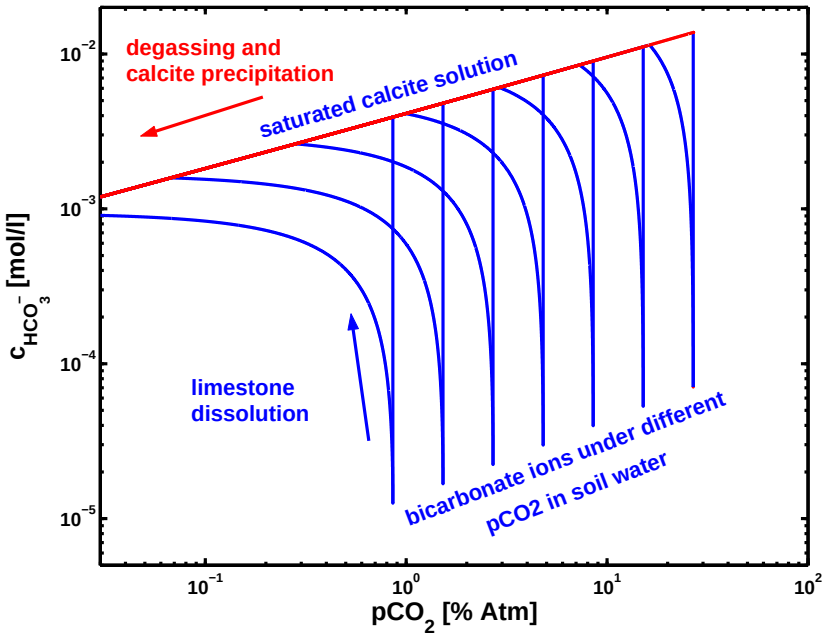

Figure 6.6: The blue lines represent the limestone dissolution process under open (straight blue lines) and closed conditions (curved blue lines) for water parcels charged with different amounts of pCO_2. The red line shows the relation of the pCO_2 of the solution and the concentration of bicarbonate ions during the degassing process. The red line also represents the saturation state of the different solutions. The left edge of the diagram is equal to a pCO_2 of 300 ppm (0.03 % atm). The cave atmosphere CO_2 content was set for this figure to be 300 ppm and, hence, the degassing process stops there. (temperature: 10°C)

However, some difficulties arise. Firstly, it is necessary to assume certain values for the soil carbon isotopes **(i)** before the calculation starts, otherwise it is not possible to allocate one carbon isotope pair to concentrations and to soil pCO_2. Using for example other soil carbon isotope parameters than those in Figure 6.7, e.g. $^{14}C_{soilair} = 100\,\mathrm{pmC}$, $\delta^{13}C_{soilair} = -23$ ‰, all lines shift to down left, and, hence, the measured carbon isotope pair indicates a higher soil pCO_2 value.

Secondly, this method works fine for closed limestone dissolution conditions due to the wide spread of the radiocarbon values in the precipitated calcite caused by different soil pCO_2 **(ii)**. On the other hand the method is difficult to apply for the open system because the carbon isotope values of the precipitated calcite are very similar for large differences of soil pCO_2 (Fig. 6.7, upper red dashed lines).

Furthermore, this model is not really an inverse model. Thus, a time consuming search algorithm is applied, running the forward model until the measured carbon isotopes agreed with the measured ones **(iii)**. The fourth point is the question where the calcite, which is supposed to precipitate before the measured carbon isotopes are reached **(iv)**, is deposited. The last point is that limestone dissolution mostly occurs under intermediate dissolution conditions **(v)**, whereas Figure 6.7 only shows the extreme cases.

The first four points are easy to address:

- **(i)** In a first attempt the soil conditions of the carbon isotopes are kept constant. That means the soil air $\delta^{13}C$ is kept at a value representing the present day situation. Variable

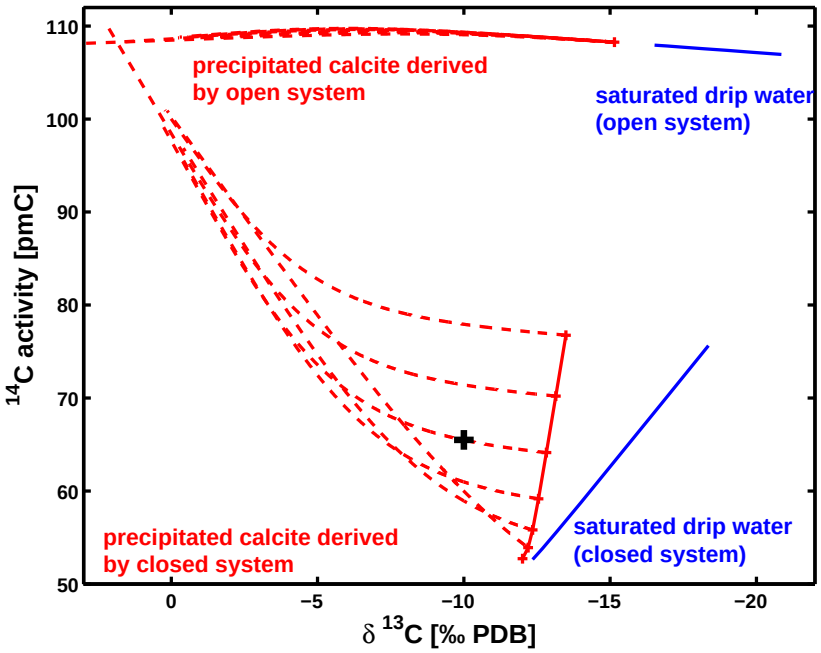

Figure 6.7: The ^{14}C and $\delta^{13}C$ plot is redrawn after Hendy (1971) using the presented model. In comparison to Hendy (1970) (Fig. 1.1) slightly different equilibrium and fractionation constants are used. The blue lines represent the isotopes in saturated drip water resulting from different soil pCO_2. The red solid line is the first calcite precipitated in equilibrium. The dashed red lines describe the carbon isotopes during the degassing process. Each of the dashed lines represents a track, whose shape depends on the pCO_2 value in the solution at the beginning of the limestone dissolution process. The lines on top represent the carbon isotopes derived under open limestone dissolution. On the bottom the carbon isotopes are derived under closed conditions. Input parameters: T = 10°C, $^{14}C_{soilair}$ = 106 pmC, $\delta^{13}C_{soilair}$ = −25 ‰. The black "+" represents carbon isotope values of $^{14}C_{stal}$ = 65.5 pmC and $\delta^{13}C_{stal}$ = -10 ‰.

soil air ^{14}C activity is applicable by using Intcal04 (Reimer et al., 2004), hence, it is not necessary to keep the soil air radiocarbon content constant. However one assumes constant soil reservoir parameters which change the atmospheric ^{14}C signal slightly.

- **(ii)** This point, concerning the similar carbon isotopes of precipitated drip water derived under open limestone dissolution conditions, is related to the chosen stalagmites. Stalagmites, which were fed from drip water composed under nearly closed conditions, should be used.

- **(iii)** This point of time consuming calculation does not matter if there is enough time to run the model or if fast computers are available.

- **(iv)** The calcite depositing before the solution reaches the stalagmite growth axis is deposited on the stalactite and concerns also possible prior calcite precipitation. Thus it is explainable why the carbon isotopes of the firstly deposited calcite simulated by the model are not measured on the growth axis. This is also the reason why this method results in reliable soil pCO_2 values in contrast to the inverse drip water approach

(Sec. 5.3.3).

The solution to point **(v)** is presented by the drip water model (Sec. 5.2). Using this model with several open to closed system ratios and the Rayleigh Distillation process (Sec. 6.2.1) enables to apply the same procedure as explained above to estimate soil pCO_2. However, here new problems arise. To illustrate these, limestone dissolution is performed once for the case of an open to closed system ratio of 20 to 80 % and once in a ratio of 15 to 85 %. The results of the modelled carbon isotopes are shown in Figure 6.8.

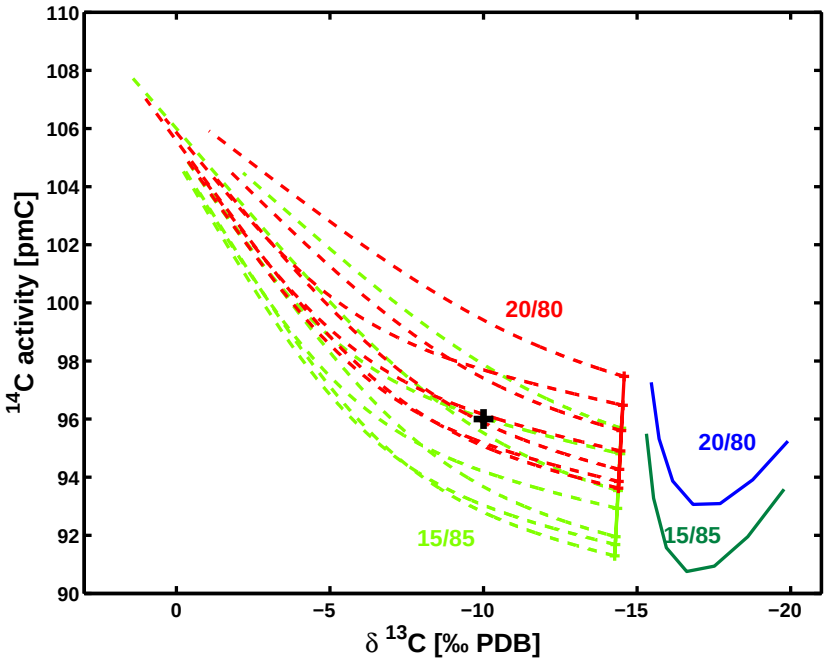

Figure 6.8: The figure visualises the same processes as Figure 6.7. The difference is the chosen open to closed dissolution systems. In blue the drip water carbon isotopes of saturated solutions derived by an open to closed system ratio of 20 to 80 % are shown. In solid green an open to closed system ratio of 15 to 85 % is used. The carbon isotopes of the corresponding deposited calcite are represented by the dashed red and green lines, respectively. Input parameters: T = 10°C, $^{14}C_{soilair}$ = 106 pmC, $\delta^{13}C_{soilair} = -25$ ‰. The black "+" represents carbon isotope values of $^{14}C_{stal}$ = 96 pmC and $\delta^{13}C_{stal}$ = -10 ‰.

The first problem is the non linear shape of the isotopes in saturated drip waters, and the second one is the unknown open to closed limestone dissolution system ratio. Hence, several soil pCO_2 values can be derived from the data pair $^{14}C_{stal}$ = 96 pmC (initial value) and $\delta^{13}C_{stal}$ = -10 ‰ (black "+" in Figure 6.8).

The non linear relationship between ^{14}C and δ^{13}C of the saturated drip water is a major problem for the estimation of soil pCO_2. The resulting first precipitated calcite is not a straight line as for the completely closed system (Fig. 6.7). The carbon isotopes of the first calcite to be precipitated are described best by a distorted "V" shape (Fig. B.12). The carbon isotopes of the degassing solution depend on the first calcite and, hence, carbon isotopes of the precipitating calcite can offer two solutions for one ^{14}C - δ^{13}C data pair measured in the stalagmite. Thus, the method described above is not applicable without using some assumptions.

One assumption is to neglect the right arm of the parabola like isotope relation of the saturated drip water (compare Figs. 6.8 and 6.9). That can be done without any big constraints. Looking at the minima of the parabola the corresponding soil pCO_2 value is around 6 % atm. That is a rather high value, which is hardly expected to result from vegetation. Any known literature, so far, did not find soils with higher pCO_2 values (Dörr and Münnich, 1980, 1986; Cerling, 1984, and citations therein). Thus, soil pCO_2 values higher than around 6 % atm were excluded for the simulations. However, for single applications the soil pCO_2 should be evaluated, at least for the present day situation. If recent soil pCO_2 above the cave is higher than 6 % atm it is not advisable to use the method in its present form.

Nevertheless with neglecting high soil pCO_2 values, Figure 6.8 can be simplified. This is shown in Figure 6.9, where all soil pCO_2 values resulting in carbon isotopes of the saturated solution located on the right hand side of the minimum shown in Figure 6.8 were neglected.

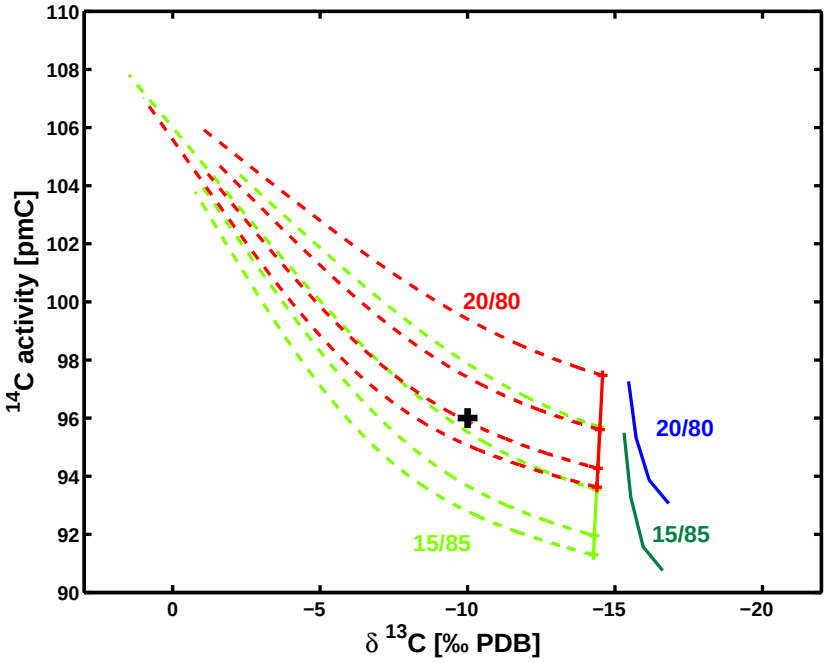

Figure 6.9: Similar as Figure 6.8. Carbon isotopes derived by high soil pCO_2 were omitted. The red and green dashed lines representing one open to closed system ratio each do not intersect. The black "+" represents carbon isotope values of $^{14}C_{stal}$ = 96 pmC and $\delta^{13}C_{stal}$ = -10 ‰.

A second major problem, which is more difficult to solve a, is the unknown behaviour of the limestone dissolution system. Figure 6.9 shows the relation between the carbon isotopes in drip water and the deposited calcite for two open to closed dissolution ratios. The problem, arising for a measurement of $^{14}C_{stal}$ = 96 pmC (initial value) and $\delta^{13}C_{stal}$ = -10 ‰ (black "+" in Figure 6.8), is to estimate the open to closed system ratio. In general, it is not possible to determine a certain value for the dissolution system ratio. Thus, several possibilities for the open to closed system ratio is to take into account and, hence, no unique solution is to expect. In Figure 6.9 two soil pCO_2 values can be determined, depending on the dissolution ratio in the karst.

Apparently, these two solutions are not the only possible. If the open to closed ratio is

between 15/85 % and 20/80 %, it is possible to trace back to several other soil pCO_2 values. Additionally, some cases yield solutions for soil pCO_2 with slightly lower or higher open to closed system ratios than shown in Figure 6.9.

The extent to which the open to closed ratio delivers a soil pCO_2 is limited. The lower limit is determined by the cave CO_2 content. If limestone dissolution results in a saturated solution with lower CO_2 than the cave atmosphere, no calcite precipitates and, hence, stalagmite growth is not possible. That means the more closed the limestone dissolution system is, the higher the soil pCO_2 has to be to allow stalagmite growth. The upper limit is introduced artificially by cutting away high soil pCO_2 values as explained above and, hence, is expected around 6 % atm.

Between the limits of the open to closed dissolution system ratios an unlimited amount of solutions for soil pCO_2 exist. The amount of pCO_2 solutions depends on the step width chosen for the open to closed system ratios. The smaller the step width, the more solutions for soil pCO_2 are available, which in turn results in lower differences between two soil pCO_2 values.

6.3 Results of the model

There are several possible solutions for soil pCO_2 derived by one measured carbon isotope pair. Hence, the best method is to treat the soil pCO_2 solutions as a probability function. For one ^{14}C - δ^{13}C data pair all possible solutions are plotted in a histogram, representing the probability function. As an example, Figure 6.10 shows such a histogram.

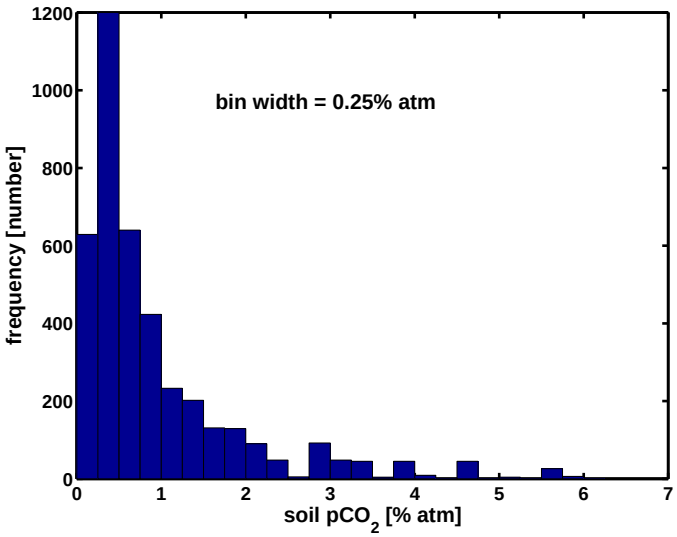

Figure 6.10: Histogram of soil pCO_2 distribution derived by the oldest radiocarbon date measured on ER-76 with a calibrated age of 5295 years BP (^{14}C = 104.18 pmC; δ^{13}C = -8.65 ‰). Most pCO_2 values are lower than 1 % atm. Bin width is 0.25 % atm and the open to closed system ratio step width is 0.01 %.

The histogram (Fig. 6.10) is used to calculate a probability function. For a conclusive histogram and probability function a sufficient amount of soil pCO_2 values is necessary. On the one hand, a too large step width in the open to closed system ratio does not result in an

adequate amount of soil pCO_2 values for a histogram, on the other hand, a too small step width is computationally too intensive. A reasonable value for the step width is 0.01 %.

In general, such a histogram and the corresponding probability function is calculated for each carbon isotope data pair measured on the stalagmite. The best way to visualise the results on a time scale is to connect all the probability functions with a contour plot.

6.3.1 Stalagmite ER-76

Now the method is applied to stalagmite ER-76. The measured radiocarbon values and the corresponding $\delta^{13}C$ data are used to estimate the open to closed ratios and soil pCO_2 values. The upper and lower limit of the open to closed system ratio[1] and of soil pCO_2 are shown in Figure 6.11.

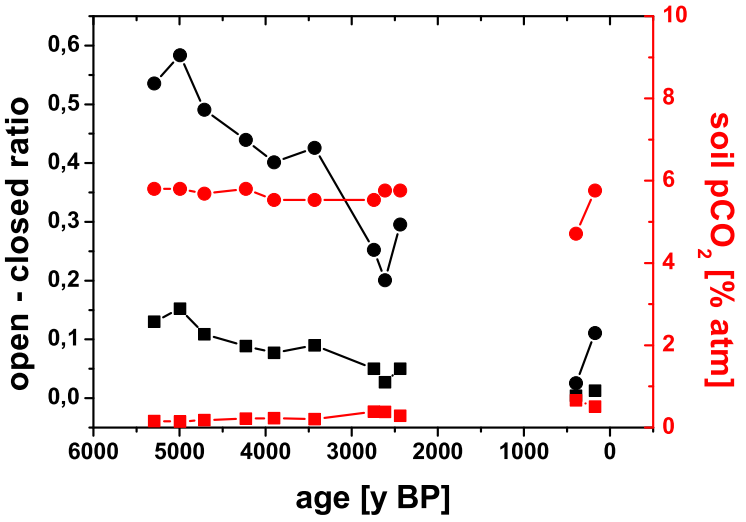

Figure 6.11: The upper (circles) and lower (squares) limits on soil pCO_2 (red) and open to closed system ratios (black) of stalagmite ER-76 are shown. The soil $\delta^{13}C$ values are kept constant at present day values ($\delta^{13}C$ = -22.48 ‰, Sec. 5.3.2). Similarly, the soil reservoir parameters (Sec. 4) of the present day soil are used, and the atmospheric radiocarbon data are taken from the IntCal04 calibration curve (Reimer et al., 2004). Additionally, a constant cave temperature of 6.6°C is assumed.

The upper and the lower limit of the open to closed system ratio decreases with time (Fig. 6.11). Despite the large difference of upper and lower limit, the gradients of both limits and the very narrow range of the open to closed system ratio of the point 400 years BP suggest that the real ratio decreases as well. This means that the limestone dissolution system of the solution feeding ER-76 changes to more closed conditions as supposed by the analysis of the dcf (Sec. 6.1.1).

[1] If the open to closed system ratio x = 1, a completely open system is modelled. x=0 represents a completely closed system.

The pCO_2 value corresponding to the upper limit of the open to closed system ratio is 6 % atm. This limit results from neglecting higher pCO_2 values (see above). More information gives the soil pCO_2 value, which corresponds to the lower limit of the open to closed system ratio, which shows an increasing trend. The increase is forced by the more closed system, which results in general in lower pCO_2 values for the saturated solution. If the cave atmosphere has a pCO_2 value higher than the solution, no calcite precipitates. This is considered in the calculations and, hence, the soil pCO_2 of the lower dissolution ratio limit increases.

While the dissolution ratio is equidistantly distributed, the probability density of the soil pCO_2 values is variable (Fig. 6.10). In Figure 6.12 the density variation of soil pCO_2 is visualised throughout the Holocene for Ernesto cave with a contour plot. Figure 6.13 shows the median value of all calculated soil pCO_2 values including error bars, which show the 1σ uncertainty. For the calculations a step width of 0.01 % for the open to closed system ratio was used.

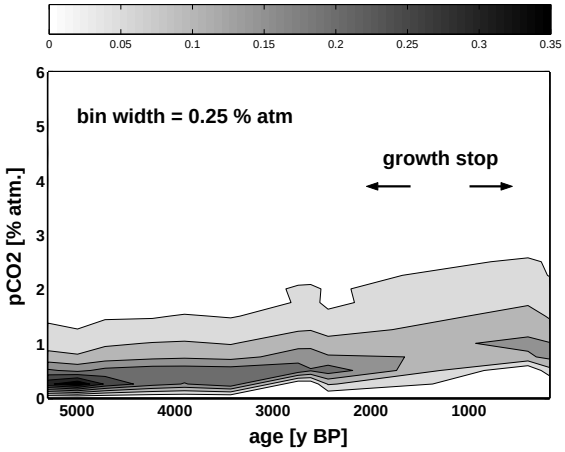

Figure 6.12: Contour plot of soil pCO_2 derived by carbon isotope measurements on stalagmite ER-76. The grey scale indicates the probability of pCO_2 values found by the model to belong to a bin. The duration of the growth stop is indicated.

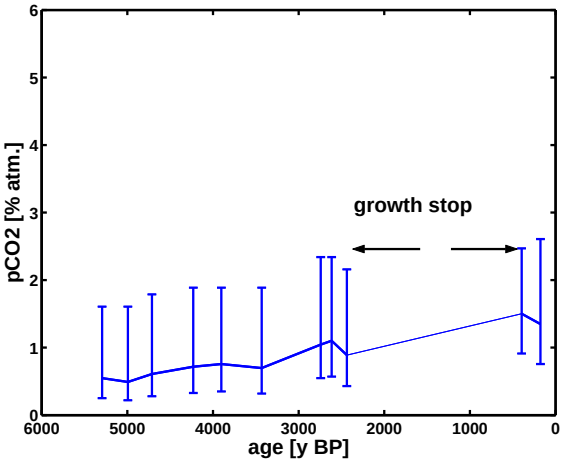

Figure 6.13: Median soil pCO_2 value derived by carbon isotope measurements on stalagmite ER-76. The duration of the growth stop is indicated.

The comparison of the most recent values (the youngest analysed carbon isotope pair corresponds to an age of 178 years BP) of the soil pCO_2 calculated for Ernesto cave from the stalagmite data and the present day measurements shows an offset. The present mean soil pCO_2 value is around 0.5 % atm (Sec. 5). The median soil pCO_2 (Fig. 6.13) derived by the most recent carbon isotope data pair is about 1.3 % atm and more than twice as high than the recent value. The darkest shaded area of Figure 6.12 for the most recent time is around 0.75 % atm and, hence, only slightly larger compared to the present day situation. Thus, feasible information of soil pCO_2 can be obtained from stalagmite carbon isotope measurements with the histogram technique.

Figure 6.12 shows an increasing trend of the soil pCO_2 values (dark shaded areas). Similarly the median soil pCO_2 values increase in Figure 6.13. The 1σ uncertainty is large compared to the gradient. A higher soil pCO_2 is caused by a more dense vegetation, higher temperature or more water supply. In the case of Ernesto cave the major reason for the

change in soil pCO_2 is a higher density of the vegetation. On a monthly time scale temperature is most important for CO_2 production (Fig. B.13). However this can not be applied for millennial time scales. Direct temperature and precipitation influences are small, because in the late Holocene only small temperature variations occurred (Mann et al., 1998; Mangini et al., 2005) compared to the range shown in Figure B.13. The indirect temperature and precipitation effect on the vegetation density are more important.

However, the result of Figures 6.12 and 6.13 is difficult to interpret in terms of climate variability, because all values were calculated assuming constant temperature, soil air $\delta^{13}C$ and soil reservoir parameters for determining soil air ^{14}C. However, a changing soil pCO_2 is induced by temperature changes and will induce soil air ^{14}C and $\delta^{13}C$ variations. Hence, the trend shown in Figures 6.12 and 6.13 maybe differ slightly, if temperature and soil carbon isotope values change.

To solve this problem, an iterative process has to be applied. If it was known, how soil pCO_2 is influenced by temperature and how soil pCO_2 influences the soil air carbon isotope composition, it would be possible to apply an iterative process. For the dependence of soil pCO_2 with the parameters the soil pCO_2 should be used, whose bin includes the highest frequency of solutions. Currently it is not possible to vary those parameters, because those dependencies are not known.

6.3.2 Stalagmite Bu1

The soil pCO_2 determination for stalagmite Bu1 is difficult. As shown in Figure 6.4 the dcf is negative in parts of the stalagmite. If there is much more radiocarbon in the stalagmite than in the atmosphere, corresponding to a dcf $\leq$ -3 %, it is not possible to determine a pCO_2 value. Hence, the soil pCO_2 can only be calculated for seven ages.

Additionally, cases with a limestone dissolution system more open than 80 % are difficult to evaluate regarding soil pCO_2, because the dashed lines start to cross each other (Fig. B.14). The more open a system is, the lighter the $\delta^{13}C$ values are, where the isotope composition lines of the precipitated calcite cross (compare the case of 90 % open and 95 % open in Figure B.14). Firstly, in the cross sections it is not possible to find only one solution for a carbon isotope pair and secondly, the search algorithm does not work properly after the crossing.

For the stalagmite Bu1 a constant soil air $\delta^{13}C$ of -22.37 ‰ was used. This is the mean value of recent soil measurements. The soil air radiocarbon content was derived by IntCal04 (Reimer et al., 2004). Additionally, the cave temperature is supposed to stay at a constant value of 10°C within the Holocene. The upper and lower limit of the limestone dissolution system as well as the corresponding soil pCO_2 values are shown in Figure 6.14.

The open to closed system ratios of five ages stays below 80 %. Only for the two oldest radiocarbon ages around 8000 years BP the open to closed system ratio is higher (86 and 91 %). The lines, which describe the carbon isotopes in precipitated calcite, cross each other for these two ages (Fig. B.14). However with the chosen soil air $\delta^{13}C$ parameter the crossing does not disturb the search algorithm because it occurs later in the calcite precipitation process when the carbon isotopes are more heavier (Fig. B.15).

No trend in the limits of the open to closed ratio is observable. The missing values between 8500 and 5500 years BP are due to too high radiocarbon values in the stalagmite. The second gap (between 3800 and 1900 years BP) is due the hiatus. In addition, no trend is visible in the corresponding soil pCO_2 values.

Figure 6.15 shows the density of calculated soil pCO_2 values, which corresponds to the equally distributed open to closed dissolution system ratio. Figure 6.16 shows the median of

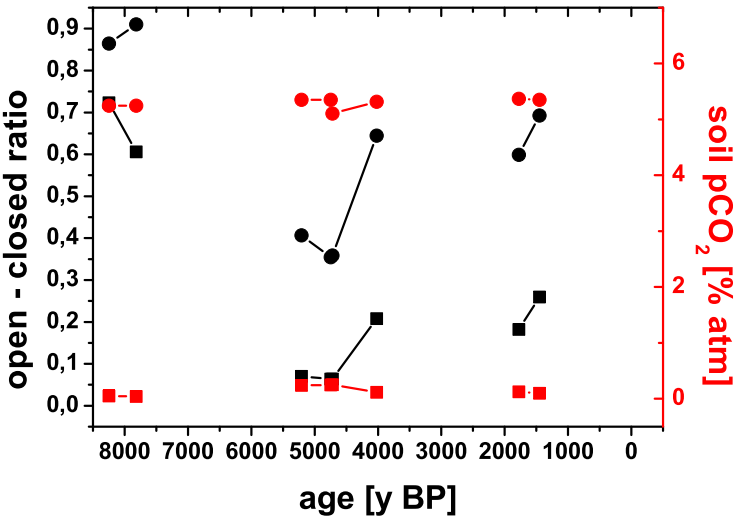

Figure 6.14: The upper (circles) and lower (squares) limits of soil pCO_2 (red) and open to closed system ratio (black) of stalagmite Bu1 are shown. The soil $\delta^{13}C$ values were kept constant at the present day annual mean (Sec. 5.3.2). The soil air radiocarbon content was taken from the IntCal04 calibration curve (Reimer et al., 2004). Additionally, a constant temperature of 10°C was assumed.

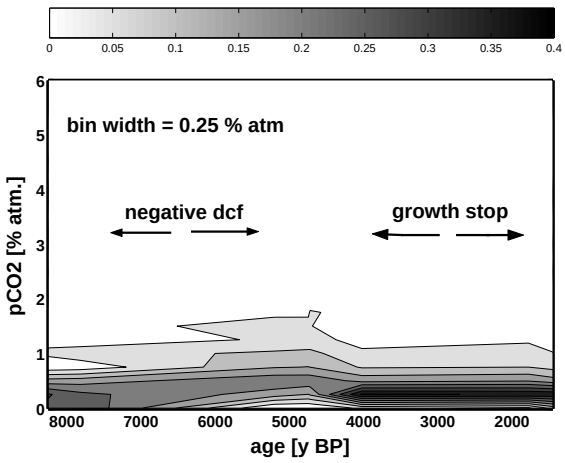

Figure 6.15: Contour plot of the soil pCO_2 derived by carbon isotope measurements on stalagmite Bu1. The grey scale indicates the probability of pCO_2 values found by the model to belong to a bin. The duration of the growth stop and times with negative dcf are indicated.

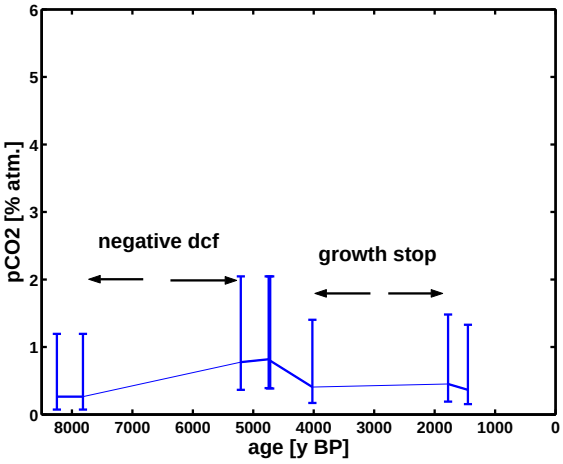

Figure 6.16: Median soil pCO_2 derived by carbon isotope measurements on stalagmite Bu1. The duration of the growth stop and times with negative dcf are indicated.

all calculated soil pCO_2 values including the 1σ uncertainty. For the calculations a step width of 0.01 % for the open to closed system ratio was used.

The last soil pCO_2 values (1550 years BP) derived by the carbon measurements are in the range of the present soil pCO_2 values. The present day measurements on soil pCO_2 show a mean value of around 0.34 % atm. The median pCO_2 value of the youngest age is around 0.37 % atm (Fig.6.16), and the darkest shaded area of Figure 6.15 is around 0.4 % atm.

Both figures (Fig. 6.15 and 6.16) show a constant soil pCO_2 over the last 8000 years. Hence, the soil characteristics as well as temperature and precipitation are supposed to be rather constant during the Holocene.

Chapter 7

Summary and outlook

Summary In this thesis radiocarbon in speleothem environments was used as a tracer to investigate soil processes. Two time approaches were applied. The first approach deals with the present day situation, where drip water samples of two drip locations of Ernesto cave and one drip location of Bunker cave were analysed. Furthermore, subsamples of the top of stalagmite ER-77 were used to derive the age spectrum of a three soil reservoir model of soil organic matter and to calculate the present soil ^{14}C content. In the second approach climate depending soil processes were studied with measurements of carbon isotopes of two stalagmites (ER-76 and Bu1), which cover the Holocene.

The ^{14}C analysis of stalagmite ER-77 shows the atmospheric radiocarbon bomb peak in the calcite. With the assumption that the total soil ^{14}C content is composed of three soil reservoirs and applying the approach by Genty and Massault (1999) it was possible to determine the soil reservoir parameters and to estimate the recent ^{14}C content of the soil air above Ernesto cave.

The present day situation in both caves was investigated with the carbon isotope analysis of monthly collected drip water. The drip water analysis revealed a seasonal cycle of the drip water radiocarbon content in all three drip locations. For the two Ernesto drip locations a constant $\delta^{13}C$ level in drip water was observed in contrast to the Bunker cave drip water where the stable carbon isotope content reveals a seasonal cycle.

Furthermore, a limestone dissolution model including the calculation of concentrations of participating ions and carbon isotopes in the solution was developed applying for the first time different open to closed system ratios. The limestone dissolution model is designed for easy application to cave drip water. Only small changes in the boundary conditions and key parameters are necessary. The obtained soil air ^{14}C values as well as the directly measured soil air $\delta^{13}C$ content and soil pCO_2 are used in the limestone dissolution model as input parameters to simulate the carbon isotope content of carbon in speleothem drip water. The comparison of modelled and measured carbon isotopes in monthly collected drip water proves the model. The good model performance can be attributed to the considered variations of the open to closed limestone dissolution system ratio.

The model results together with additionally measured data for temperature, precipitation of the atmosphere above the cave as well as soil pCO_2, drip water pH values and finally the ion concentrations of drip and soil water, allow to attribute the seasonal radiocarbon cycle in drip water to changes of precipitation infiltration (Ernesto cave) and to changes of soil air ^{14}C (Bunker cave).

The information about the soil-cave-systems obtained in the investigation of the present day situation was applied to interpret the carbon isotopes of two Holocene stalagmites (ER-76

and Bu1) of both caves. For both stalagmites a ^{14}C time series was analysed. The calcite of stalagmite Bu1 was derived by drip water, which dissolved the limestone above the cave at nearly completely open conditions. The limestone dissolution system of water feeding stalagmite ER-76 changed from a more open to a more closed limestone dissolution system.

A Rayleigh distillation model with gas exchange processes (Hendy, 1971) was used to simulate the carbon isotopes during the growth of the stalagmite. With the use of both models, the limestone dissolution and the Rayleigh distillation model, a method was developed to derive the soil pCO_2 from paired ^{14}C and $\delta^{13}C$ values of the stalagmite. This method revealed that the soil pCO_2 above Ernesto cave increased within the last 4000 years. The pCO_2 increase can be attributed to a growing vegetation density. For the soil above Bunker cave no large soil pCO_2 changes were observed.

Outlook The model results for soil pCO_2 were simulated for constant cave temperature and soil parameter values. To obtain more realistic results, variations in those parameters should be included in future. This will be possible by iterating between the soil pCO_2 and other cave and soil parameters. Iterations of the model can be performed in case a transfer function between the soil pCO_2 and the mean annual temperature is known. The changes of the soil air $\delta^{13}C$ composition depends also on soil pCO_2, which is already modelled by Cerling (1984). Soil air radiocarbon values change mainly with atmospheric ^{14}C variations and, thus, are already included in the model.

Additionally, the model can be improved by replacing the Rayleigh distillation process with recently developed more sophisticated modelling approaches that take into account the stable carbon isotope composition of precipitated calcite, e.g. the models of Mühlinghaus et al. (2007) and Romanov et al. (2008b). This future model can be fed by the results of the developed drip water model after a radiocarbon calculation chain for the calcite precipitation is added.

To find a tracer in the soil-karst-cave system, which describes changes in the limestone dissolution system quantitatively, will be a further challenge in the future. With such a tracer it will be possible to limit the possible open to closed system ratios, which give soil pCO_2 solutions for a ^{14}C - $\delta^{13}C$ pair of a stalagmite subsample. This improvement will result in less solutions of soil pCO_2 values compared to the present status of this method. In the best case of a clearly defined limestone dissolution ratio even an unique solution could be obtained.

Appendix A

^{14}C data

Table A.1: Radiocarbon ages of marble background samples. The errors for samples measured in Lund (indicated by "LuS...") were not provided except the both for M1 and M2. "EM..." and "ETH..." samples were measured in Zurich. Samples are listed in chronological order of preparation. For comments to single background samples see the text of Section 2.2.

sample name	inventory nr.	analysis nr. (HD-)	Lund/Zurich nr.	^{14}C age [y BP]	1 σ [y]	δ^{13}C [‰]
marble M1	26666	25062	LuS50033	41921	887	
marble M2	26666	25063	LuS50037	41921	887	
marble M3	26666	25182	LuS50075	37309		0.1
marble M4	26666	25183	LuS50076	37309		5.2
marble M7	26666	25406	LuS50116	34952		
marble M9	26666	25436	LuS50117	34952		
marble M11	26666	25465	LuS50153	37642		
marble M12	26666	25466	LuS50154	37642		
marble M15	26666	25716	LuS50198	34994		
marble M16	26666	25717	LuS50199	34994		
marble M17	26666	26043	LuS50230	40000		
marble M18	26666	26044	LuS50231	40000		
marble M19	26666	26045	LuS50297	38400		
marble M20	26666	26059	LuS50298	38400		
Island Spar 1	27829	26161	LuS50335	38500		
Island Spar 2	27830	26162	LuS50336	38500		
marble M21	26666	26344	LuS50369	40773		0.8
marble M23	26666	26359	LuS50370	40773		0.8
marble M26	26666	26652	EM1003	48164	808	-2.5
marble M27	26666	26653	EM1009	52413	1375	3.5
marble M28	26666	26654	EM1015	47942	1345	2.3
marble M29	26666	26689	EM1043	47333	1204	1.5
marble M31	26666	26690	EM1049	49450	1301	-0.8
marble M30	26666	26929	ETH-35000	43664	584	0.1
marble M32	26666	26930	ETH-35001	46309	650	3.6

Table A.2: Radiocarbon activity of oxalic acid II standard

sample name	inventory nr.	analysis nr. (HD-)	Lund/Zurich nr.	^{14}C activity [pmC]	1 σ [pmC]	δ^{13}C [‰]
Oxalic Acid 04b	769	25797	LuS50226	134.12	0.71	
Oxalic Acid 04b	769	26019	LuS50227	132.37	0.9	
Oxalic Acid 04b	769	26020	LuS50228	133.99	0.7	
Oxalic Acid 04b	769	26021	LuS50229	134.73	0.55	
Oxalic Acid 04b	769	25115	LuS50071	134.58	0.84	-17.8
Oxalic Acid 04b	769	25197	LuS50072	135	0.65	-17.8
Oxalic Acid 04b	769	25198	LuS50073	134.51	0.69	-17.8
Oxalic Acid 04b	769	25199	LuS50074	133.19	0.47	-17.8
Oxalic Acid 04b	769	25673	LuS50184	133.61		
Oxalic Acid 04b	769	25674	LuS50185	134.39		
Oxalic Acid 04b	769	25682	LuS50186	133.56		
Oxalic Acid 04b	769	25683	LuS50187	134.71		
Oxalic Acid 04b	769	25486	LuS50147	134.2		
Oxalic Acid 04b	769	25487	LuS50148	134.76		
Oxalic Acid 04b	769	25495	LuS50149	133.35		
Oxalic Acid 04b	769	25496	LuS50150	133.96		
Oxalic Acid 04b	769	26198	LuS50293	134.06	0.53	
Oxalic Acid 04b	769	26199	LuS50294	133.94	0.35	
Oxalic Acid 04b	769	26200	LuS50295	134.16	0.61	
Oxalic Acid 04b	769	26209	LuS50296	134.36	0.62	
Oxalic Acid 04b	769	26210	LuS50331	133.77	0.40	
Oxalic Acid 04b	769	26211	LuS50332	134.22	0.36	
Oxalic Acid 04b	769	26212	LuS50333	133.54	0.41	
Oxalic Acid 04b	769	26213	LuS50334	134.26	0.23	
Oxalic Acid 04b	769	25815	LuS50194	134.66	0.6	
Oxalic Acid 04b	769	25798	LuS50195	134.18	0.43	
Oxalic Acid 04b	769	25814	LuS50196	133.92	0.59	
Oxalic Acid 04b	769	25816	LuS50197	133.19	0.69	
Oxalic Acid 04b	769	25351	LuS50110	134.29		
Oxalic Acid 04b	769	25350	LuS50111	133.55		
Oxalic Acid 04b	769	25407	LuS50112	134.73		
Oxalic Acid 04b	769	25408	LuS50113	133.69		
Oxalic Acid 04b	769	25051	LuS50032	133.49	0.69	-17.8
Oxalic Acid 04b	769	25052	LuS50034	134.93	0.55	-17.8
Oxalic Acid 04b	769	25053	LuS50036	133.81	0.35	-17.8
Oxalic Acid 04b	769	25074	LuS50039	134.23	0.62	-17.8
Oxalic Acid 04b	769	26214	LuS50371	133.74	0.6	-17.8
Oxalic Acid 04b	769	26341	LuS50372	134.27	0.42	-17.8
Oxalic Acid 04b	769	26342	LuS50373	133.98	0.58	-17.8
Oxalic Acid 04b	769	26343	LuS50374	134.06	0.58	-17.8
Oxalic Acid 04b	769	26369	LuS50409	134.05	0.4	
Oxalic Acid 04b	769	26370	LuS50410	133.98	0.42	
Oxalic Acid 04b	769	26371	LuS50411	134.68	0.41	

Continued on next page

Table A.2 – continued from previous page

sample name	inventory nr.	analysis nr. (HD-)	Lund/Zurich nr.	^{14}C activity [pmC]	1 σ [pmC]	δ^{13}C [‰]
Oxalic Acid 04b	769	26408	LuS50412	133.46	0.44	
Oxalic Acid 04b	769	26540	EM1001	133.65	0.22	-18
Oxalic Acid 04b	769	26633	EM1002	133.82	0.23	-17.2
Oxalic Acid 04b	769	26634	EM1008	134.16	0.24	-18
Oxalic Acid 04b	769	26635	EM1014	134.81	0.24	-18.3
Oxalic Acid 04b	769	26640	EM1021	133.91	0.23	-18.1
Oxalic Acid 04b	769	26641	EM1022	133.91	0.22	-16.9
Oxalic Acid 04b	769	26642	EM1028	134.02	0.23	-19.4
Oxalic Acid 04b	769	26643	EM1034	134.4	0.23	-16.8
Oxalic Acid 04b	769		EM1041	134.24	0.29	-17.3
Oxalic Acid 04b	769		EM1042	133.6	0.28	-18.2
Oxalic Acid 04b	769		EM1048	133.72	0.28	-18
Oxalic Acid 04b	769		EM1054	134.79	0.28	-17.5
Oxalic Acid 04b	769		ETH-35000	134.4	0.23	-18.8
Oxalic Acid 04b	769		ETH-35000	134	0.23	-18.1
Oxalic Acid 04b	769		ETH-35015	133.72	0.23	-16.8
Oxalic Acid 04b	769		ETH-35019	134.18	0.23	-17.5

Table A.3: Radiocarbon measurements on the top section of ER-77. The dft (distance from top) of the stalagmite is corrected for the different locations between sample collection and laminar counting.

sample name	inventory nr.	analysis nr. (HD-)	Lund nr.	dft [mm]	age [yr AD]	^{14}C activity [pmC]	1σ [pmC]	δ^{13}C [‰]
ER - 77 A	27810	26149	LuS50301	12.62	1888.87	87.90	0.35	-8.7
ER - 77 B	27811	26150	LuS50302	12.02	1898.67	86.96	0.38	-2.3
ER - 77 C	27812	26151	LuS50303	11.43	1905.99	87.01	0.35	-4.1
ER - 77 D	27813	26152	LuS50304	10.83	1911.92	88.02	0.36	-8.3
ER - 77 E	27814	26153	LuS50305	10.23	1917.69	87.47	0.35	-8.8
ER - 77 F	27815	26140	LuS50306	9.63	1922.27	87.26	0.35	-9.4
ER - 77 G	–	–	–	9.04	1926.29	–	–	–
ER - 77 H	27817	26141	LuS50307	8.44	1930.89	87.30	0.34	-9.4
ER - 77 I	27818	26142	LuS50308	7.84	1935.65	87.04	0.34	-7.1
ER - 77 J	27819	26144	LuS50309	7.25	1939.6	87.52	0.36	-2.3
ER - 77 K	27820	26145	LuS50310	6.65	1944.53	86.76	0.36	-8.3
ER - 77 L	27821	26154	LuS50311	6.05	1950.08	86.70	0.36	-2.0
ER - 77 M	–	–	–	5.45	1955.03	–	–	–
ER - 77 N	27823	26158	LuS50312	4.86	1960	87.61	0.34	-5.3
ER - 77 O	27824	26159	LuS50313	4.26	1964.34	91.26	0.34	-6.8
ER - 77 P	27825	26172	LuS50314	3.66	1967.62	106.88	0.40	-4.6
ER - 77 Q	27826	26173	LuS50315	3.06	1971.42	118.19	0.42	-13.0
ER - 77 R	27827	26174	LuS50316	2.47	1975.43	119.07	0.44	-11.1
ER - 77 S	27828	26160	LuS50317	1.87	1979.63	112.79	0.44	-11.7

Table A.4: Radiocarbon drip water measurements on drip location ER-G1. The time period of collection was from November 2005 until October 2007. In general all samples were collected during some hours only those marked by a † were collected over a full month.

sample name	month	inventory nr.	analysis nr. (HD-)	Lund/Zurich nr.	^{14}C activity [pmC]	1 σ [pmC]	δ^{13}C [‰]
ER-G1 47	Nov 05	26300	24871	LuS50011	95.28	0.32	-7.9
ER-G1 48	Dec 05	26425	24882	LuS50012	99.47	0.36	-7.9
ER-G1 49	Jan 06	26427	24884	LuS50013	100.02	0.39	-14.1
ER-G1 52	Apr 06	26942	25302	LuS50082	94.47	0.34	-9.9
ER-G1 53	May 06	26944	25304	LuS50084	96.82	0.39	-6.8
ER-G1 54	Jun 06	26946	25306	LuS50086	98.79	0.36	-0.7
ER-G1 55†	Jul 06	26948	25348	LuS50088	101.00	0.39	-13.5
ER-G1 56	Aug 06	27028	25410	LuS50090	100.70	0.37	-13.7
ER-G1 57	Sep 06	27081	25464	LuS50144	100.10	0.44	-5.9
ER-G1 58	Oct 06	27263	25597	LuS50206	98.70	0.41	-6.2
ER-G1 59†	Nov 06	27265	25739	LuS50204	98.28	0.38	-16.2
ER-G1 60	Dec 06	27361	25789	LuS50208	98.91	0.39	-18.7
ER-G1 61	Jan 07	27363	25791	LuS50203	101.47	0.41	-16.1
ER-G1 62	Feb 07	27461	25822	LuS50201	96.60	0.49	3.8
ER-G1 63	Mar 07	27598	25974	LuS50256	97.48	0.40	-13.2
ER-G1 64	Apr 07	27625	25979	LuS50258	98.28	0.43	-13.1
ER-G1 65	May 07	27672	26047	LuS50260	98.68	0.55	-5.3
ER-G1 66	Jun 07	27953	26202	LuS50357	99.02	0.49	-12.3
ER-G1 67	Jul 07	27988	26266	LuS50361	101.35	0.38	-16.9
ER-G1 68	Aug 07	28036	26368	LuS50363	101.46	0.38	-13.0
ER-G1 69†	Sep 07	28128	26475	EM1005	100.01	0.26	-11.6
ER-G1 70	Oct 07	28130	26477	EM1007	98.91	0.25	-11.2

Table A.5: Radiocarbon drip water measurements on drip location ER-76. The time period of collection was from November 2005 until October 2007. In general all samples were collected over a full month.

sample name	month	inventory nr.	analysis nr. (HD-)	Lund/Zurich nr.	^{14}C activity [pmC]	1 σ [pmC]	δ^{13}C [‰]
ER-76 47	Nov 05	26299	24870	LuS50014	97.32	0.38	-12.0
ER-76 48	Dec 05	26424	24881	LuS50015	98.82	0.36	-4.7
ER-76 49	Jan 06	26426	24883	LuS50016	98.84	0.34	-1.3
ER-76 51	Mar 06	26554	25032	LuS50017	99.43	0.42	-6.9
ER-76 52	Apr 06	26941	25301	LuS50091	96.21	0.41	-6.1
ER-76 53	May 06	26943	25303	LuS50083	97.09	0.35	-9.6
ER-76 54	Jun 06	26945	25305	LuS50085	97.65	0.35	-11.0
ER-76 55	Jul 06	26947	25349	LuS50087	99.11	0.36	-16.4
ER-76 56	Aug 06	27027	25409	LuS50089	95.96	0.36	-12.5
ER-76 57	Sep 06	27080	25463	LuS50145	98.75	0.42	-15.4
ER-76 58	Oct 06	27262	25596	LuS50207	97.46	0.39	-16.9
ER-76 59	Nov 06	27264	25738	LuS50205	97.04	0.39	-18.2
ER-76 60	Dec 06	27360	25788	LuS50209	96.26	0.38	-15.9
ER-76 61	Jan 07	27362	25790	LuS50202	98.79	0.39	-11.6
ER-76 62	Feb 07	27460	25821	LuS50200	99.08	0.41	-7.7
ER-76 63	Mar 07	27597	25973	LuS50255	90.61	0.37	-15.1
ER-76 64	Apr 07	27624	25978	LuS50257	99.32	0.40	-12.4
ER-76 65	May 07	27671	26046	LuS50259	99.23	0.46	-8.8
ER-76 66	Jun 07	27952	26201	LuS50356	95.90	0.36	-14.0
ER-76 67	Jul 07	27987	26265	LuS50360	98.21	0.54	-13.9
ER-76 68	Aug 07	28037	26384	LuS50364	98.75	0.37	-11.2
ER-76 69	Sep 07	28127	26474	EM1004	97.01	0.25	-11.6
ER-76 70	Oct 07	28129	26476	EM1006	98.25	0.24	-10.2

Table A.6: Radiocarbon drip water measurements on drip location Bu-TS2. The time period of collection was from March 2007 until February 2008. All samples were collected over a full month.

sample name	month	inventory nr.	analysis nr. (HD-)	Lund/Zurich nr.	^{14}C activity [pmC]	1 σ [pmC]	δ^{13}C [‰]
Bu TS2 03/07	Mar 07	27627	25981	LuS50261	98.14	0.42	0.8
Bu TS2 04/07	Apr 07	27626	25980	LuS50262	98.80	0.44	2.0
Bu TS2 05/07	May 07	27673	26048	LuS50263	99.18	0.43	4.8
Bu TS2 06/07	Jun 07	27954	26203	LuS50358	100.32	0.54	-11.0
Bu TS2 07/07	Jul 07	27959	26267	LuS50359	100.45	0.37	-8.4
Bu TS2 08/07	Aug 07	28035	26367	LuS50362	101.85	0.38	-9.4
Bu TS2 10/07	Oct 07	28386	26630	EM1010	99.94	0.26	-5.3
Bu TS2 11/07	Nov 07	28387	26631	EM1011	99.59	0.26	-5.5
Bu TS2 12/07	Dec 07	28638	26791	ETH-35016	99.19	0.26	-5.1
Bu TS2 01/08	Jan 08	28639	26792	ETH-35017	99.49	0.25	-4.4
Bu TS2 02/08	Feb 08	28718	26931	ETH-35018	98.80	0.26	-4.6

Table A.7: Radiocarbon ages of stalagmite subsamples of ER-76. The corresponding distance from top (dft) as well as true ages according to the best age model are shown including the 1σ value. All samples have the Heidelberg inventory number 26620.

sample name	analysis nr. (HD-)	Lund/Zurich nr.	dft [mm]	^{14}C age [y BP]	1 σ [y]	age and 1 σ [y]	δ^{13}C [‰]
ER-76 L	25236	LuS50079	10.5	1479	33	176 ± 10	-0.2
ER-76 M	25237	LuS50080	18.8	2696	35	396 ± 10	-4.6
ER-76 A	25022	LuS50001	22.3	2508	31	– ± –	-3.6
ER-76 B	25023	LuS50002	24.9	2894	43	– ± –	-17.8
ER-76 N	25238	LuS50081	33.6	3218	34	2437.41 ± 151	-9.3
ER-76 C	25024	LuS50003	39.4	3529	37	2613.86 ± 140	-5.9
ER-76 D	25025	LuS50004	44.3	3440	40	2742 ± 135	-13.9
ER-76 E	25026	LuS50005	60.7	3751	36	3431 ± 103	-15.5
ER-76 F	25027	LuS50006	87.7	4182	36	3902 ± 154	-12.3
ER-76 G	25028	LuS50007	107.75	4363	38	4230 ± 135	-7
ER-76 H	25029	LuS50008	130.9	4642	39	4713 ± 155	-7.9
ER-76 I	25030	LuS50009	145.4	4752	40	4994 ± 168	-12.4
ER-76 J	25031	LuS50010	167.8	4966	39	5295 ± 153	-7.6

Table A.8: Radiocarbon ages of stalagmite subsamples of Bu1. The corresponding distance from top (dft) as well as true ages according to the best age model are shown including the 1σ value. All samples have the Heidelberg inventory number 27278.

sample name	analysis nr. (HD-)	Zurich nr.	dft [mm]	^{14}C age [y BP]	1 σ [y]	age and 1 σ [y]	δ^{13}C [‰]
Bu1 - X	26607	EM1037	1	745	22	1120 ± 125	-9.5
Bu1 - I	26580	EM1024	90	1705	23	1449 ± 110	-9.6
Bu1 - II	26581	EM1025	140.4	2110	24	1778 ± 115	-12.3
Bu1 - III	26582	EM1026	170.5	3933	29	4023 ± 185	-10.8
Bu1 - XI	26608	EM1038	275	4857	27	4720 ± 305	-9.9
Bu1 - XII	26609	EM1039	281	4869	28	4745 ± 300	-10.6
Bu1 - IV	26583	EM1027	351.7	5114	19	5206 ± 80	-6
Bu1 - XVIII	26693	EM1047	421.15	5531	32	6335 ± 100	-7.7
Bu1 -V	26584	EM1030	440.2	5722	30	6580 ± 210	-8.4
Bu1 - XVII	26692	EM1046	465.2	5708	34	6855 ± 260	-6
Bu1 - XV	26676	EM1044	490.2	5828	33	7085 ± 315	-6.2
Bu1 - VI 1.7cm	26718	EM1050	524	6226	31	7346 ± 180	-13.4
Bu1 - VI	26585	EM1031	526.1	6237	40	7362 ± 180	-20.8
Bu1 - VII	26604	EM1032	535	6281	32	7432 ± 175	-10.8
Bu1 - VIII	26605	EM1033	555.1	6652	47	7593 ± 165	-24.2
Bu1 - IX	26606	EM1036	579.5	7115	33	7817 ± 165	-10.7
Bu1 - XIII	26678	EM1045	620.9	7606	37	8249 ± 180	-6.9

Appendix B

Additional figures

Additional figures to Chapter 4

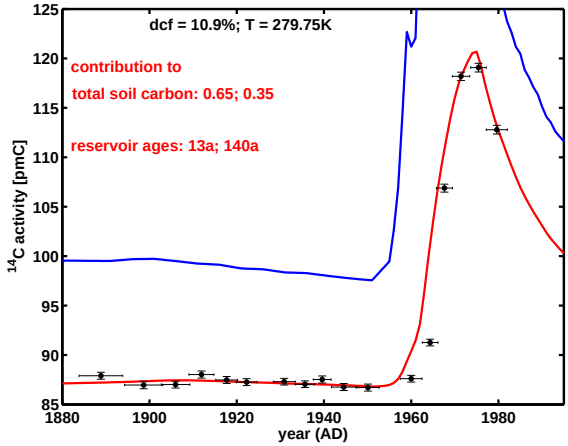

Figure B.1: By using only two soil reservoirs the onset, the maximum and the decrease of the radiocarbon bomb peak in the stalagmite are not well reproduced. The best fit with two soil reservoirs is shown here (red line).

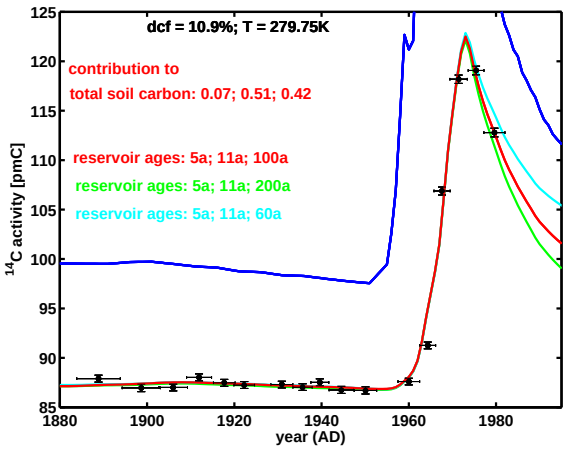

Figure B.2: The old soil reservoir is changed from 100 years (red) to 60 years (cyan) and to 200 years (green). All three lay in the range of the ^{14}C measurements of the stalagmite. Therefore, the age of the old reservoir is not constrained well. Nevertheless, the best fit is represented by an age of the old reservoir of 100 years.

Additional figures to Chapter 5

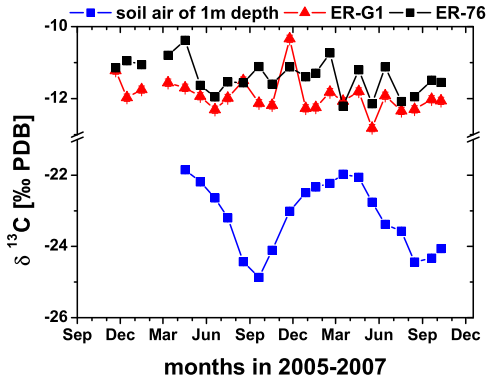

Figure B.3: Monthly measured δ^{13}C data of the drip water samples collected on drip locations ER-G1 (black squares) and ER-76 (red triangles) as in figure 5.2 but additionally with the δ^{13}C content of one meter deep soil air. The errors are within the symbol size.

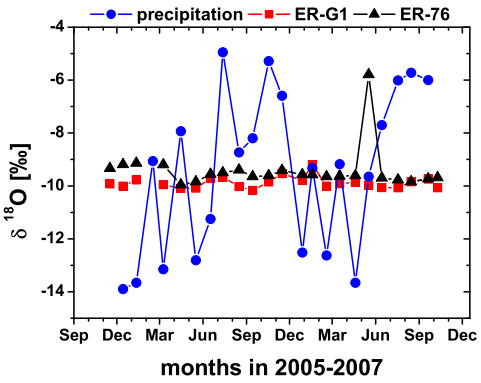

Figure B.4: Monthly measured δ^{18}O data of the drip water samples collected on drip locations ER-G1 (black squares) and ER-76 (red triangles) and precipitation values (blue circles).

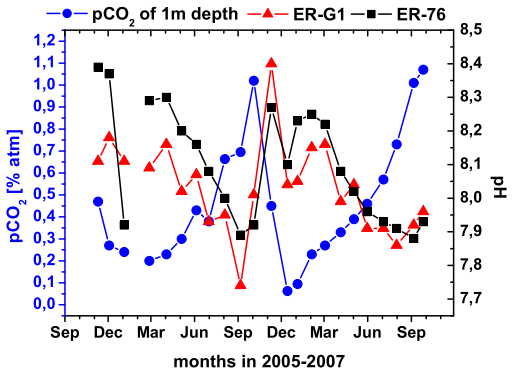

Figure B.5: Monthly measured soil pCO_2 (blue circles) and pH of ER-G1 (red triangles) as well as the pH of ER-76 (black squares).

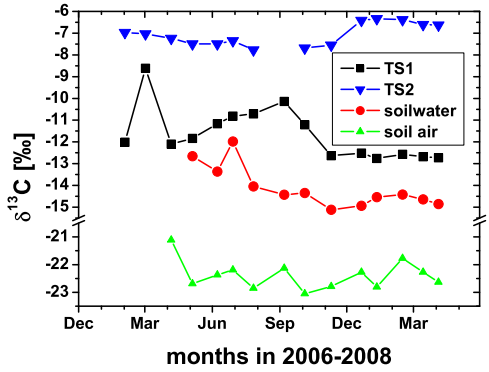

Figure B.6: Monthly measured δ^{13}C data of the drip water samples (Bu-TS1 – black squares, Bu-TS2 – blue face down triangles), soil water (red circles) and soil air (green triangles) both at 0.5 m depth. The errors are within the symbol size.

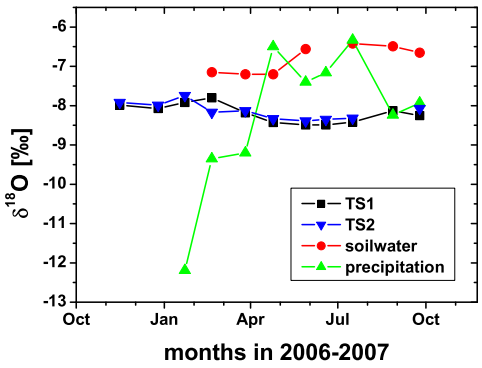

Figure B.7: Monthly measured δ^{18}O data of the drip water samples (Bu-TS1 – black squares, Bu-TS2 – blue face down triangles), soil water (red circles) and precipitation (green triangles). The errors are within the symbol size.

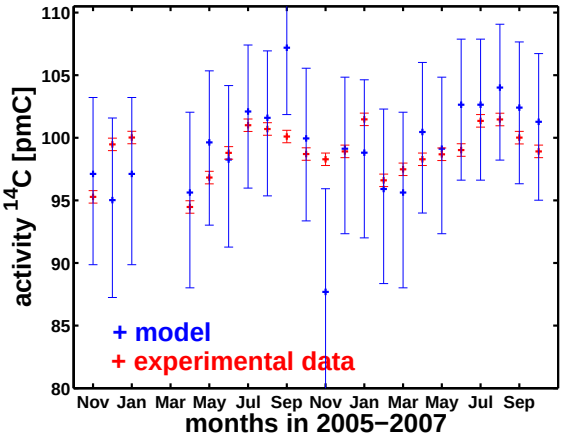

Figure B.8: Monthly measured ^{14}C data of drip water samples (red) collected on drip place ER-G1 compared to the modelled radiocarbon content of the drip water (blue). The range the model calculates is correct and also the annual cycle is reproduced. The outliers can be explained by difficulties with the drip water pH measurements. The errors are given under an uncertainty of mean soil pCO_2 of 0.1 % atm.

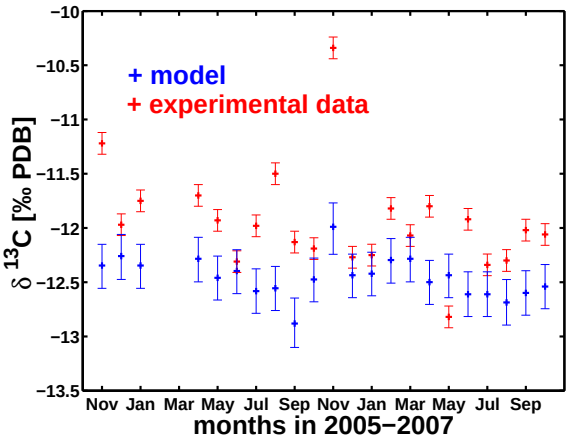

Figure B.9: Monthly measured δ^{13}C data of drip water samples (red) collected on drip place ER-G1 compared to the modelled δ^{13}C content of the drip water (blue). The calculated magnitude is underestimated, but in general satisfying. The modelled data points are not consistent with the measured data. The errors are given under a an uncertainty of mean soil pCO_2 of 0.1 % atm.

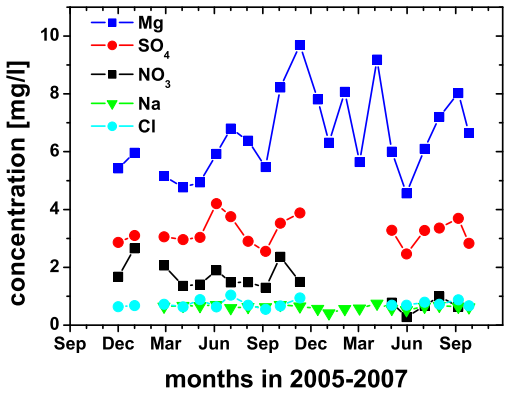

Figure B.10: Magnesium, sulphate, nitrate, sodium and chlorine in drip water of location ER-G1 are variable throughout the two years of investigation. The variability can explain the non-high correlation between measured and modelled calcium concentration. Data were measured by A. Schröder-Ritzrau.

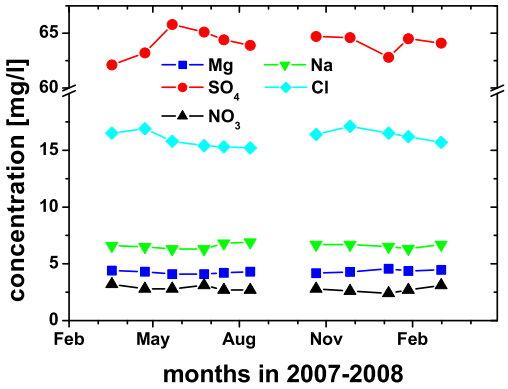

Figure B.11: Magnesium, sulphate, nitrate, sodium and chlorine in drip water of location Bu-TS2 are shown throughout the two years of investigation. Most elements are rather constant, only SO_4 shows variations. Sulphate has the highest concentration besides calcium in the drip water of this location. Data were measured by A. Schröder-Ritzrau.

Additional figures to Chapter 6

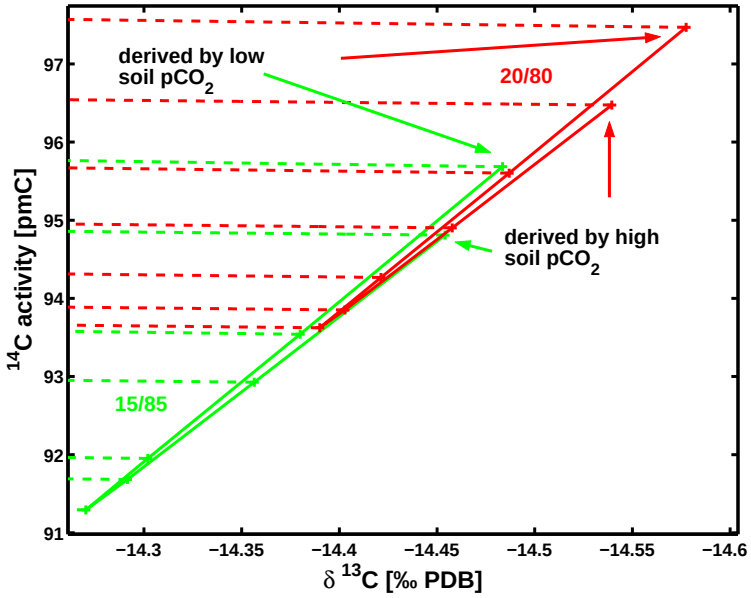

Figure B.12: This figure zooms into Figure 6.8 and shows the small differences of the first calcite to be precipitated (distorted "V" shapes in red and in green). From the first calcite to be precipitated the calcite precipitated during the degassing steps leads to heavier isotopic compositions (dashed red and green lines). Hence, two solutions exist for every measured carbon isotope pair. Input parameters: T = 10°C, $^{14}C_{soilair}$ = 106 pmC, $\delta^{13}C_{soilair}$ = −25 ‰

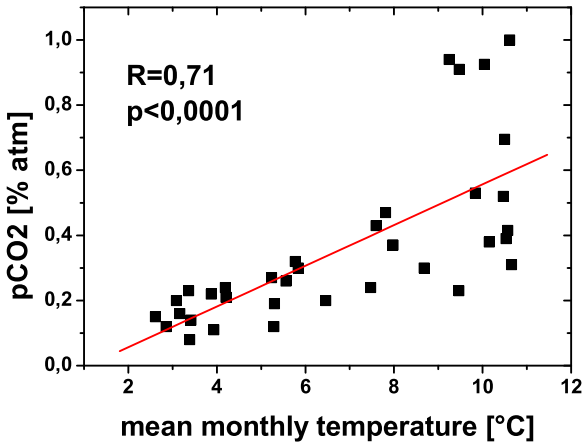

Figure B.13: The soil pCO_2 depends strongly on temperature. As an example the soil above Ernesto cave was chosen. Three years of monthly measurements of temperature and soil pCO_2 of one meter depth were used for the correlation calculation.

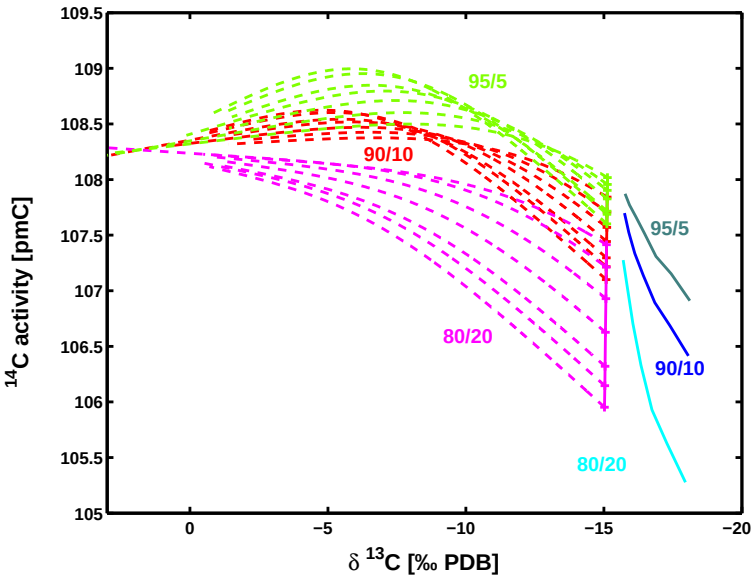

Figure B.14: The figure visualises the same processes as Figure 6.7. The difference is the chosen open to closed dissolution system ratio. In blue the drip water carbon isotopes derived by open/closed ratio of 90/10 % is shown. In cyan an open/closed ratio of 80/20 % and in dark green an open to closed ratio of 95 to 5 % is used. The carbon isotopes of the corresponding deposited calcite are drawn in red, pink and light green, respectively. At a ratio of 80/20 % the dashed lines do not cross. With a ratio higher than 80/20 % the isotopes in precipitated calcite derived by different soil pCO_2 form lines, which cross (e.g. 90/10 %). Input parameters: T = 10°C, ${}^{14}C_{soilair} = 106\,\mathrm{pmC}$, $\delta^{13}C_{soilair} = -25$ ‰

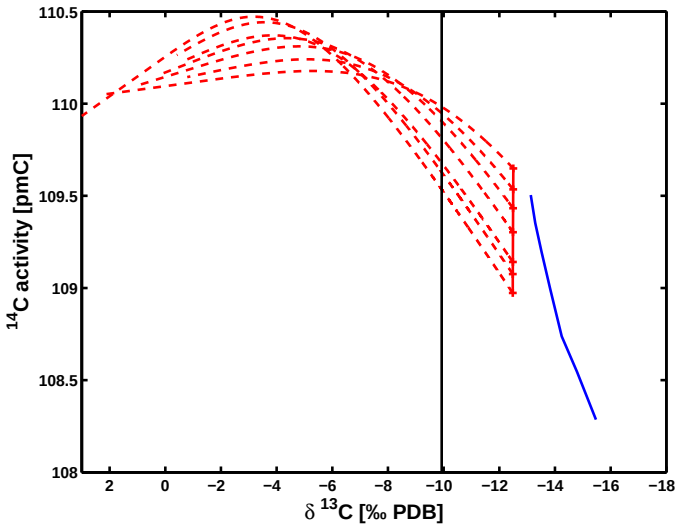

Figure B.15: The figure visualises the same processes as Figure 6.7. The difference is the chosen 91 % open dissolution system, the highest value in the Bu1 simulation (Sec. 6.3.2). The chosen soil air parameters and temperature correspond to the simulation of the soil pCO_2 derived from Bu1 (see caption of Figure 6.14). The black line is the δ^{13}C value (-9.93 ‰), which corresponds to the measured value of the carbon isotope pair at the age of 7817 years BP. The crossing of the dashed lines starts at higher δ^{13}C values. Hence, the search algorithm is not disturbed.

Bibliography

Aitken, M.: Physics and Archaeology, Interscience Publishers, Inc., New York, London, 1961.

Anderson, E. C. and Libby, W. F.: World-Wide Distribution of Natural Radiocarbon, Phys. Rev., 81, 64–69, doi:10.1103/PhysRev.81.64, 1951.

Beck, J., Richards, D., Edwards, R., Silverman, B., Smart, P.L. andDonahue, D., Hererra-Osterheld, S., Burr, G., Calsoyas, L., Jull, A., and Biddulph: Extremely Large Variations of Atmospheric ^{14}C Concentration During the Last Glacial Period, Science, 292, 2453 – 2458, 2001.

Bennet, C., Beukens, R., Clover, M., Gove, H., Lievert, R. B., Litherland, A., Purser, K., and Sondheim, W.: Radiocarbon Dating Using Accelerators: Negative Ions Provide the Key, Science, 198, 508 – 509, 1977.

Borsato, A.: Dripwater Monitoring at Grotta di Ernesto (NE-Italy): a Contribution to the Understanding of Karst Hydrology and the Kinetics of Carbonate Dissolution, in Proceedings of the 12th International Congress of Speleology,, vol. 2, pp. 57 – 60, 1997.

Bourdon, B., Turner, S., Henderson, G., and Lundstrom, C. C.: Introduction to U-Series Geochemistry, in Uranium-Series Geochemistry, edited by B. Bourdon, G. Henderson, C. Lundstrom, and S. Turner, p. 656 ff., Mineralogical Society of America, Washington, DC., 2003.

Broecker, W., Olson, E., and Orr, P.: Radiocarbon Measurements and Annual Rings in Cave Formations, Nature, 185, 93 – 94, 1960.

Cerling, T.: The Stable Isotopic Composition of Modern Soil Carbonate and Its Relationships to Climate, Earth and Planetary Science Letters, 71, 229 – 240, 1984.

Cruz Jr., F., Burns, S., Karmann, I., Sharp, W., Vuille, M., and Ferrari, J.: A Stalagmite Record of Changes in Atmospheric Circulation and Soil Processes in the Brazilian Subtropics During the Late Pleistocene, Quaternary Science Reviews, 22, 2749 – 2761, 2006.

de Vries, H.: Variation in Concentration of Radiocarbon with Time and Location on Earth, Koninklijke Nederlandse Akademie van Wetenschappen, B61, 94 – 102, 1958.

Deevey, E. J., Gross, M., Hutchinson, G., and Kraybill, H.: The Natural ^{14}C Contents of Materrials frem Hard-Water Lakes, Proceedings of the National Academy of Sciences of the United States of America, 40, 285 – 288, 1954.

Deines, P.: The Isotopic Composition of Reduced Organic Soil, in Handbook of Isotope Geochemistry, 1 The Terrestrial Environment, edited by P. Fritz and J. C. Fontes, pp. 329–406, Elsevier, Amsterdam-Oxford-New York-Tokio, 1980.

Deines, P., Langmuir, D., and Harmon, R.: Stable Carbon Isotope Ratios and the Existence of a Gas Phase in the Evolution of Carbonate Ground Waters, Geochimica et Cosmochimica Acta, 38, 1147 – 1164, 1974.

Denniston, F., Gonzáles, L., Asmerom, Y., Reagan, M., and Recelli-Snyder, H.: Speleothem Carbon Isotopic Records of Holocene Environments in the Ozark Highlands, USA, Quaternary International, 67, 21 – 27, 2000.

Dorale, J., Gonzáles, L., Reagan, M., Pickett, D., Murrell, M., and Baker, R.: A High-Resolution Record of Holocene Climate Change in Speleothem Calcite from Cold Water Cave, Northeast Iowa, Science, 258, 1626 – 1630, 1992.

Dorale, J., Edward, R., Ito, E., and Gonzáles, L.: Climate and Vegetation History of the Midcontinent from 75 to 25 ka: A Speleothem Record from Crevice Cave, Missouri, USA., Science, 282, 1871 – 1874, 1998.

Dörr, H. and Münnich, K.: Carbon-14 and Carbon-13 in Soil CO_2, Radiocarbon, 22, 909 – 918, 1980.

Dörr, H. and Münnich, K.: Annual Variations of the ^{14}C Content, Radiocarbon, 28, 338 – 345, 1986.

Dreybrodt, W.: Processes in Karst Systems - Physics, Chemistry and Geology, Springer Verlag, Berlin, Heidelberg, New York, London, Paris, Tokio, 1988.

Drysdale, R., Zanchetta, G., Hellstrom, J., Fallick, A., Zhao, J., Isola, I., and Bruschi, G.: Palaeoclimatic Implications of the Growth History and Stable Isotope ($\delta^{18}O$ and $\delta^{13}C$) Geochemistry of a Middle to Late Pleistocene Stalagmite from Central-Western Italy, Earth and Planetary Science Letters, 227, 215 – 229, 2004.

Dulinsky, M. and Rozanski, K.: Formation of $^{13}C/^{12}C$ Isotope Ratios in Speleothems: A Semi-Dynamic Model, Radiocarbon, 32, 7 – 16, 1990.

Dykoski, C., Edwards, R., Cheng, H., Yuan, D., Cai, Y., Zhang, M., Lin, Y., Qing, J., An, Z., and Revenaugh, J.: A High-Reolution, Absolute-Dated Holocene and Deglacial Asian Monsoon Record from Dongge Cave, China, Earth and Planetary Science Letters, 233, 71 – 86, 2005.

Fairchild, I., Borsato, A., Tooth, A., Frisia, S., Hawkesworth, C., Huang, Y., McDermott, F., and Spiro, B.: Controls on Trace Element (Sr-Mg) Compositions of Carbonate Cave Water: Implications for Speleothem Climatic Records, Chemical Geology, 166, 255 – 269, 2000.

Fairchild, I., Smith, C., Baker, A., Fuller, L., Spötl, C., Mattey, D., McDermott, F., and EIMF: Modification and Preservation of Environmental Signals in Speleothems, Earth Science Reviews, 75, 105 – 153, 2006.

Finkel, R. and Suter, M.: AMS in the Earth Sciences: Technique and Application, Advances in Analytical Geochemistry, 1, 1 – 114, 1993.

Franke, W.: Altersbestimmung von Kalzitkonkretionen mit radioaktivem Kohlenstoff, Naturwissenschaften, 38, 527 – 528, 1951.

Friedman, I. and O'Neil, R.: Compilation of Stable Isotope Fractionation Factors of Geochemical Interest, chap. Data of Geochemistry, pp. KK1 – KK12, US Govt. Print. Office, 1977.

Frisia, S., Borsato, A., Preto, N., and McDermott, F.: Late Holocene Annual Growth in Three Alpine Stalagmites Records the Influence of Solar Activity and the North Atlantic Oscillation on Winter Climate, Earth and Planetary Sience Letters, 216, 411 – 424, 2003.

Garrels, R. and Christ, C.: Solutions, Minerals and Equilibria, Harper & Row, New York, 1965.

Genty, D. and Massault, M.: Bomb ^{14}C recorded in Laminated Speleothems: Calculations of Dead Carbon Proportion, Radiocarbon, 39, 33 – 48, 1997.

Genty, D. and Massault, M.: Carbon Transfer Dynamics from Bomb-^{14}C and $\delta^{13}C$ Time Series of a Laminated Stalagmite from SW France – Modeling and Comparison with other Stalagmite Records, Geochimica et Cosmochimica Acta, 63, 1537 – 1548, 1999.

Genty, D., Vokal, B., Obelic, B., and Massault, M.: Bomb ^{14}C Time History Recorded in Two Modern Stalagmites – Importance for Soil Organic Matter Dynamics and Bomb ^{14}C Distribution over Continents, Earth and Planetary Science Letters, 160, 795 – 809, 1998.

Genty, D., Massault, M., Gilmour, M., Baker, A., Verheyden, S., and Kepens, E.: Calculation of Past Dead Carbon Proportion and Variability by the Comparison of AMS ^{14}C and TIMS U/Th Ages on Two Holocene Stalagmites, Radiocarbon, 41, 251 – 270, 1999.

Genty, D., Baker, A., Massault, M., Proctor, C., Gilmour, M., Pons-Branchu, E., and Hamelin, B.: Dead Carbon in Stalagmite: Carbonate Bedrock Paleodissolution vs. Ageing of Soil Organic Matter. Implications for ^{13}C Variations in Speleothems, Geochimica et Cosmochimica Acta, 65, 3443 – 3457, 2001.

Geyh, M.: An Overview of ^{14}C Analysis in the Study of Groundwater, Radiocarbon, 42, 99 – 114, 2000.

Geyh, M. and Franke, H.: Zur Wachstumsgeschwindigkeit von Stalagmiten, Atompraxis, 16, 46 – 48, 1970.

Glynn, S., Southon, J., and Sinha, A.: Stalagmite Based Reconstruction of Atmospheric Radiocarbon Levels during Deglaciation: Implications for Radiocarbon Calibration , EOS Trans. AGU, 87, Abstract, 2006.

Godwin, H.: Half-Life of Radiocarbon, Nature, 195, 984, 1962.

Goslar, T. and Czernik, J.: Sample Preparation in the Gliwice Radiocarbon Laboratory for the AMS ^{14}C Dating of Sediments, Geochronometria, 18, 1 – 8, 2000.

Grebe, W.: Die Bunkerhöhle in Iserlohn-Letmathe (Sauerland), Mitt. Verb. Dt. Höhlen- und Karstforsch, 39, 22 – 23, 1993.

Hamon, W.: Estimating Potential Evapotranspiration., Journal of the Hydraulics Division, Proceedings of the American Society of Civil Engineers, pp. 107 – 120, 1961.

Haude, W.: Zur praktischen Bestimmung der aktuellen und potentiellen Evaporation und Evapotranspiration, Mitteilungen des deutschen Wetterdienstes, 1, 1954.

Heegaard, E., Birks, H. J. B., and Telford, R. J.: Relationships Between Calibrated Ages and Depth in Stratigraphical Sequences: An Estimation Procedure by Mixed-Effect Regression, The Holocene, 15, 612 – 618, 2005.

Hellstrom, J., McCulloch, M., and Stone, J.: A Detailed 31,000-Year Record of Climate and Vegetation Change from the Isotope Geochemistry of Two New Zealand Speleothems, Quarternary Research, 50, 167 – 178, 1998.

Hendy, C.: The Use of ^{14}C in the Study of Cave Processes, in Radiocarbon Variations and Absolute Chronology, edited by I. Olsson, Wiley Interscience Devision, New York, 1970.

Hendy, C.: The Isotopic Geochemistry of Speleothems – I. The Calculation of the Effects of Different Modes of Formation on the Isotopic Composition of Speleothems and Their Applicability as Palaeoclimatic Indicators, Geochimica et Cosmochimica Acta, 35, 801 – 824, 1971.

Hendy, C. and Wilson, A.: Palaeoclimatic Data from Speleothems, Nature, 216, 48 – 51, 1968.

Hodge, E., Zhao, J., Feng, Y., Wu, J., Fink, D., and Hua, Q.: Coupled U-series and Radiocarbon Dating of a Chinese Stalagmite from 15 to 33 ka: Testing Calibration Applicability and Dead Carbon Correction Variability, Geochimica et Cosmochimica Acta, 70, A255, 2006.

Hu, C., Henderson, G., Huang, J., Xie, S., Sun, Y., and Johnson, K.: Quantification of Holocene Asian Monsoon Rainfall from Spatially Separated Cave Records, Earth and Planetary Science Letters, 266, 221 – 232, 2008.

Huang, Y., Fairchild, I., Borsato, A., Frisia, S., Cassidy, N., McDermott, F., and Hawkesworth, C.: Seasonal Variations in Sr, Mg and P in Modern Speleothems (Grotta di Ernesto, Italy), Chemical Geology, 175, 429 – 448, 2001.

Hughen, K., Baillie, M., Bard, E., Beck, J., and et al: Marine04 Marine Radiocarbon Age Calibration, 0-26 cal kyr BP.), Radiocarbon, 46, 1059–1086, 2004.

Kim, S.-T. and O'Neil, J.: Equilibrium and Nonequilibrium Oxygen Isotope Effects in Synthetic Carbonates, Geochimica et Cosmochimica Acta, 61, 3461 – 3475, 1997.

Klein, M., van Staveren, H., Mous, D., and Gottdang, A.: Performance of the Compact HVE 1MV Multi-Element AMS System, Nuclear Instruments and Methods in Physics Research B, 259, 184 – 187, 2007.

Levin, I. and Kromer, B.: The Tropospheric $^{14}CO_2$ Level in Mid-Latitudes of the Northern Hemisphere (1959-2003), Radiocarbon, 46, 1261 – 1272, 2004.

Libby, W., Anderson, E., and Arnold, J.: Age determination by Radiocarbon Content: World-Wide Assay of Natural Radiocarbon, Science, 109, 227 – 228, 1949.

Mangini, A., Spötl, C., and Verdes, P.: Reconstruction of temperature in the Central Alps During the Past 2000 yr from a $\delta^{18}O$ Stalagmite Record, Earth and Planetary Science Letters, 235, 741 – 751, 2005.

Mann, M., Bradley, R., and Hughes, M.: Global-Scale Temperature Patterns and Climate Forcing over the Past Six Centuries, Nature, 392, 779 – 787, 1998.

Mann, W.: An International Reference Material for Radiocarbon Dating, Radiocarbon, 25, 519 – 527, 1983.

McDermott, F., Frisia, S., Huang, Y., Longinelli, A., Spiro, B., Heaton, T. H. E., Hawkesworth, C. J., Borsato, A., Keppens, E., Fairchild, I. J., van der Borg, K., Verheyden, S., and Selmo, E. M.: Holocene Climate Variability in Europe: Evidence from δ^{18}O, Textural and Extension-Rate Variations in Three Speleothems, Quaternary Science Reviews, 18, 1021 – 1038, 1999.

Mook, W. and de Vries, J.: Environmental Isotopes in the Hydrological Cycle Principles and Applications - Volume I: Introduction - Theory, Methods, Review, IAEA, Vienna, 2000.

Morse, J. and Arvidson, R.: The Dissolution Kinetics of Major Sedimentary Carbonate Minerals, Earth-Science Reviews, 58, 51 – 84, 2002.

Mühlinghaus, C., Scholz, D., and Mangini, A.: Modelling Stalagmite Growth and δ^{13}C as a Function of Drip Interval and Temperature, Geochimica et Cosmochimica Acta, 71, 2780 – 2790, 2007.

Muller, R.: Radioisotope Dating with a Cyclotron, Science, 196, 489 – 494, 1977.

Münnich, K.: Messung des ^{14}C-Gehaltes von hartem Grundwasser, Naturwissenschaften, 44, 32 – 33, 1957.

Münnich, K.: Der Kreislauf des Radiokohlenstoffs in der Natur, Naturwissenschaften, 50, 211 – 218, 1963.

Nelson, D., Korteling, R., and Stott, W.: Carbon-14: Direct Detection at Natural Concentrations, Science, 198, 507 – 508, 1977.

Olsson, I.: A Warning Against Radiocarbon Dating of Samples Containing Little Carbon, Boreas, 8, 203 – 207, 1979.

Penman, H.: Natural Evaporation from Open Water, Bare Soil and Grass, Proceedings of the Royal Society of London. Series A, Mathematical and Physical Sciences, 193, 120 – 145, 1948.

Plummer, L. and Mackenzie, F.: Predicting Mineral Solubility from Rate Data: Application to the Dissolution of Magnesian Calcite, American Journal of Science, 274, 61 – 83, 1974.

Reimer, P., Baillie, M., Bard, E., Bayliss, A., and et al.: IntCal04 Terrestrial Radiocarbon Age Calibration, 0–26 cal kyr BP, Radiocarbon, 46, 1029 – 1058, 2004.

Roberts, M., Smart, P., and Baker, A.: Annual Trace Element Variations in a Holocene Speleothem, Earth and Planetary Science Letters, 154, 237 – 246, 1998.

Romanek, C., Grossman, E., and Morse, J.: Carbon Isotopic Fractionation in Synthetic Aragonite and Calcite: Effects of Temperature and Precipitation Rate, Geochimica et Cosmochimica Acta, 56, 419 – 430, 1992.

Romanov, D., Kaufmann, G., and Dreybrodt, W.: Modeling Stalagmite Growth by First Principles of Chemistry and Physics of Calcite Precipitation, Geochimica et Cosmochimica Acta, 72, 423 – 437, 2008a.

Romanov, D., Kaufmann, G., and Dreybrodt, W.: δ^{13}C Profiles along Growth Layers of Stalagmites: Comparing Theoretical and Experimental Results, Geochimica et Cosmochimica Acta, 72, 438 – 448, 2008b.

Salièges, J. and Fontes, J.: Essai de Détermination Expérimentale du Fractionnement des Isotopes ^{13}C et ^{14}C du Carbone au cours de Processus Naturels, International Journal of Applied Radiation and Isotopes, 35, 55 – 62, 1984.

Salomons, W. and Mook, W.: Isotope Geochemistry of Carbonates in the Weathering Zone, in Handbook of Isotope Geochemistry, edited by P. Fritz and J. C. Fontes, vol. 2, Elsevier, Amsterdam-Oxford-New York-Tokio, 1986.

Scharf, A., Uhl, T., Luppold, W., Rottenbach, A., Kritzler, K., Ohneiser, A., and Kretschmer, W.: Status Report on the Erlangen AMS facility, Nuclear Instruments and Methods in Physics Research B, 259, 50 – 56, 2007.

Scholz, D. and Hoffmann, D.: ^{230}Th/U-Dating of Fossil Reef Corals and Speleothems, Quaternary Science Journal, 57, 52 – 77, 2008.

Scholz, D., Frisia, S., Borsato, A., Miorandi, R., Spötl, C., J., F., Kromer, B., Mühlinghaus, C., Mangini, A., and Mudelsee, M.: Holocene Stalagmite Documents Alternating Influence of Central European and Mediterranean Climate in Northern Italy, in prep.

Schwarcz, H.: Geochronology and Isotopic Geochemistry of Speleothems, in Handbook of Isotope Geochemistry, edited by P. Fritz and J. C. Fontes, vol. 2, Elsevier, Amsterdam-Oxford-New York-Tokio, 1986.

Skog, G.: The Single Stage AMS Machine at Lund University: Status Report, Nuclear Instruments and Methods in Physics Research B, 259, 1 – 6, 2007.

Stuiver, M. and Braziunas, T.: Modeling Atmospheric ^{14}C Influences and ^{14}C Ages of Marine Samples to 10,000 BC., Radiocarbon, 35, 137 – 189, 1993.

Stuiver, M. and Polach, H.: Discussion Reporting of ^{14}C Data, Radiocarbon, 19, 355 – 363, 1977.

Suess, H.: Radiocarbon Concentration in Modern Wood, Science, 122, 415 – 417, 1955.

Synal, H.-A., Jacob, S., and Suter, M.: The PSI/ETH Small Radiocarbon Dating System, Nuclear Instruments and Methods in Physics Research B, 172, 1 – 7, 2000.

Tegen, I. and Dörr, H.: ^{14}C Measurments of Soil Organic Matter, Soil CO_2 and Dissolved Organic Carbon, Radiocarbon, 38, 247 – 251, 1996.

Thornthwaite, C. W.: An Approach toward a Rational Classification of Climate, Geographical Review, 38, 55–94, 1948.

Tooth, A. and Fairchild, I.: Soil and Karst Aquifer Hydrological Controls on the Geochemical Evolution of Speleothem-Forming Drip Waters, Crag Cave, Southwest Ireland, Journal of Hydrology, 273, 51 – 68, 2003.

Treble, P., Shelley, J., and Chappell, J.: Comparison of High Resolution Sub-Annual Records of Trace Elements in a Modern (1911 – 1992) speleothem with Instrumental Climate Data from Southwest Australia, Earth and Planetary Science Letters, 216, 141 – 153, 2003.

Trumbore, S.: Age of Soil Organic Matter and Soil Respiration: Radiocarbon Constraints on Belowground C Dynamycs, Ecological Applications, 10, 399 – 411, 2000.

Unkel, I.: Chronostratigraphie der Nasca-Kultur und Paläoklimarekonstruktion der Region Palpa (Peru) mittels AMS-^{14}C Datierung, Master's thesis, Universität Heidelberg, Institut für Umweltphysik, 2006.

Verheyden, S., Keppens, E., Fairchild, I., McDermott, F., and Weis, D.: Mg, Sr and Sr Isotope Geochemistry of a Belgian Holocene Speleothem: Implications for Paleoclimate Reconstructions, Chemical Geology, 169, 131 – 144, 2000.

Vollweiler, N., Scholz, D., Mühlinghaus, C., Mangini, A., and Spötl, C.: A Precisely Dated Climate Record for the Last 9 kyr from Three High Alpine Stalagmites, Spannagel Cave, Austria, Geophysical Research Letters, 33, L20 703, 2006.

Wang, Y., Cheng, H., Edwards, R., An, Z., Wu, J., Shen, C.-C., and Dorale, J.: A High-Resolution Absolute-Dated Late Pleistocene Monsoon Record from Hulu Cave, China, Science, 294, 2345 – 2348, 2001.

Wang, Y., Cheng, H., Edwards, R., He, Y., Kong, X., An, Z., Wu, J., Kelly, M., Dykoski, C., and Li, X.: The Holocene Asian Monsoon: Links to Solar Changes and North Atlantic Climate, Science, 308, 854 – 857, 2005.

Warembourg, F. and Paul, E.: The Use of $^{14}CO_2$ Canopy Techniques for Measuring Carbon Transfer Through the Plant-Soil System, Plant and Soil, 38, 331 – 345, 1973.

Wendt, I., Stahl, W., Geyh, M., and Fauth, F.: Model Experiments for ^{14}C Water-Age Determinations, in Isotopes in Hydrology, Proceedings of the IAEA, pp. 321 – 337, Vienna, 1967.

Zhang, M., Yuan, D., Lin, Y., Qin, J., Bin, L., Cheng, H., and Edwards, R.: A 6000-Year High-Resolution Climatic record from a stalagmite in Xiangshui Cave, Guilin, China, The Holocene, 14, 697 – 702, 2004.

Danksagung

Zum Ende meiner Arbeit möchte ich mich bei allen Kollegen und Freunden bedanken, die zum Gelingen meiner Doktorarbeit beigetragen haben.

Als erstes möchte ich Dr. Bernd Kromer und Prof. Dr. Augusto Mangini danken, die mir die Möglichkeit gaben meine Doktorarbeit über ein solch interessantes und komplexes Thema zu schreiben. Beide haben mich herzlichst empfangen, als ich mich bei ihnen im Juli 2005 zum ersten mal vorstellte und auch als ich drei Monate später mit der Arbeit begann. Sie halfen mir bei schwierigen wissenschaftlichen Fragen und förderten meine Entwicklung als Forscher. Es war und ist eine Freude in der Radiometrie-Arbeitsgruppe zu arbeiten. Es hat jederzeit viel Spass gemacht sich in der Gruppe einzubringen und wissenschaftlich zu diskutieren. Die gemeinsamen Mittagessen und Gruppenausflüge, sowie die Daphnetreffen und -workshops waren eine Bereicherung. Deshalb ein ganz herzliches Dankeschön an: Alex, Andrea, Anne, Augusto, Bernd, Christian, Claudia, Daniel, Daniela, Denis, Eva, Helga, Ingmar, Jörg, Karoline, Mario, Marleen, Nicole, René, Sabine, Sahra und Susanne.

Ich danke Bernd und Ingmar, die mir die Präparation von Proben für AMS Messungen beigebracht haben. Weiterhin möchte ich gerne Eva, Helga, Marleen and Susanne danken, die mir mit Rat und Tat bei schwierigen Suchen über den Verbleib nach "verschollenen" Arbeitsgeräten zur Seite standen und mir auch besonders am Anfang meiner Arbeit als Doktorand bei Fragen über die Laborорganisation auf die Sprünge halfen.

Weiterhin geht mein Dank auch an Prof. Dr. Christoph Spötl, in dessen Labor ich Proben mit der "miromill" nehmen durfte. Dana Riechelmann und Renza Miorandi gebührt mein Dank für das fleissige Sammeln von Daten über die Höhlen- und Bodenparameter, und für das schnelle Antworten auf Fragen bezüglich "ihrer" Höhle.

Eine Freude waren die mitunter witzigen aber vor allem ergiebigen Diskussionen mit Andrea und Denis über die Höhlen- und Bodenprozesse in der Ernestohöhle und Bunkerhöhle. Für die Hilfe bei Matlab- und sonstigen computertechnischen Problemen danke ich Daniela und Christian.

Das Lesen und Beurteilen einer Doktorarbeit ist viel Arbeit. Daher auch ein extragroßes Danke an meine Gutachter Prof. Dr. Augusto Mangini und Prof. Dr. Werner Aeschbach-Hertig.

Der gleiche Dank und größter Respekt gilt Andrea, Bernd, Denis, Janine, Susanne und Thomas, die meine Arbeit Korrektur gelesen haben. Es war sicherlich nicht einfach mein Englisch zu kontrollieren und meine Gedankengänge zu verstehen.

Es ist eine Freude meinen Kollegen im Büro zu danken. Danke Barbara, Florian, Mario, Thomas K. und Thomas L., es war unterhaltsam mit Euch das Büro zu teilen.

Ein großer Dank geht an meine Eltern Doris und Bernd sowie an meine Schwester Julia die mich während der drei Jahre meiner Doktorarbeit aus weiter Ferne so gut es ging unterstützten.

Ein besonders großen Dank möchte ich meiner nicht mehr ganz so kleinen Familie aussprechen. Danke Janine, Henry und auch Edwin, dass ihr für mich da seid. Ihr habt mir Kraft und einen triftigen Grund gegeben innerhalb von drei Jahren pünktlich meine Doktorarbeit abzuschliessen.